Non-Hydrostatic and Hydrostatic AROME experiments with the setting of Low and High Diffusion

Manuel João Lopes

Sylvie Malardel

Toulouse, december 2007

Introduction

In order to evaluate the importance of non-hydrostatic and hydrostatic modes on AROME model and also the importance of the intensity of the numerical diffusion used on the model, some experiments were made using two particular meteorological situations. The first one, occurred on the 1th of March 2007, is associated with the developing of orographical waves; the second one, occurred on the 6th September 2005, is associated with deep convection. The experiments include Non-Hydrostatic (*NH*) and Hydrostatic (*H*) experiments with different settings for the diffusion: Standard Diffusion (*Std Diff*) and Low Diffusion (*Low Diff*).

Furthermore, the performances of two AROME shallow cumulus convection schemes were compared, one from the cycle al32t3_arome-main.01 and the other one from a tested version with a new shallow cumulus convection scheme (Malardel, 2007). This comparison was made setting non-hydrostatic mode, low diffusion and No Predictor/Corrector in an experiment with the frontal case occurred on the 21th of November 2007.

1. – AROME experiments for the 1th of March 2007

This situation is characterized by the developing of orographical waves on the *Massif Central* zone.

On a first stage, two *NH* AROME experiments were made: one with Standard Diffusion (or High Diffusion) and Predictor/Corrector (*NH _ Std Diff _ PC*), the reference (*REF*) experiment[1]; another one with Low Diffusion and Predictor/Corrector (*NH _ Low Diff _ PC*)[2]. However the second experiment did "*blow up*" for the wind field on the step H+13 at the model level 19. As the previous experiment of Yann Seit - an *NH* AROME experiment with Low Diffusion and No Predictor/Corrector (*NH _ Low Diff _ No PC*) from a more recent cycle[3] - did succeed well, a new experiment was made[4].
The new experiment was similar to the second one but includes on its Forecast Part a new namelist *Gnam* for the No PC, similar to the namelist with the same name included on the Yann's experiment. This experiment with *No PC* ran all the Forecast Part well which means that maybe there exists a problem with the Predictor/Corrector on this case.

Furthermore, two *H* AROME experiments[5] were made: one with Standard Diffusion and Predictor/Corrector (*H _ Std _ PC*); another one with Low diffusion and Predictor Corrector (*H _ Low Diff _ PC*).

The area used is FRAN004, sometimes with a zoom over the *Massif Central* area, defined by the SW point 43°N 1°E and the NE grid 47°N 5.5°E.

[1] Experiment from cycle al32t3_arome-main.01 with coupling every 3hour.
[2] Experiment with the same cycle and the same frequency of coupling as the *REF* experiment.
[3] Experiment from cycle al31t2_arome-main.01 with canopy and coupling every 3 hours.
[4] Experiment with the same cycle and the same frequency of coupling as the *REF* experiment.
[5] Experiment with the same cycle and the same frequency of coupling as the *REF* experiment.

1.1 Forecasts for 12h from the *NH* experiments

(A) Pressure Departure ($P_{NH} - P_H$)

By the comparison of the forecasts of the pressure departure at ML 32, it is possible to identify orographical waves above the *Massif Central* zone by the long areas with very strong gradient of the field – "red" ("blue") areas followed by "blue" ("red") areas. The forecast of the experience *Low Diff _ PC* is very different from the forecasts of the other two experiments on the N-NW Part of the domain where the field shows a "numerical anomaly" with very strong values, which is related with the *"blow up"* of this experiment at the 13h forecast. The fields forecasted by the REF experiment and the experiment *Low Diff _ No PC* are similar in magnitude and present some differences in patterns. While the REF experiment shows larger areas with strong values of the pressure departure over the Eastern Part of the domain (Western Alps), the experiment *Low Diff _ No PC* shows a lined structure with strong values of the field on the NW part of the domain.

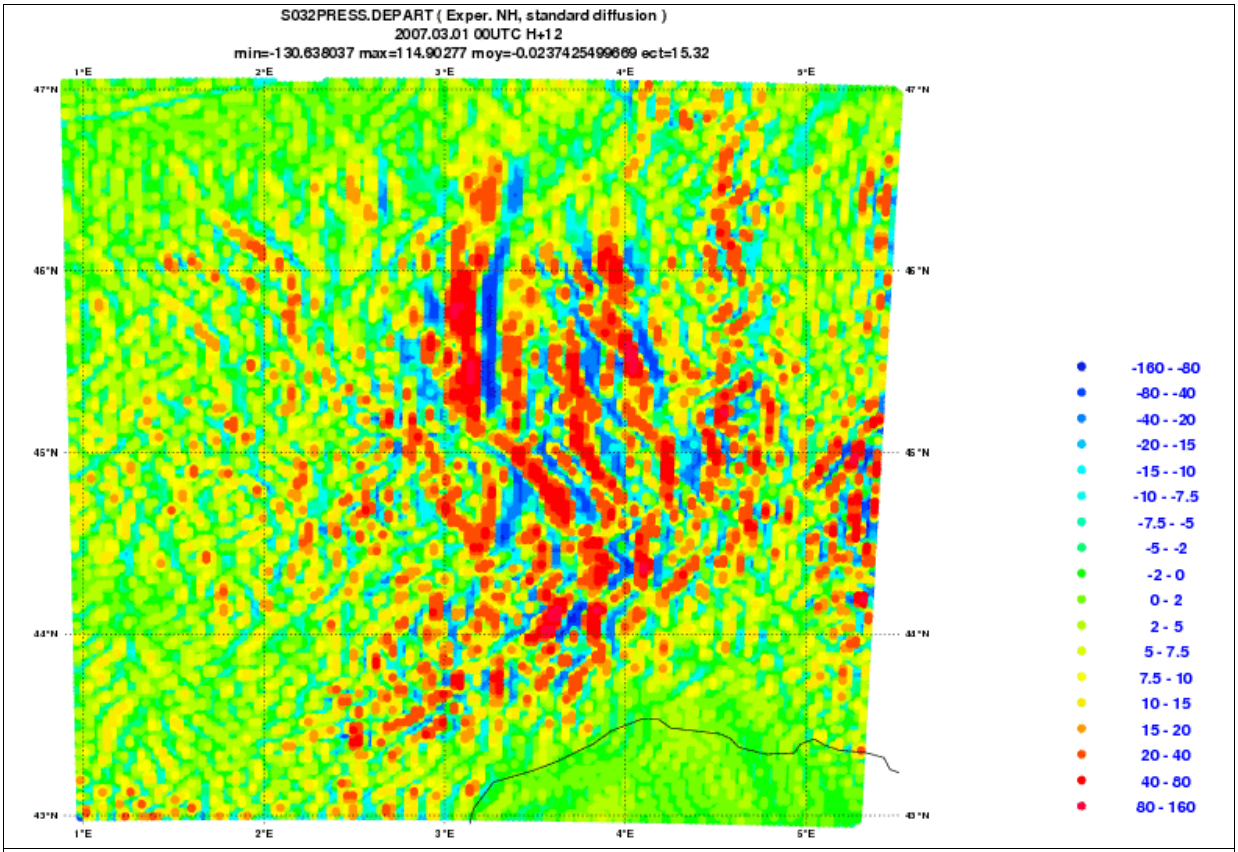

Figure 1.1 *NH _ Std Diff _ PC*: forecast H+12 of the Pressure Departure (Pa) at ML 32 from the 00UTC run of the 1th of March (zoom on the *Massif Central* zone).

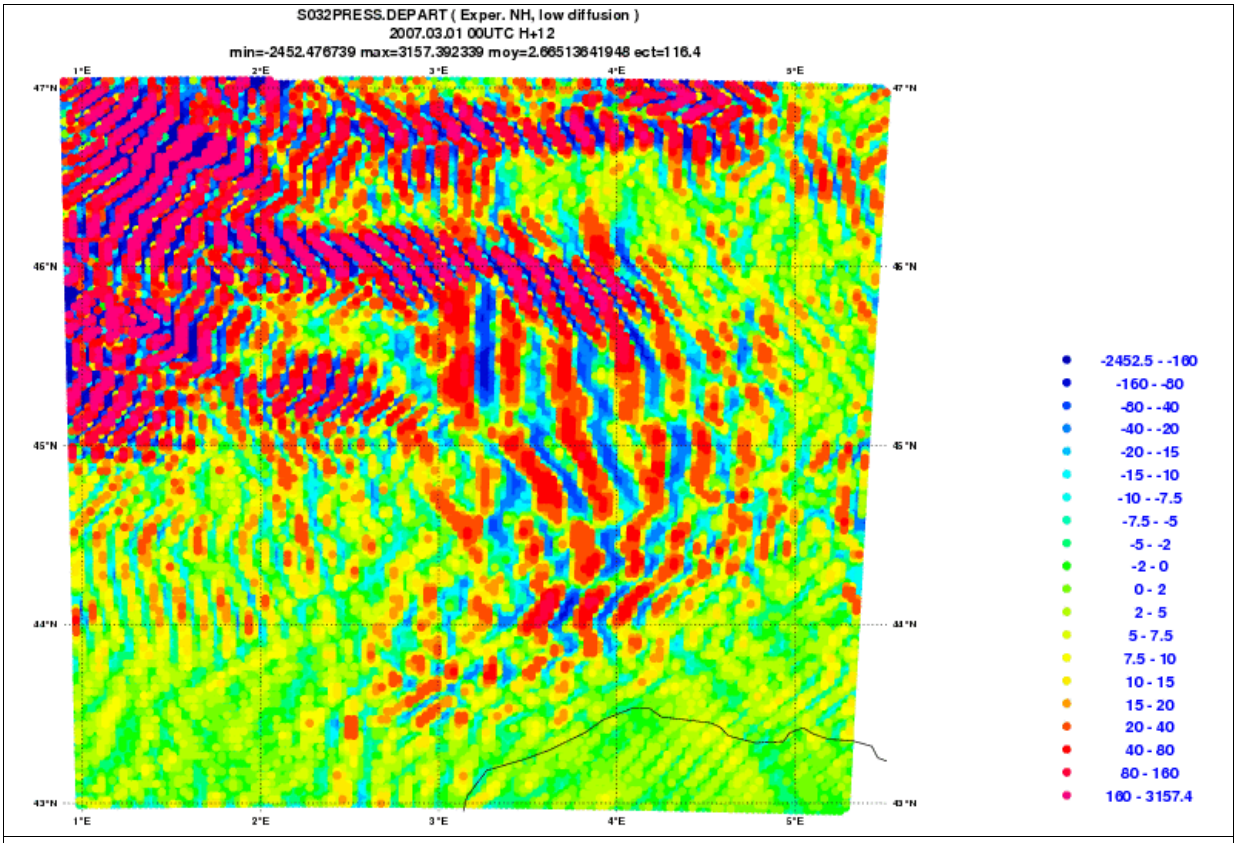

Figure 1.2 *NH _ Low Diff _ PC*: forecast H+12 of the Pressure Departure (Pa) at ML 32 from the 00UTC run of the 1th of March (zoom on the *Massif Central* zone).

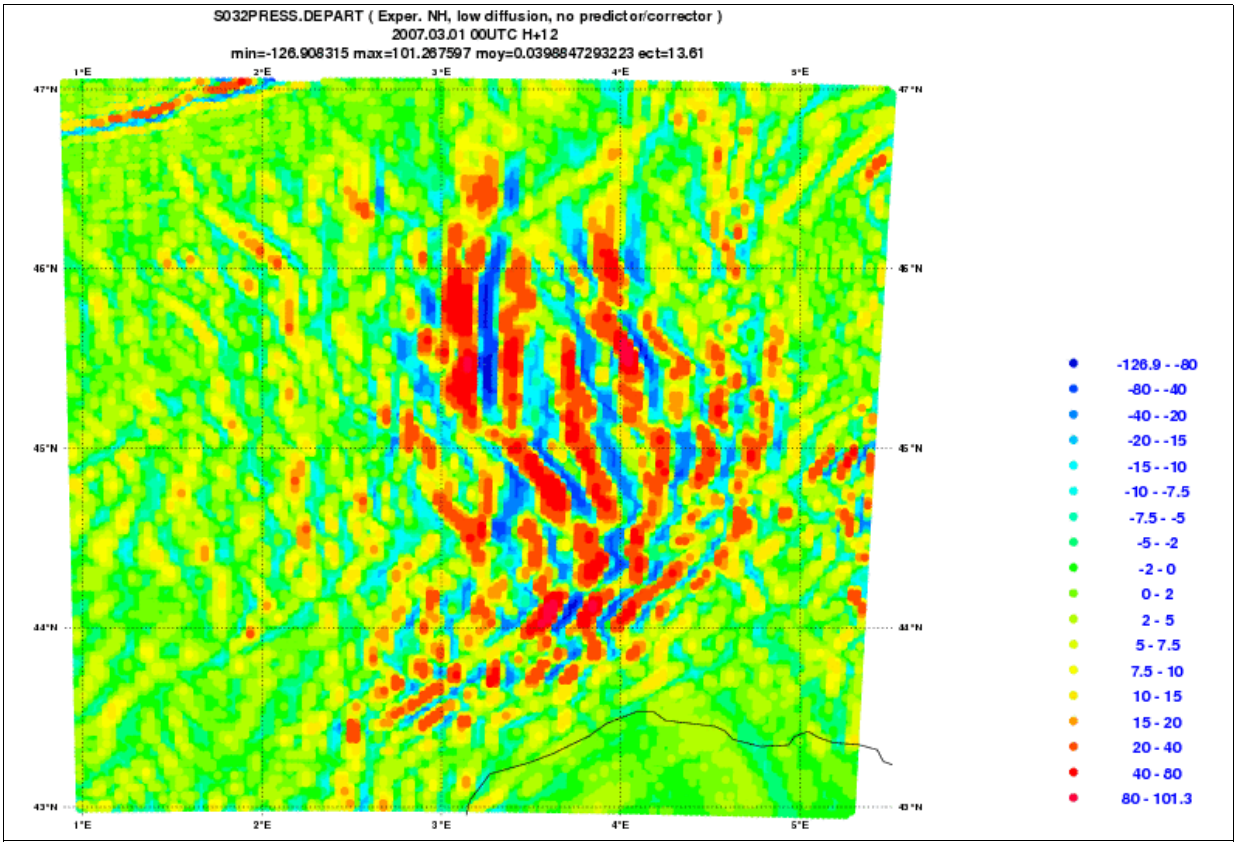

Figure 1.3 *NH _ Low Diff _ No PC*: forecast H+12 of the Pressure Departure (Pa) at ML 32 from 00UTC run of the 1th of March (zoom on the *Massif Central* zone).

(B) Relative Humidity (RH)

On the forecasts of RH at 700hPa (figures 1.4 - 1.6) the orographical waves can be identified by the longitudinal areas in the region of the *Massif Central* where the values of this field decreases below 90%, sometimes to values between 35% and 65%. The fields forecasted by the experiment *Std Diff _ PC* and the experiment *Low Diff _ No PC* are very similar. The field forecasted by the experimented *Low Diff _ PC* shows again a strange behaviour on the NW-N Part of the domain.

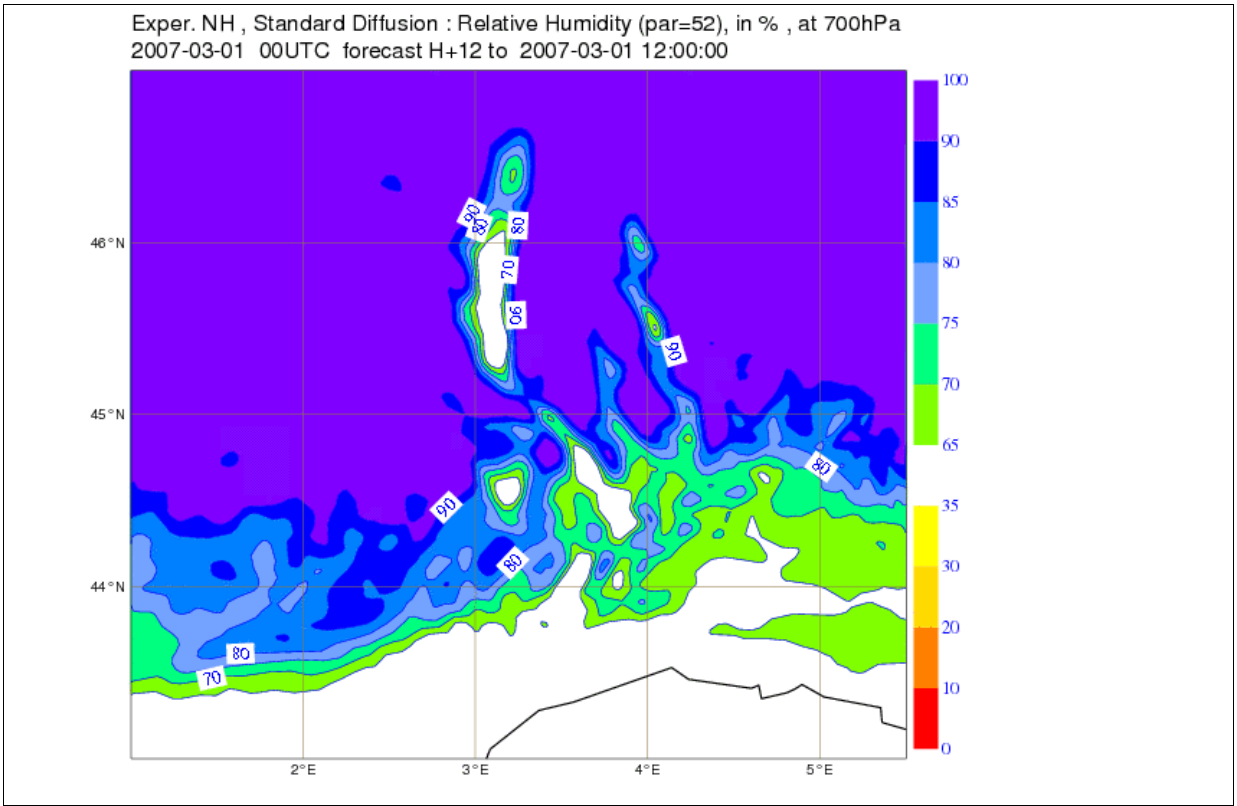

Figure 1.4 *NH _ Std Diff _ PC*: forecast H+12 of RH (%) from 00UTC run of the 1th of March (zoom on the *Massif Central* zone; cylindrical projection).

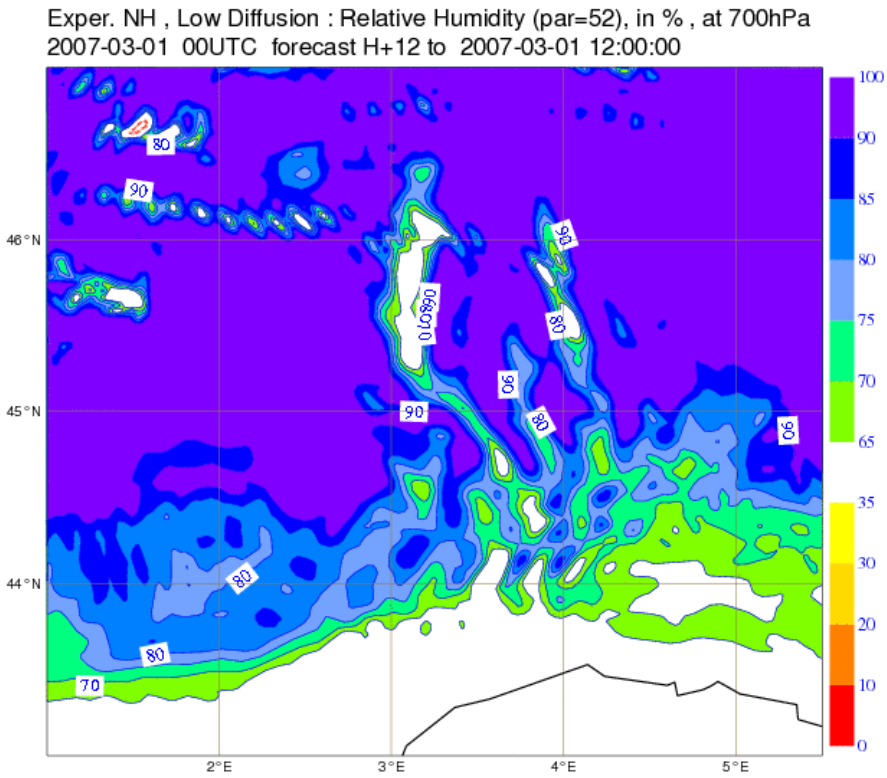

Figure 1.5 *NH _ Low Diff _ PC*: forecast H+12 of RH (%) from 00UTC run of the 1th of March (zoom on the *Massif Central* zone; cylindrical projection).

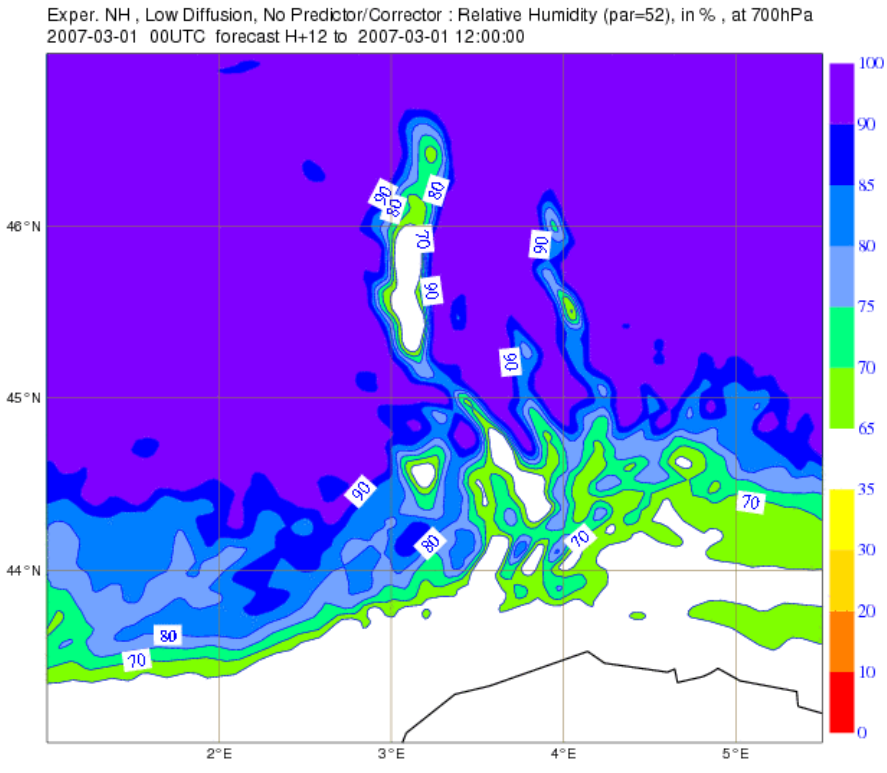

Figure 1.6. *NH _ Low Diff _ No PC*: forecast H+12 of RH (%) from 00UTC run of the 1th of March (zoom on the *Massif Central* zone; cylindrical projection).

(C) Vertical cross-sections of the Temperature (T) and the Cloud Water (CW)

Vertical cross-sections of T and CW between the points 45.8°N 2.5°E and 45.8°N 4.5°E located on the region of the *Massif Central* are presented below.

By the analysis of the cross-sections of T derived from the experiments *Std Diff _ PC* and *Low Diff _ No PC* (figures 1.7 and 1.9), it seems that the waves on the lower layers are also orographical. In agreement with the problem on the experiment *NH _ Low Diff _PC*, the field derived from this experiment is very unstable.

The cross-sections of CW (figures 1.10 – 1.12) present broken areas in the low levels that may be associated also with the orographical waves.

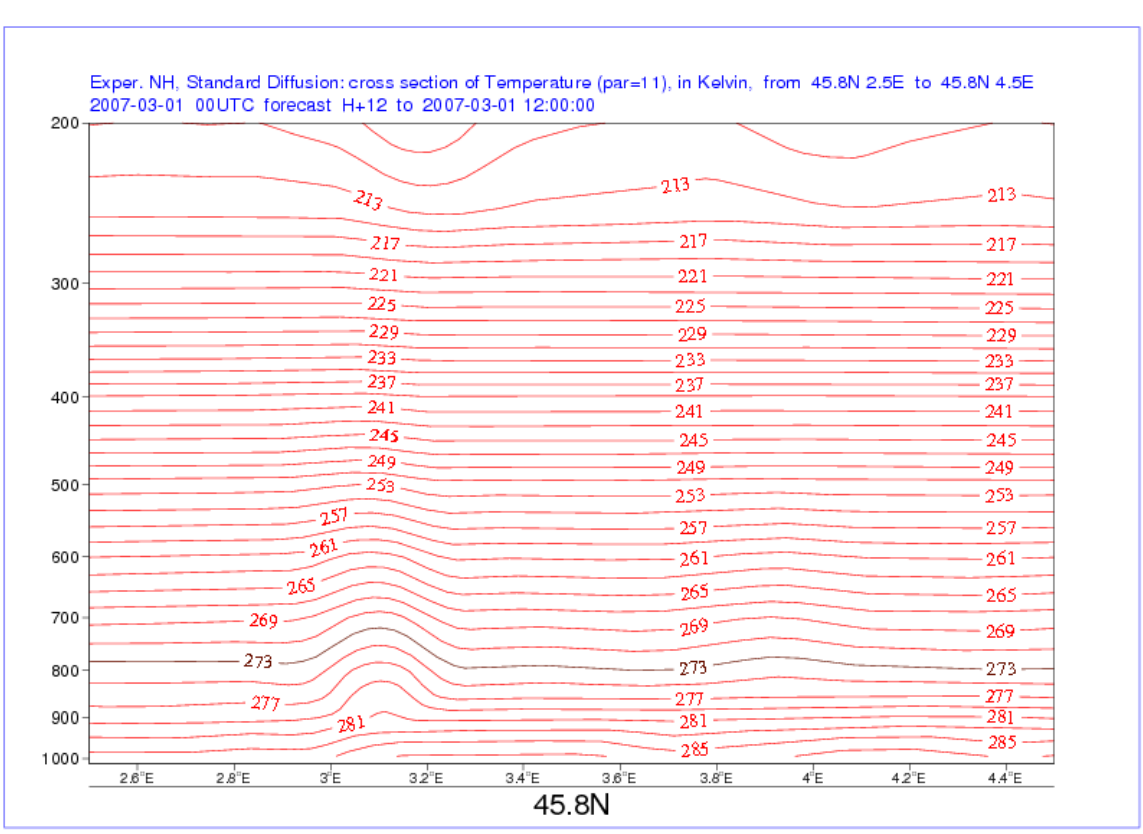

Figure 1.7 *NH _ Std Diff _ PC*: forecast H+12 of the Temperature (K) from 00UTC run of the 1th of March .

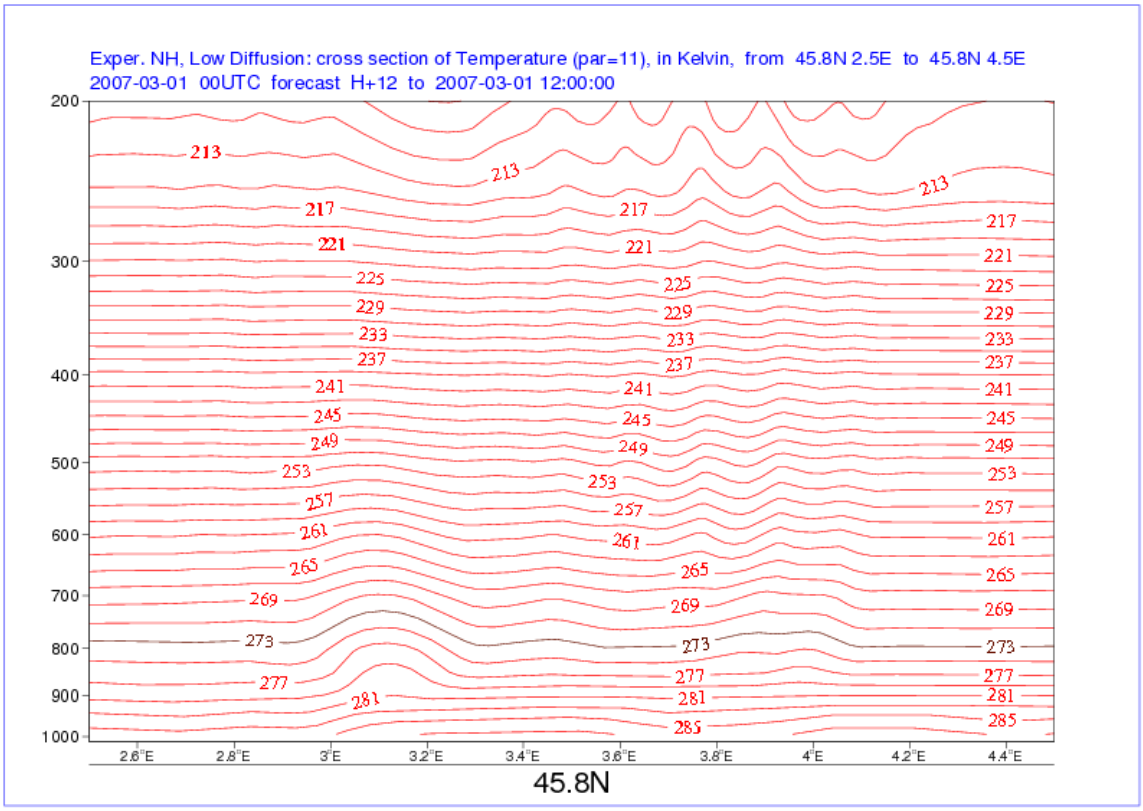

Figure 1.8 *NH _ Low Diff _PC*: forecast H+12 of the Temperature (K) from 00UTC run of the 1th of March .

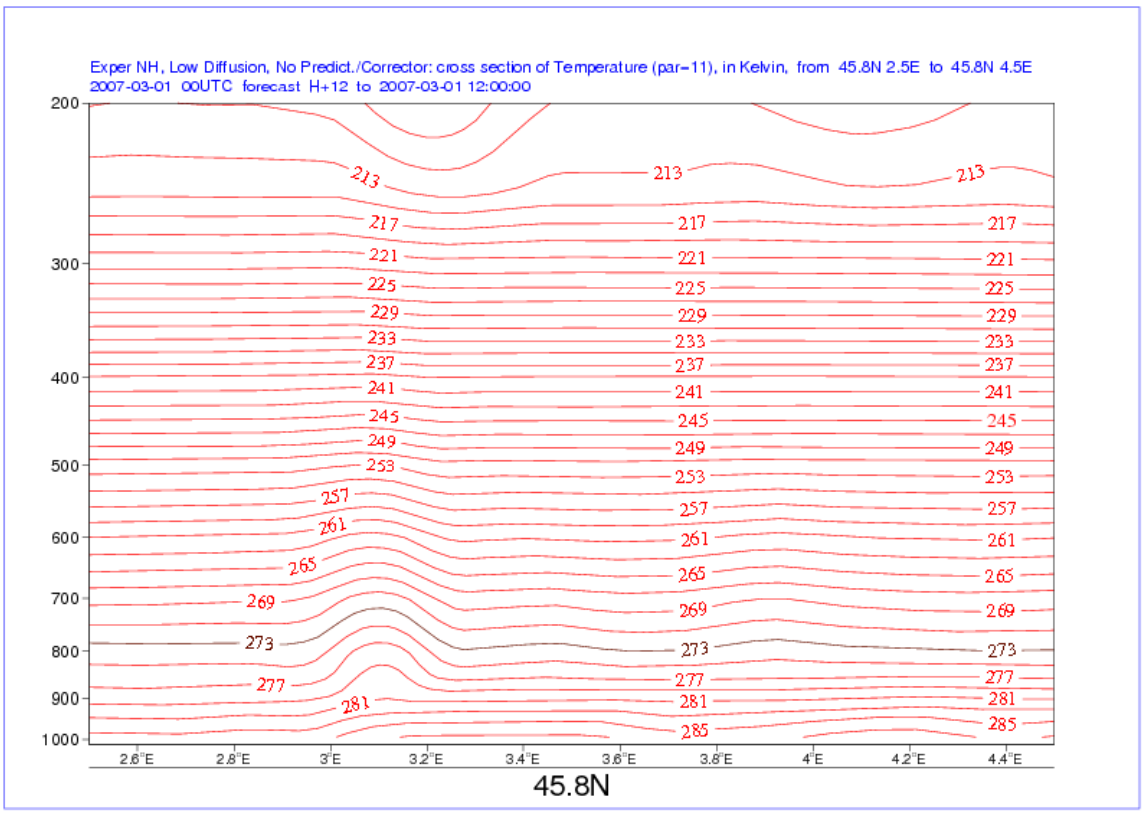

Figure 1.9 *NH _ Low diff _ No PC*: forecast H+12 of the Temperature (K) from 00UTC run of the 1th of March .

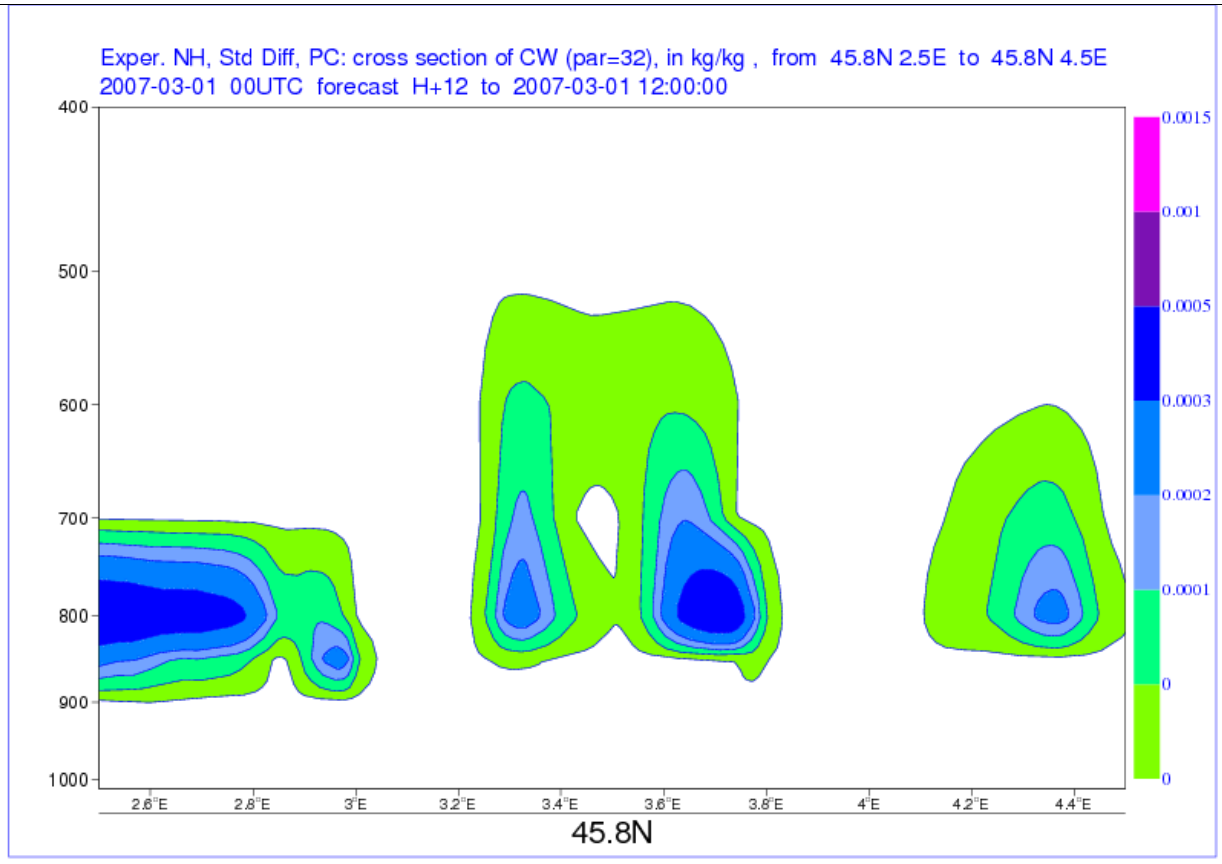

Figure 1.10 ***NH _ Std Diff _PC*****: forecast H+12 of the Cloud Water (Kg Kg^{-1}) from 00UTC run of the 1th of March .**

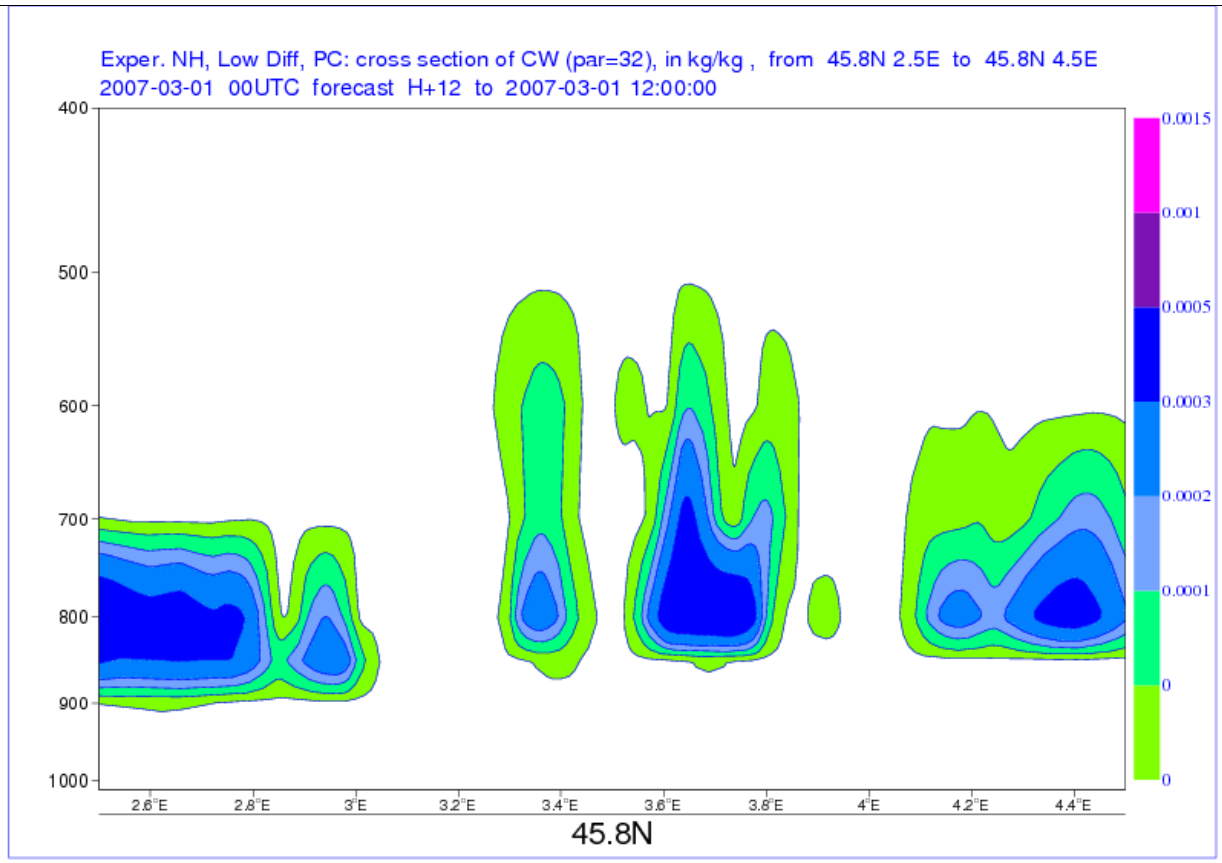

Figure 1.11 ***NH _ Low Diff _ PC*****: forecast H+12 of the Cloud Water (Kg Kg^{-1}) from 00UTC run of the 1th of March .**

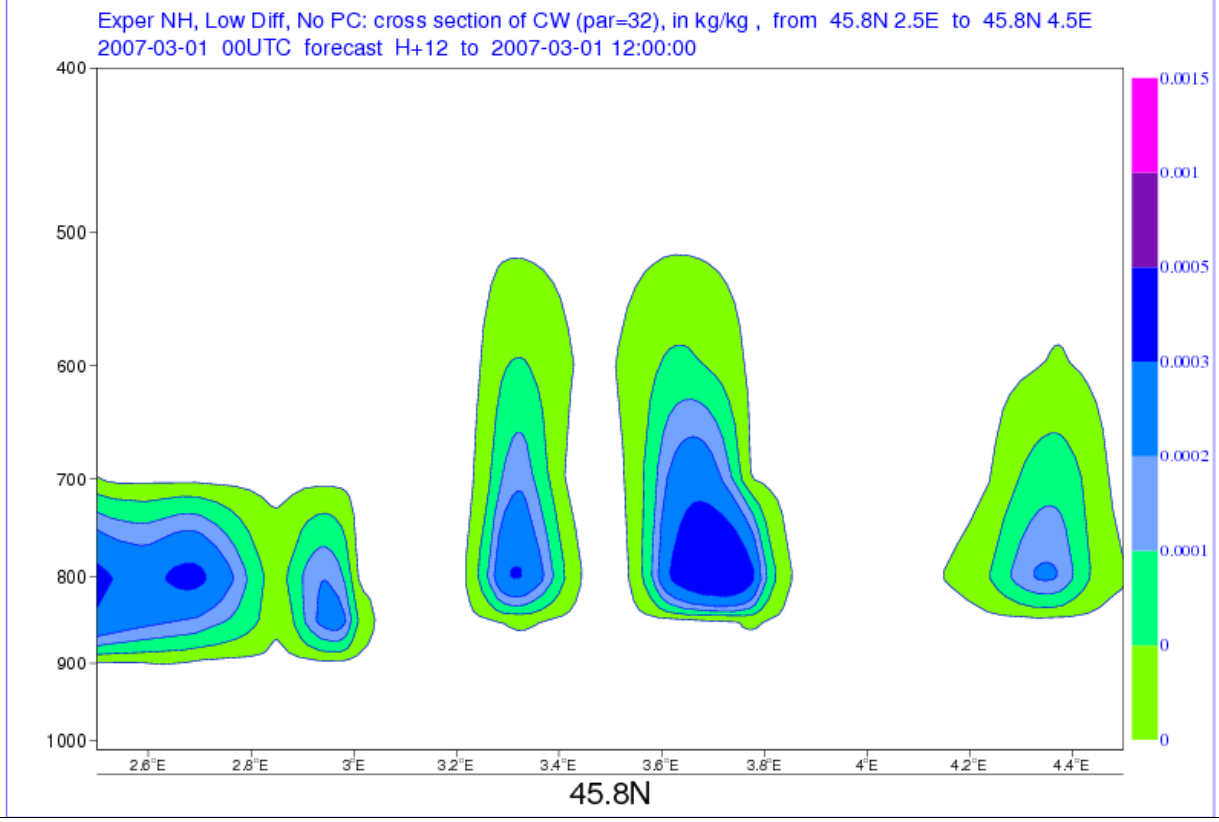

Figure 1.12 ***NH _ Low Diff _ No PC*****: forecast H+12 of the Cloud Water (Kg Kg^{-1}) from 00UTC run of the 1th of March .**

1.2 Comparison between the forecasts of the *NH* experiments and the forecasts of the *H* experiments

Using a similar analysis for the fields forecasted by the *H* experiments, it can be concluded that the orographical waves are also detected on the hydrostatic mode of the model.

(A) Vertical Velocity

By the comparison of the vertical velocity at 700hPa (figures 1.13 – 1.16) on the centre of the domain (*Massif Central*), it can be verified that:

- The values of the field are strong on both *NH* and *H* experiments.

- As would be expected, the magnitude of the fields produced by the *NH* experiments is higher than the magnitude of the fields produced by the *H* experiments.

- For each dynamical mode, there are no significant differences between the field produced by the experiment *Std Diff* and the field produced by the experiment *Low Diff*.

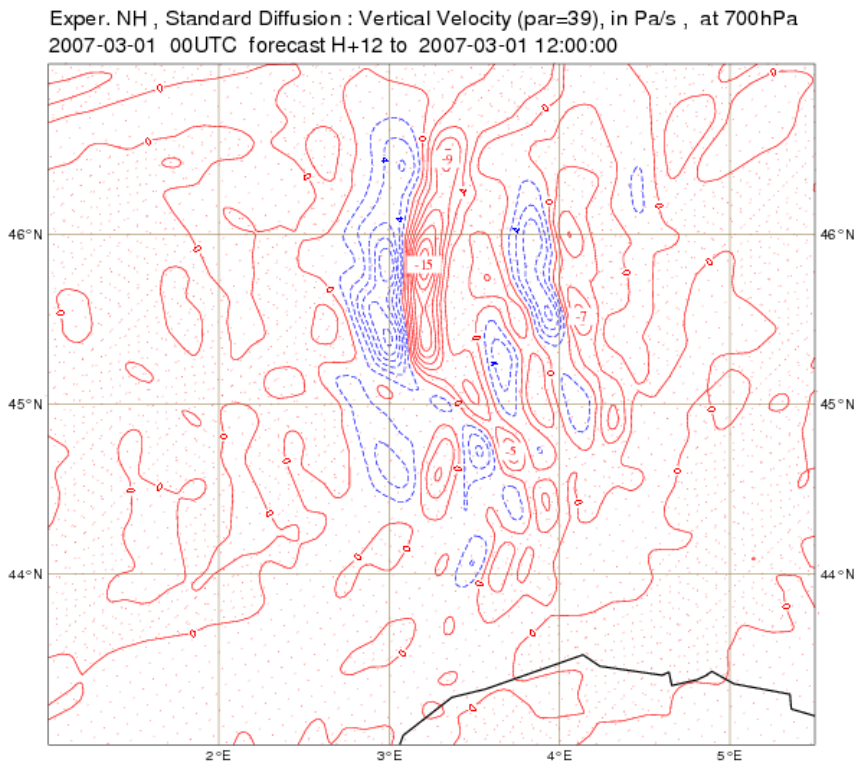

Figure 1.13 *NH _ Std Diff _ PC*: forecast H+12 of the Vertical Velocity (Pa s^{-1}) at 700hPa from 00UTC run of the 1th of March (zoom on the *Massif Central* zone; cylindrical Projection).

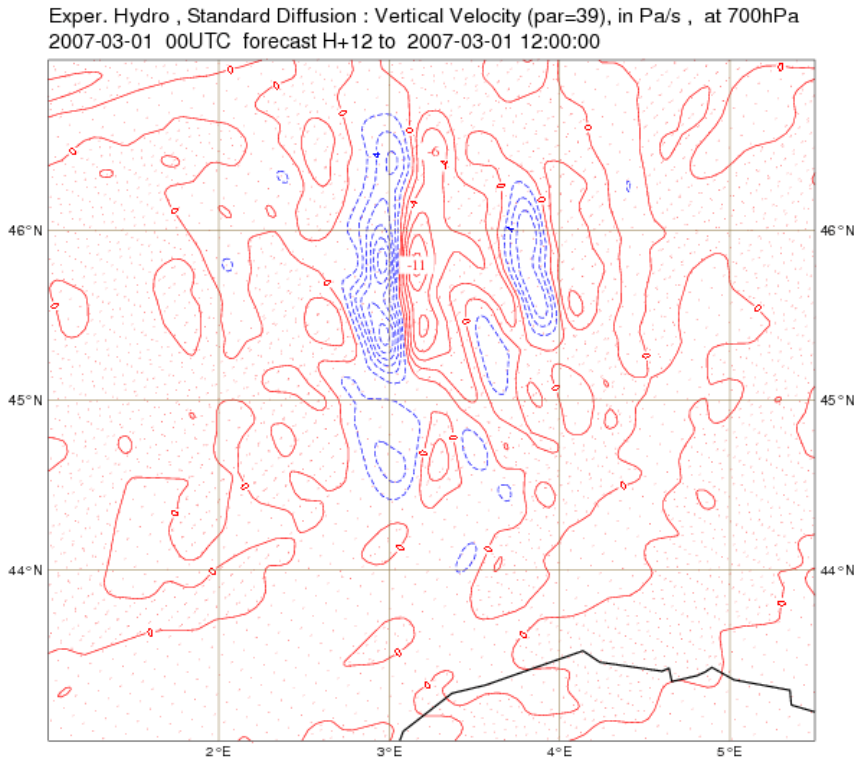

Figure 1.14 *H _ Std Diff _ PC*: forecast H+12 of the Vertical Velocity (Pa s^{-1}) at 700hPa from 00UTC run of the 1th of March (zoom on the *Massif Central* zone; cylindrical Projection).

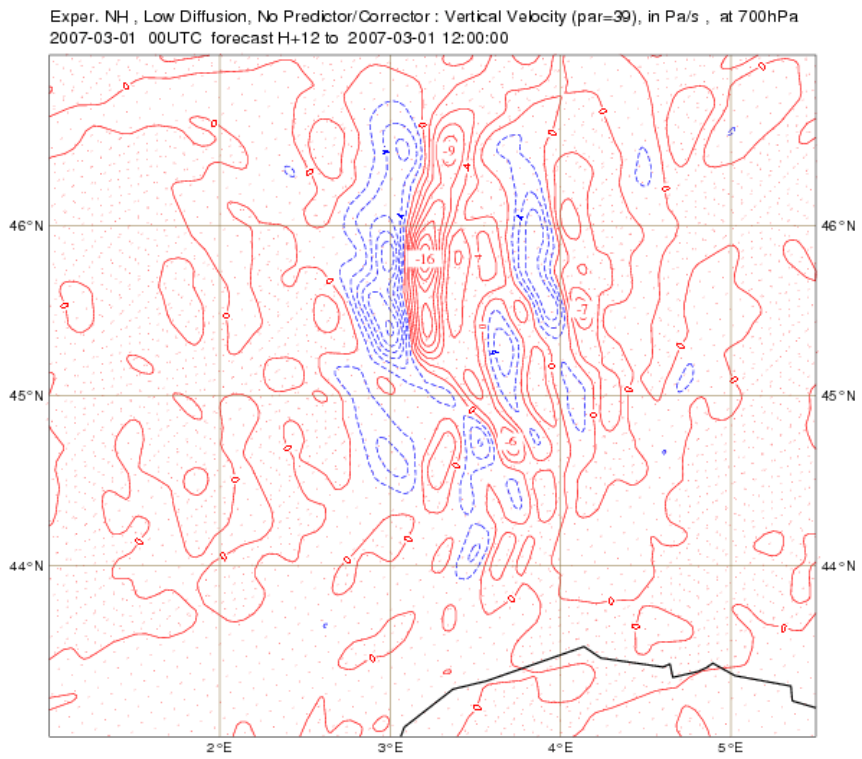

Figure 1.15 *NH _ Low Diff _ No PC*: forecast H+12 of the Vertical Velocity (Pa s^{-1}) at 700hPa from 00UTC run of the 1th of March (zoom on the *Massif Central* zone; cylindrical Projection).

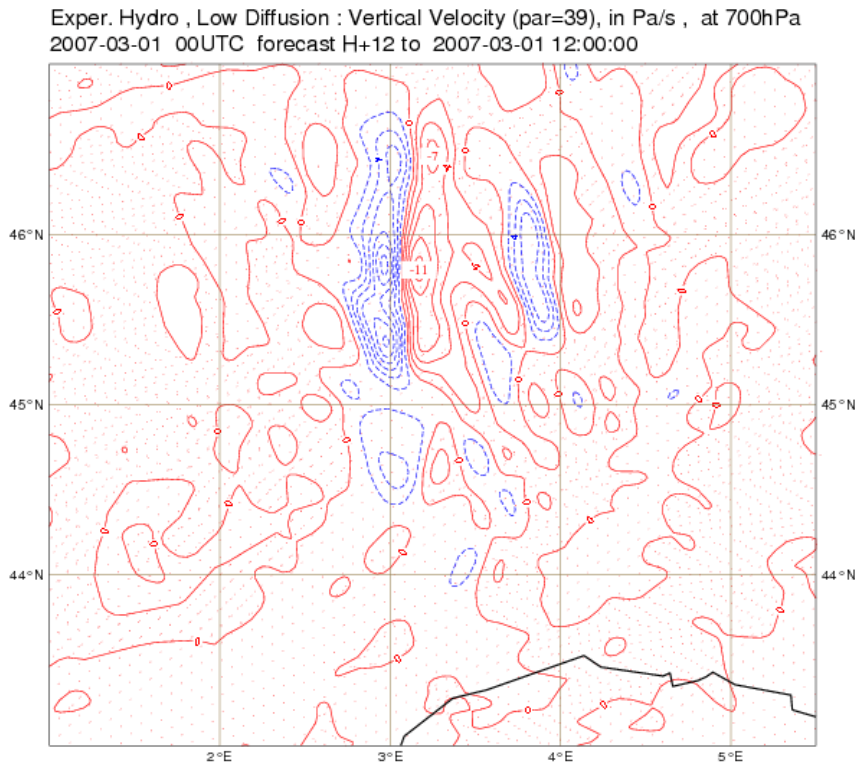

Figure 1.16 *H _ Low Diff _ PC*: forecast H+12 of the Vertical Velocity (Pa s^{-1}) at 700hPa from 00UTC run of the 1th of March (zoom on the *Massif Central* zone; cylindrical Projection).

(B) Low cloud Cover (LCC)

With the analysis of the low clouds on the area of the *Massif Central*, it can be concluded that:

- As for the vertical velocity, there are no significant differences between the field produced by the experiment *Std Diff* and the field produced by the experiment *Low Diff* in each dynamical mode.

- However, there are some differences not well understood between the patterns of the fields produced by the *NH* and those produced by the *H* experiments on this situation.

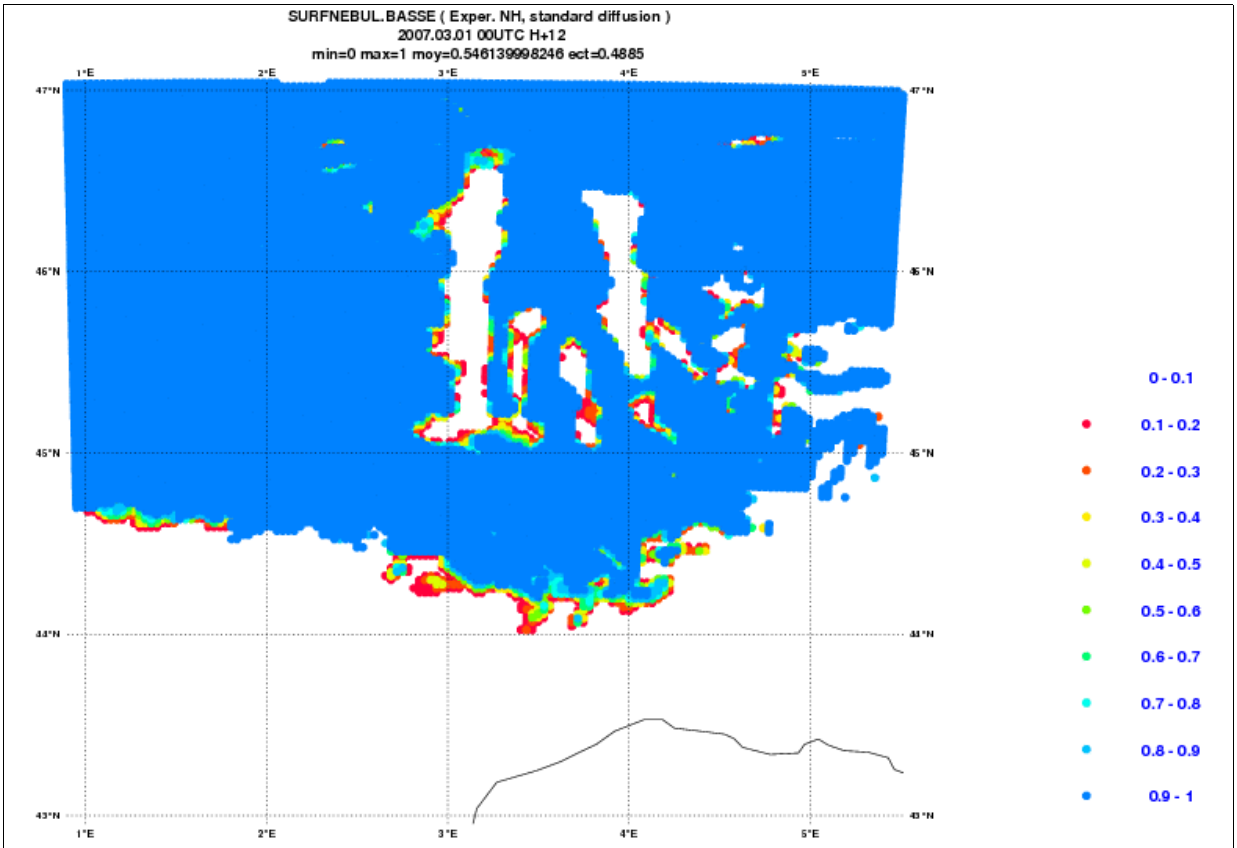

Figure 1.17 *NH _ Std Diff _ PC*: forecast H+12 of LCC (tenth) from the 00UTC run of the 1th of March (zoom on the *Massif Central* zone; cylindrical projection).

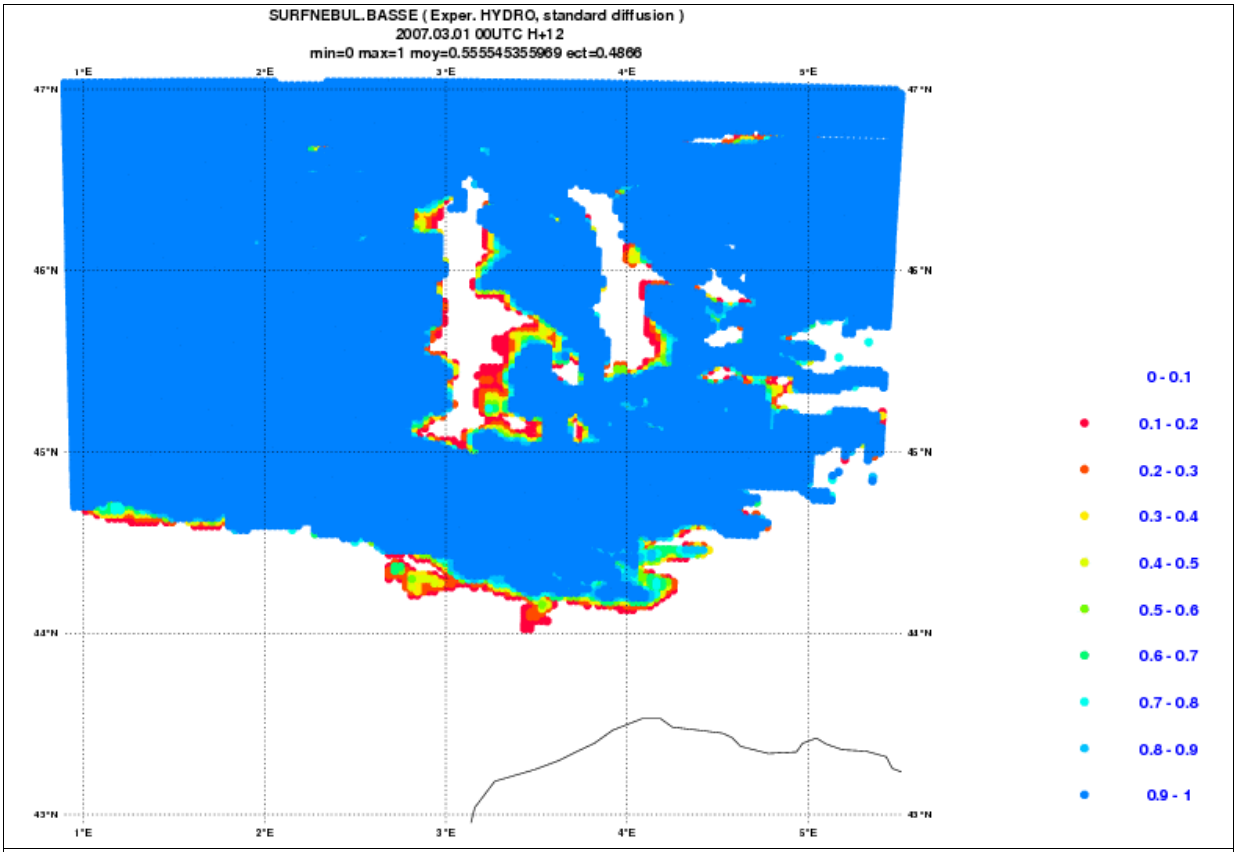

Figure 1.18 *H _ Std Diff _ PC*: forecast H+12 of LCC (tenth) from the 00UTC run of the 1th of March (zoom on the *Massif Central* zone; cylindrical projection).

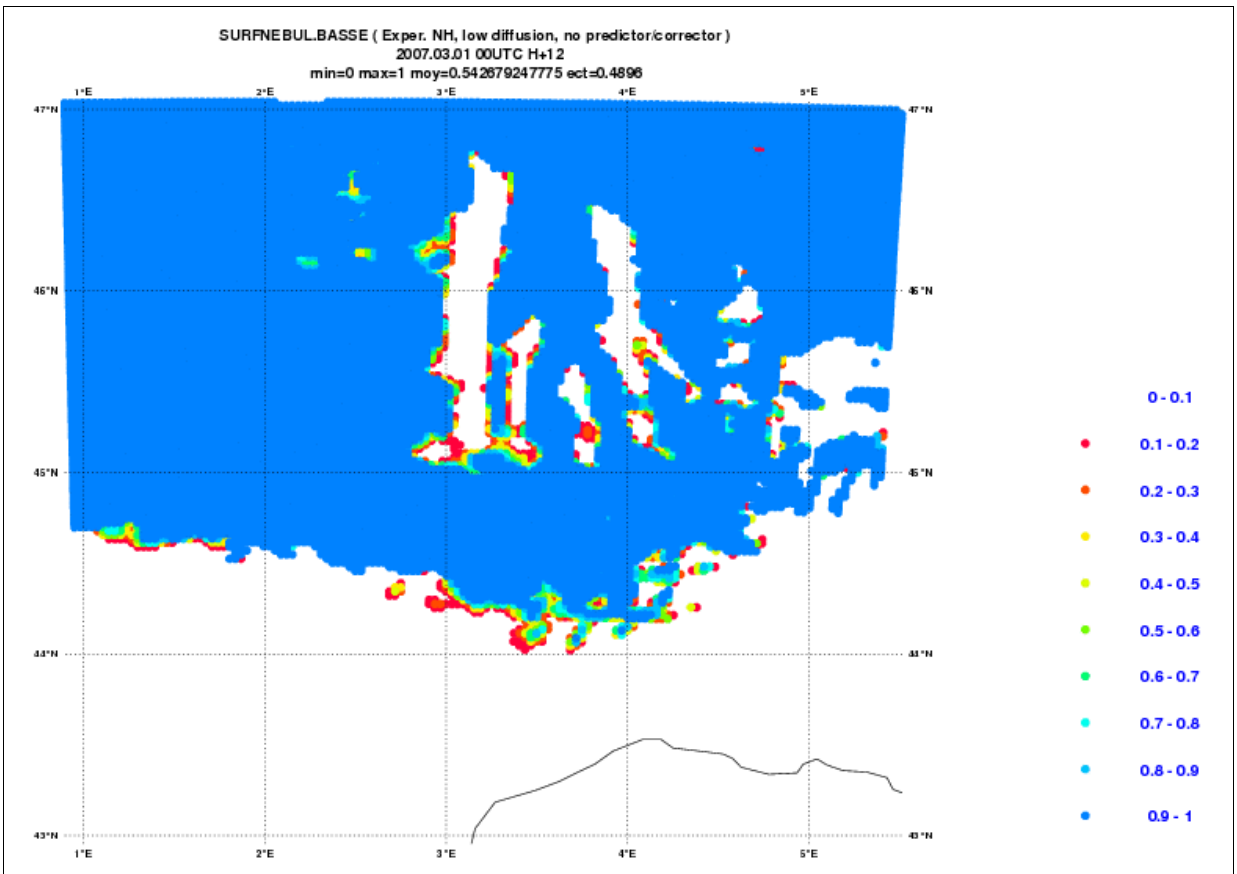

Figure 1.19 *NH _ Low Diff _ No PC*: forecast H+12 of LCC (tenth) from the 00UTC run of the 1th of March (zoom on the *Massif Central* zone; cylindrical projection).

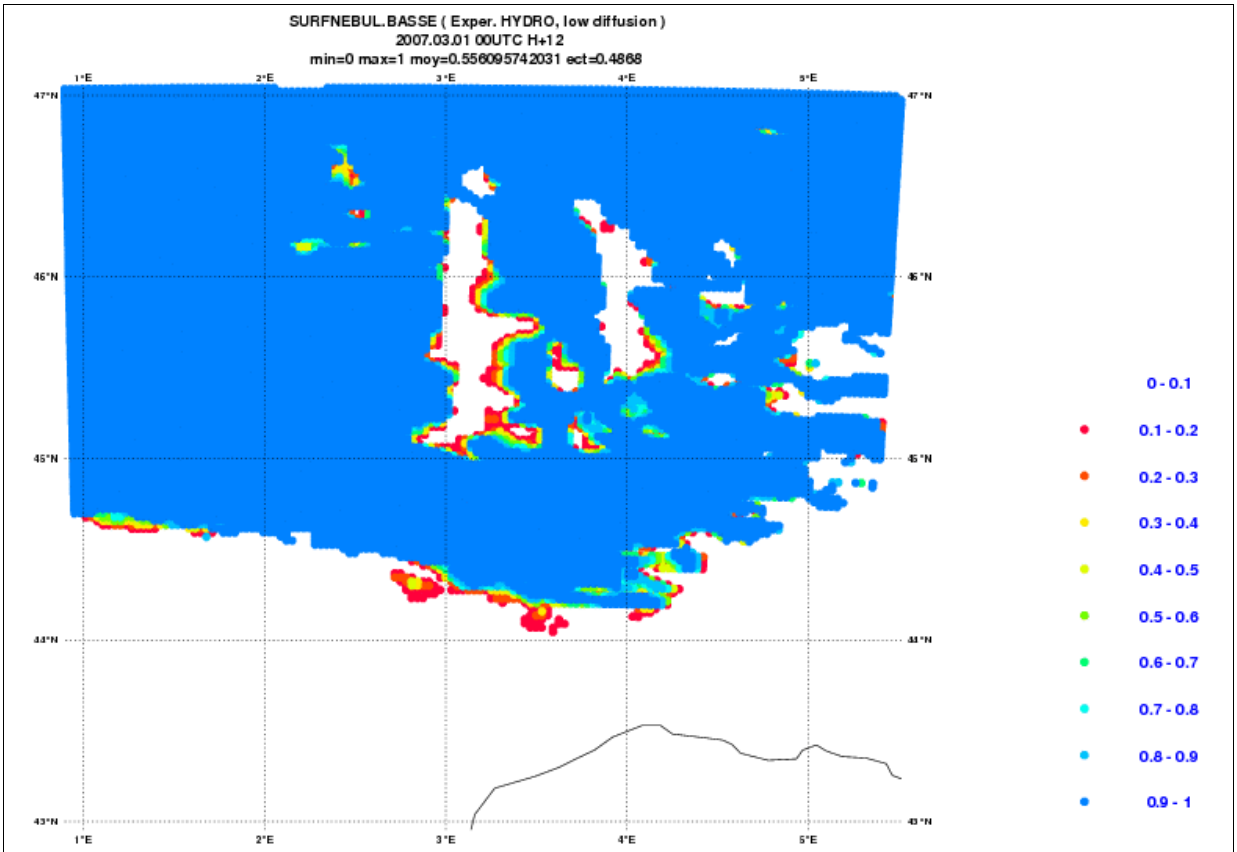

Figure 1.20 *H _ Low Diff _ PC*: forecast H+12 of the LCC (tenth) from the 00UTC run of the 1th of March (zoom on the *Massif Central* zone; cylindrical projection).

1.3 Forecasts for the 13h

(A) *u* and *v*-components of the wind at ML 19

By the comparison of the forecasts of the u and the v-components of the wind (figures 1.21 – 1.32), it can be verified that:

- The components of the wind produced by the experiments *NH _ Std Diff _PC* are very similar to the ones produced by the experiments *NH _ Low Diff _ No PC* (e.g., the ones derived from the experiment of Yann and the ones derived from the experiment with the same cycle as the REF experiment).

- The u and v-components of the wind produced by the *H* experiments are similar to the same components forecasted by the *NH* experiments mentioned before.

- However the components of the wind derived from the experiment *NH _ Low Diff _ PC* show an non-physical behaviour (more clear on the u-component) that can be probably related with strong and oscillating winds at the origin of the model explosion.

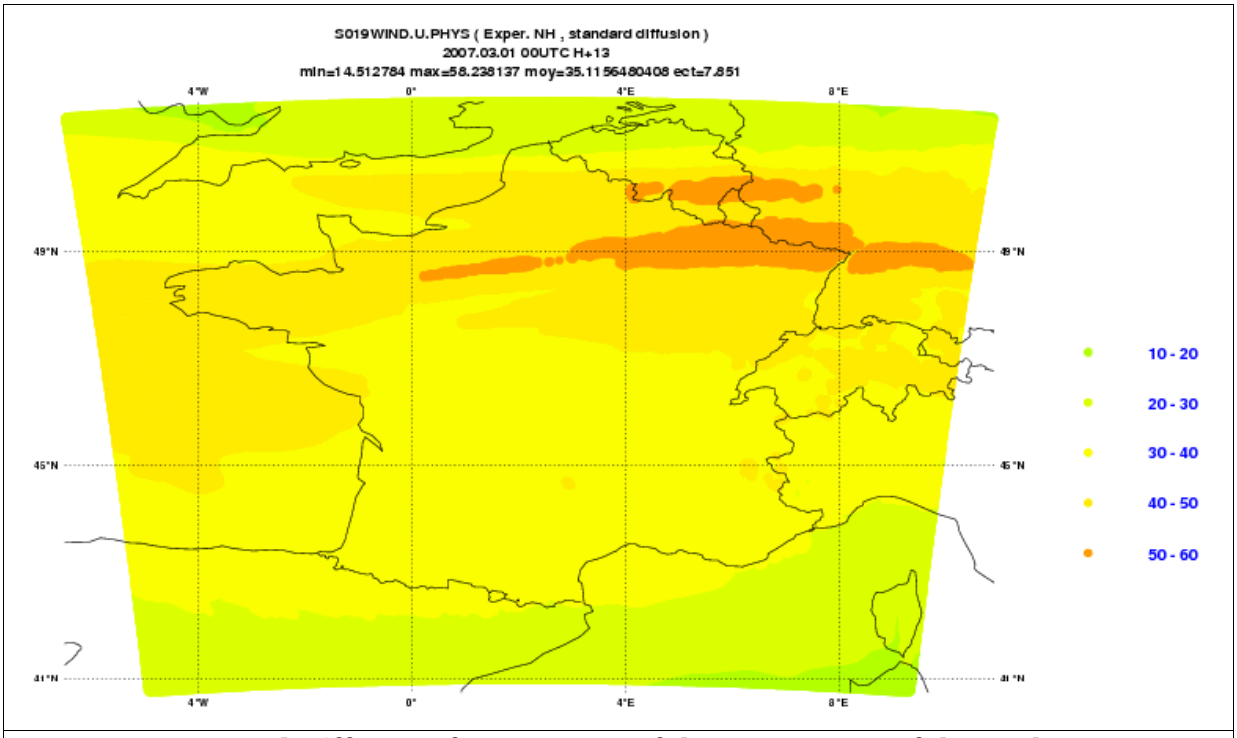

Figure 1.21 ***NH _ Std Diff _ PC*****: forecast H+13 of the u-component of the wind (m s^{-1}) at ML 19 from the 00UTC run of the 1th of March.**

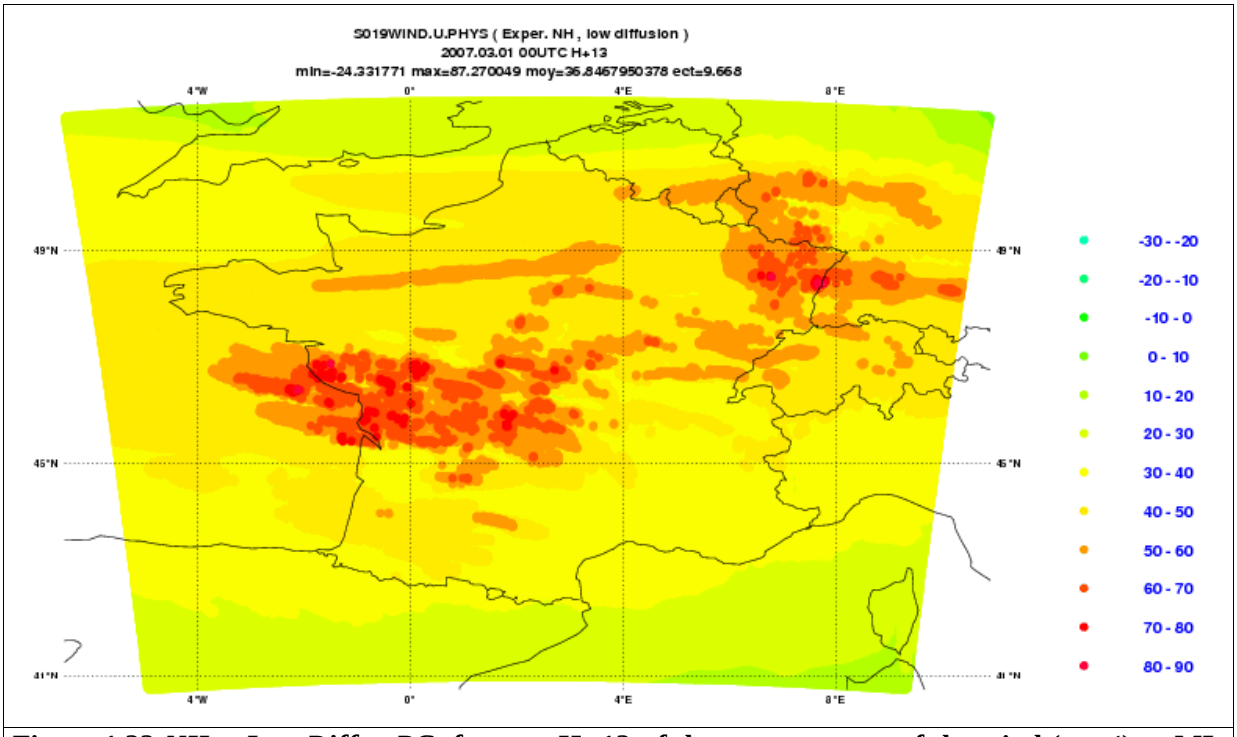

Figure 1.22 ***NH _ Low Diff _ PC*****: forecast H+13 of the u-component of the wind (m s^{-1}) at ML 19 from the 00UTC run of the 1th of March.**

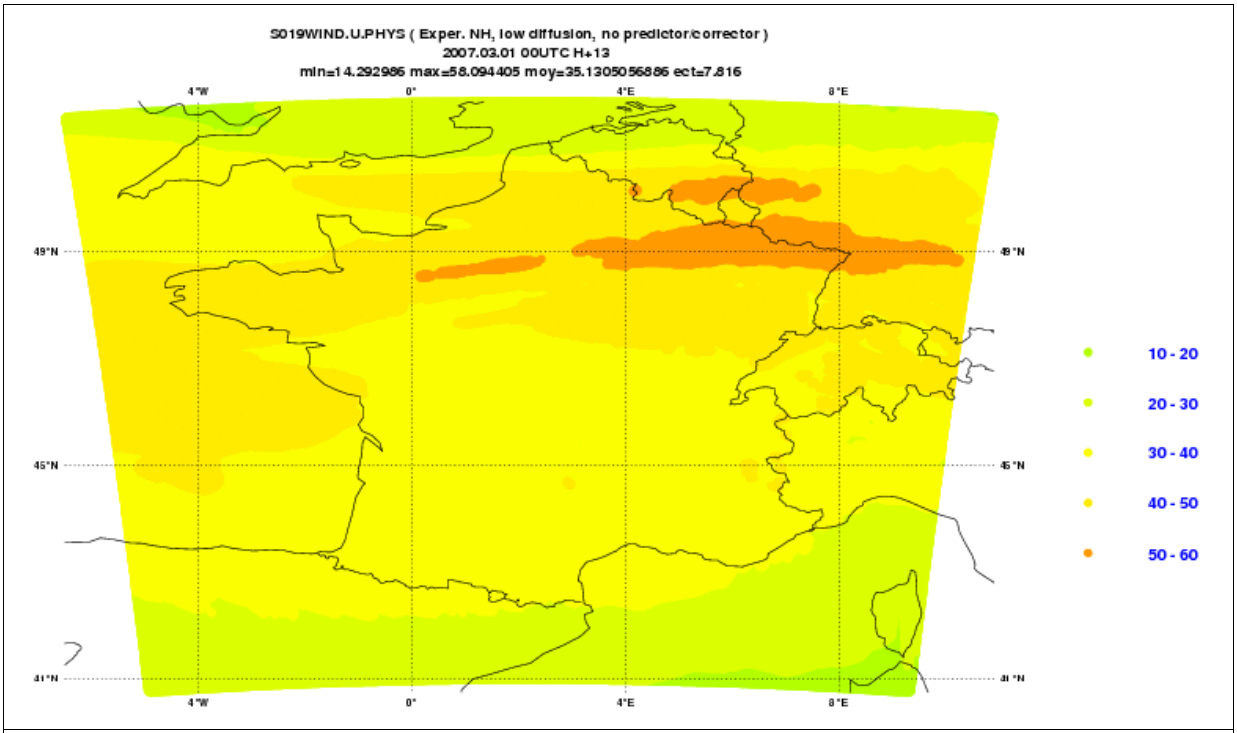

Figure 1.23 *NH _ Low Diff _ No PC* (same cycle as the *REF* experiment): forecast H+13 of the u-component of the wind (m s^{-1}) at ML 19 from the 00UTC run of the 1th of March.

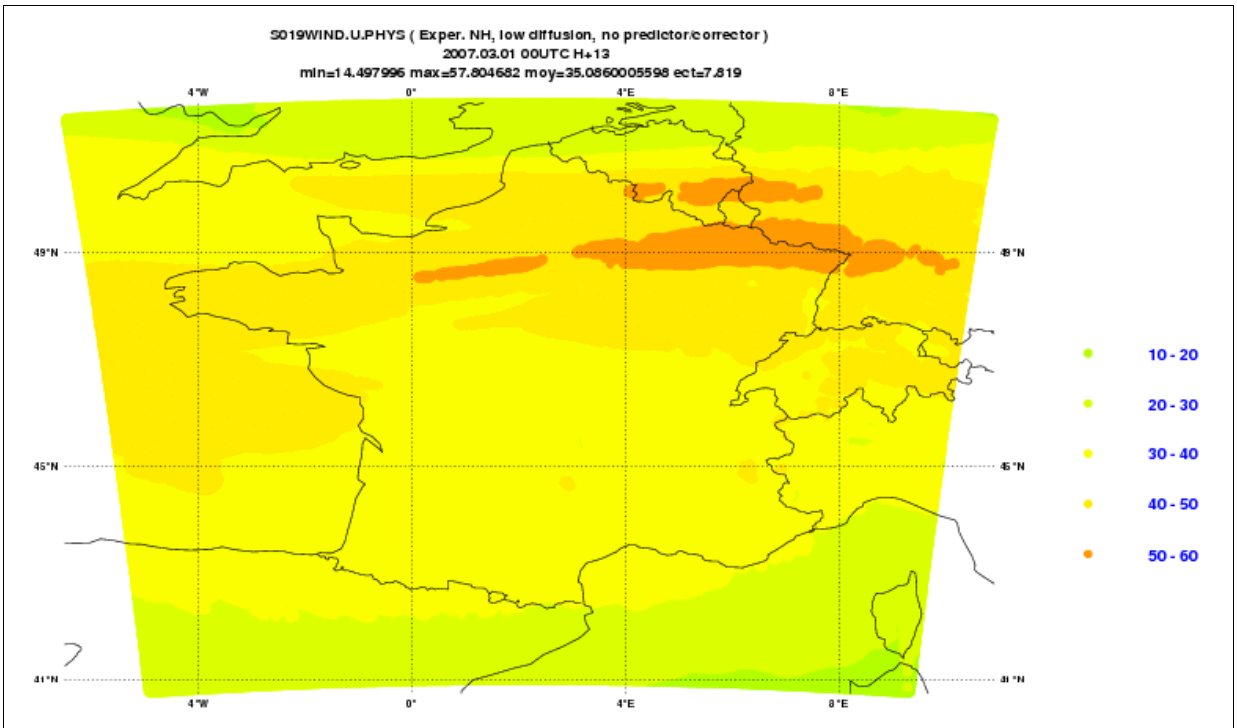

Figure 1.24 *NH _ Low Diff _ No PC* (Yann's experiment): forecast H+13 of the u-component of the wind (m s^{-1}) at ML 19 from the 00UTC run of the 1th of March.

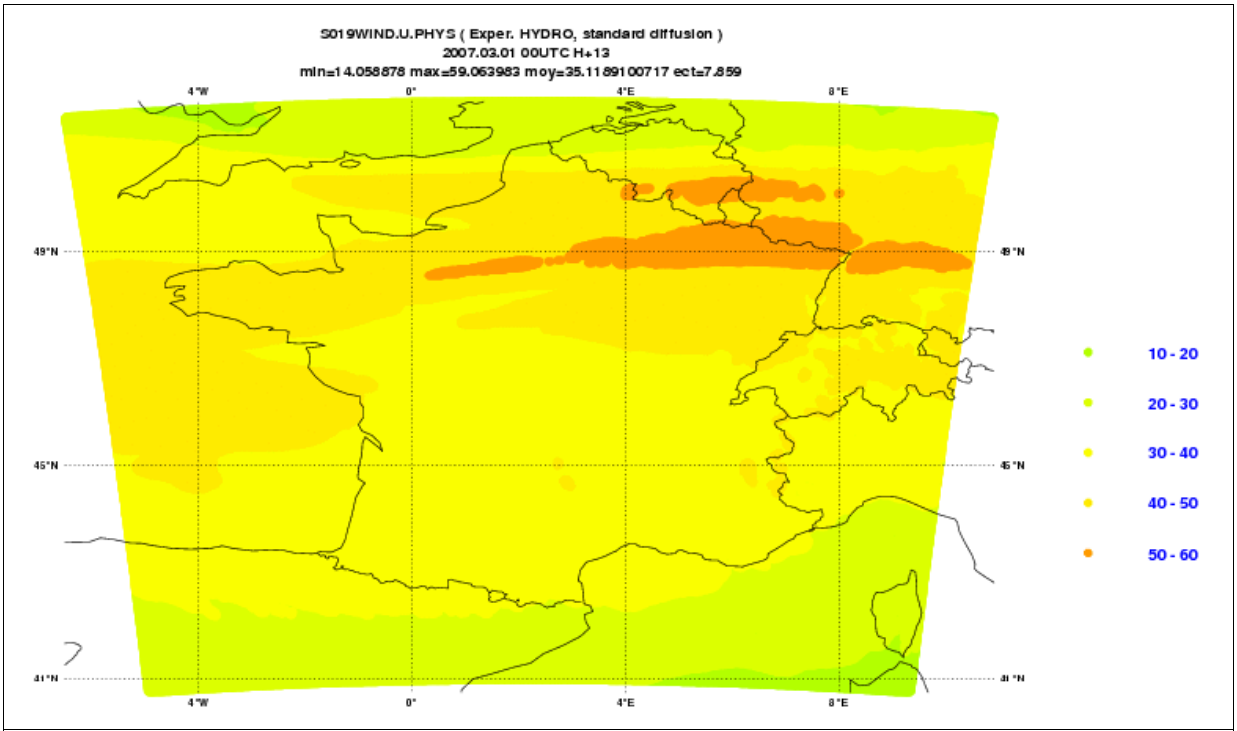

Figure 1.25 *H _ Std Diff _ PC*: forecast H+13 of the u-component of the wind (m s^{-1}) at ML 19 from the 00UTC run of the 1th of March.

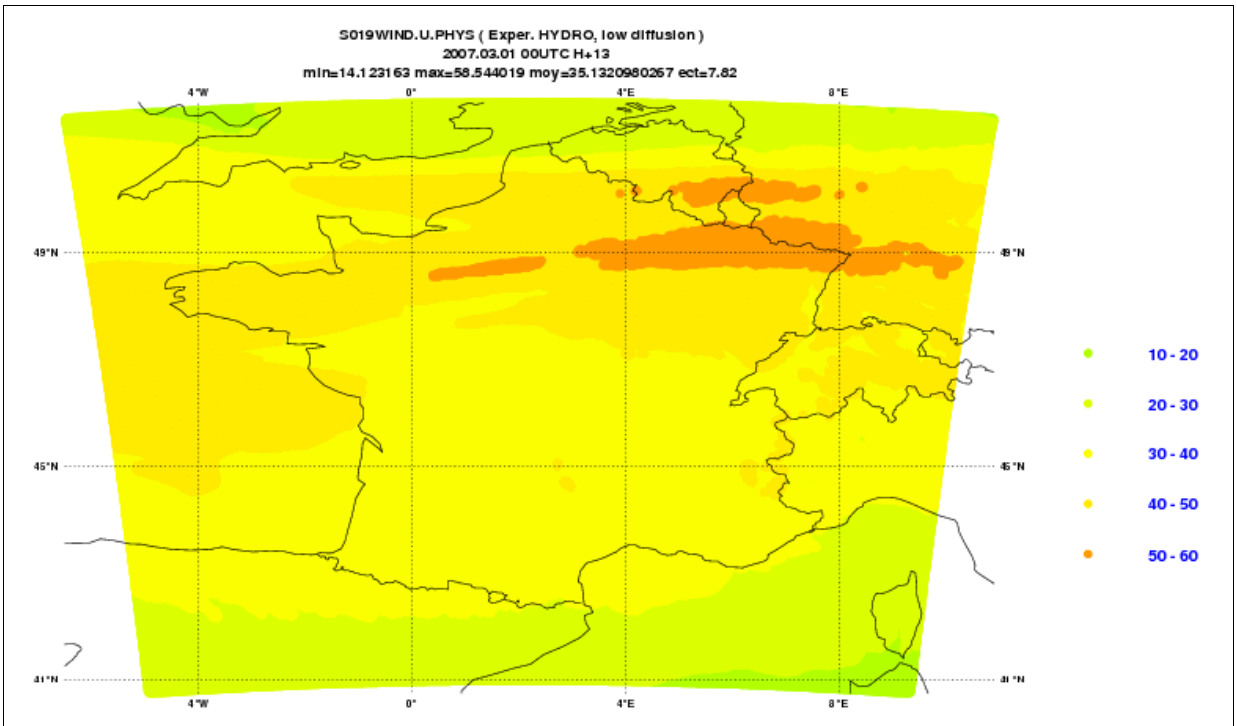

Figure 1.26 *H _ Low Diff _ PC*: forecast H+13 of the u-component of the wind (m s^{-1}) at ML 19 from the 00UTC run of the 1th of March.

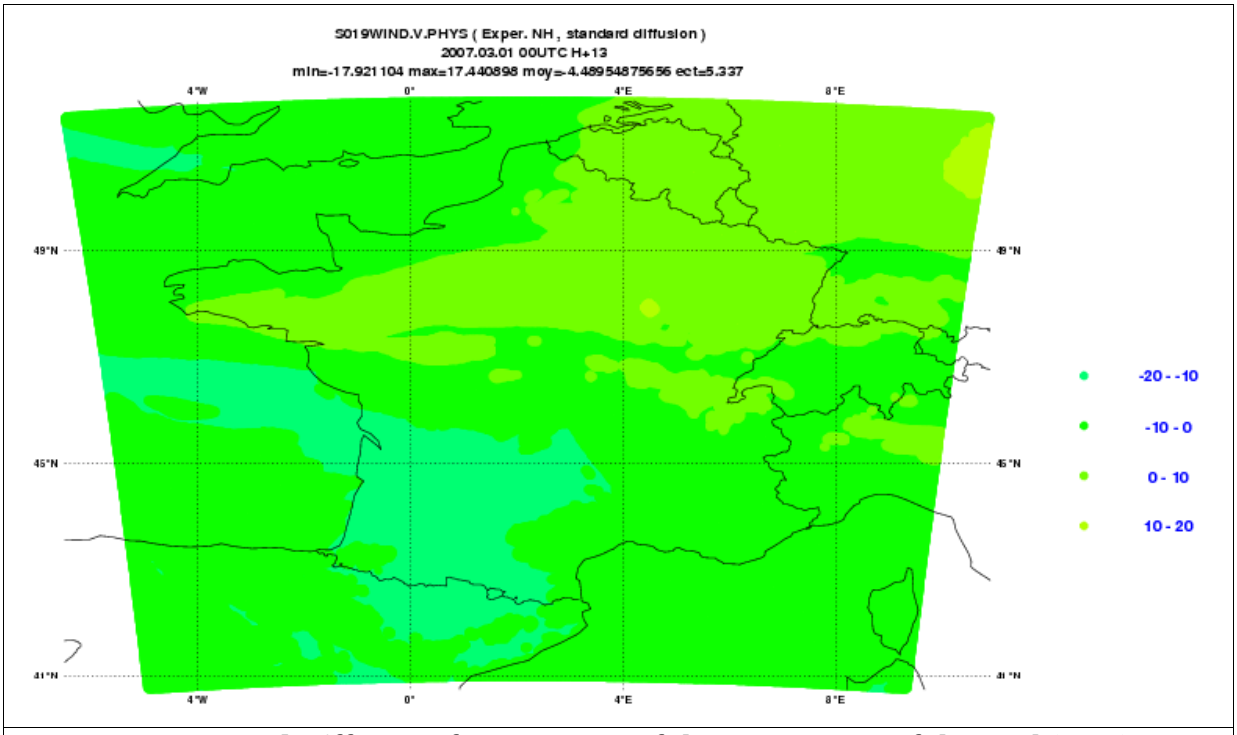

Figure 1.27 *NH _ Std Diff _ PC*: forecast H+13 of the v-component of the wind (m s^{-1}) at ML 19 from the 00UTC run of the 1th of March.

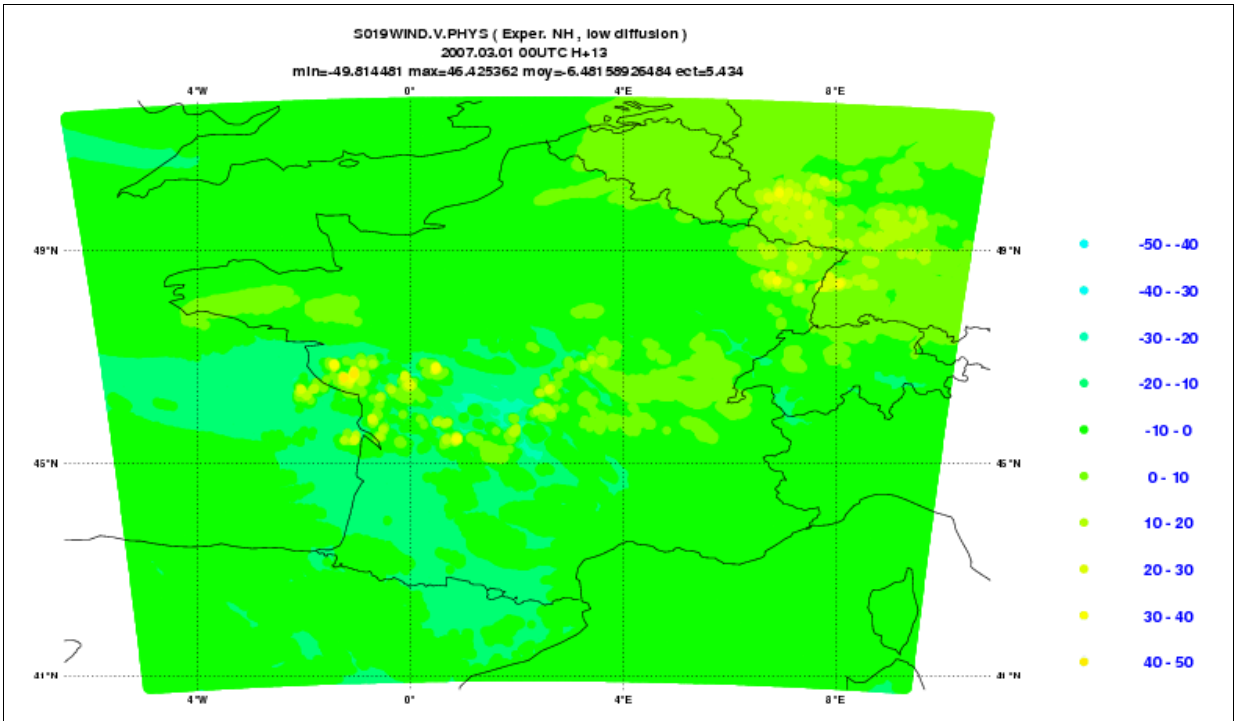

Figure 1.28 *NH _ Low Diff _ PC*: forecast H+13 of the v-component of the wind (m s^{-1}) at ML 19 from the 00UTC run of the 1th of March.

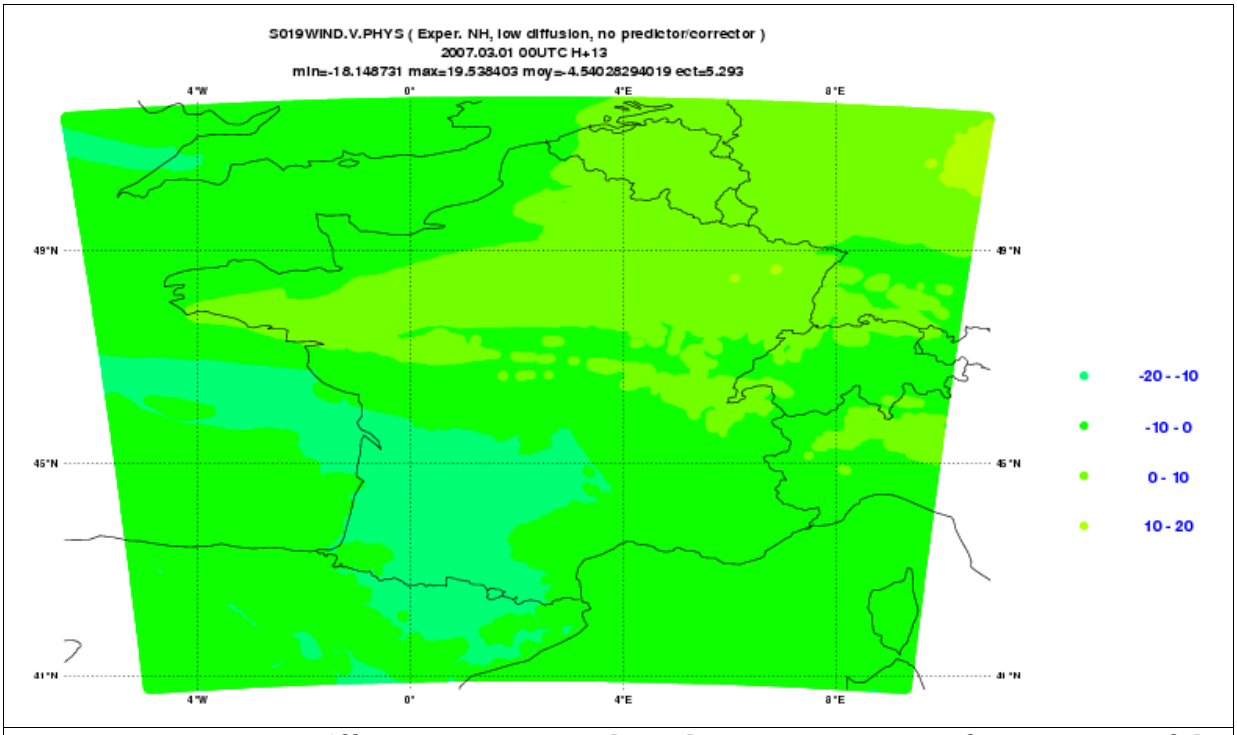

Figure 1.29 *NH _ Low Diff _ No PC* (same cycle as the REF experiment): forecast H+13 of the v-component of the wind (m s^{-1}) at ML 19 from the 00UTC run of the 1th of March.

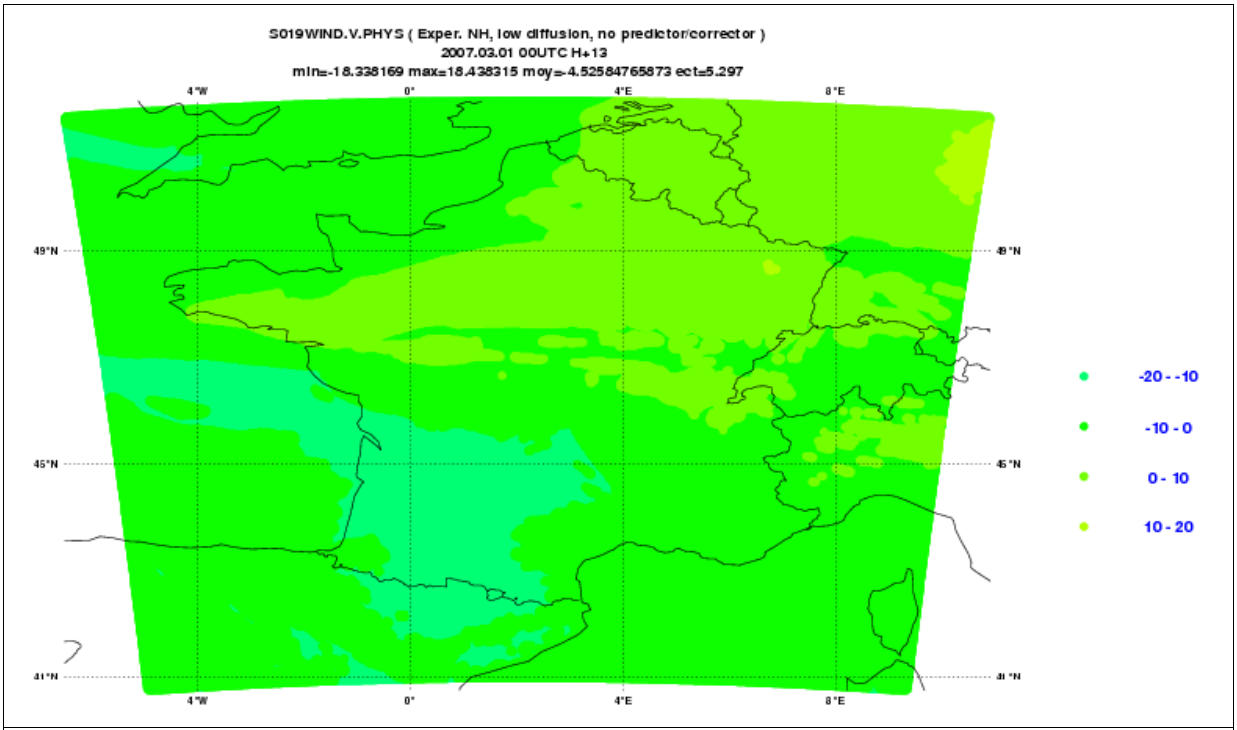

Figure 1.30 *NH _ Low Diff _ No PC* (Yann's experiment): forecast H+13 of the v-component of the wind (m s^{-1}) at ML 19 from the 00UTC run of the 1th of March.

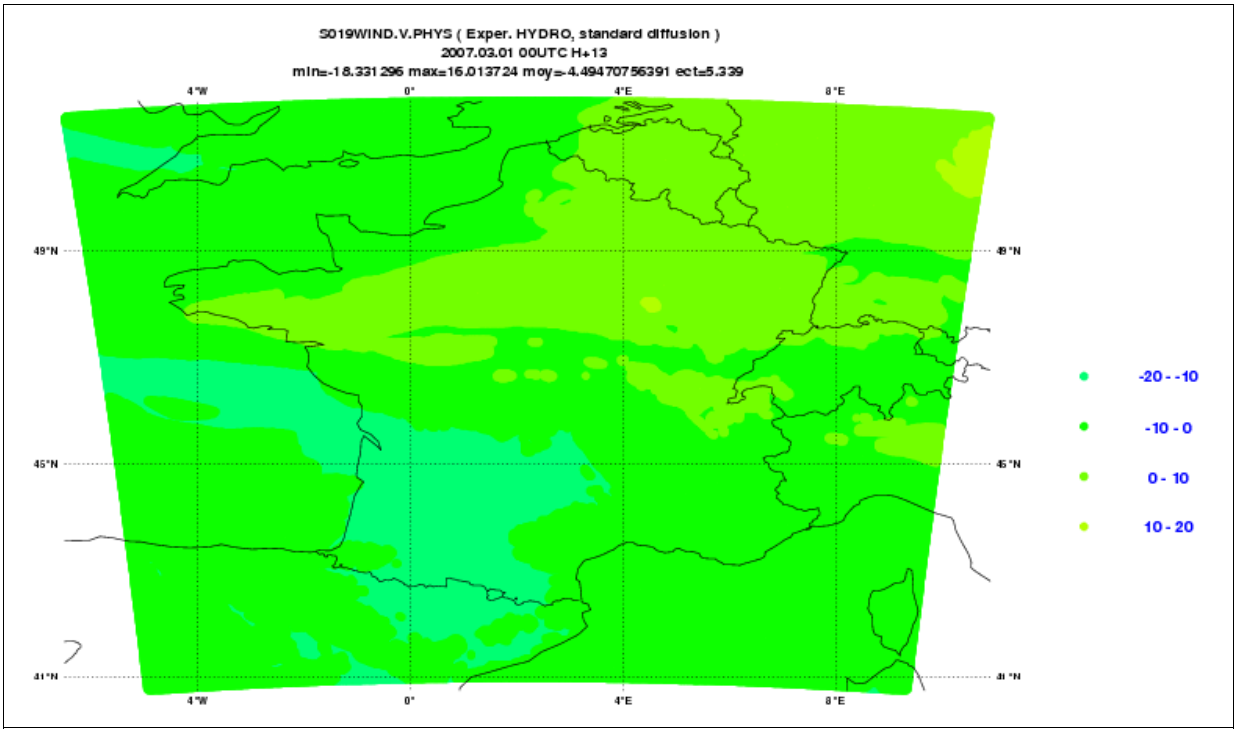

Figure 1.31 *H _ Std Diff _ PC*: forecast H+13 of the v-component of the wind (m s^{-1}) at ML 19 from the 00UTC run of the 1th of March.

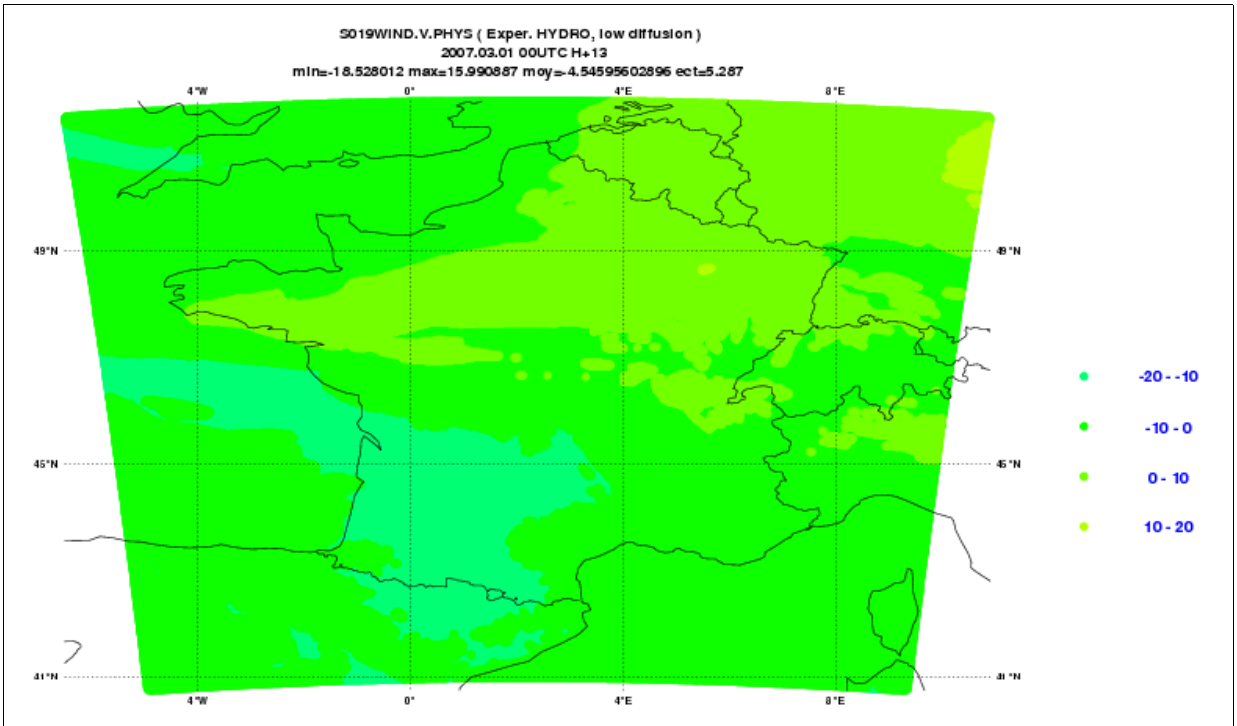

Figure 1.32 *H _ Low Diff _ PC*: forecast H+13 of the v-component of the wind (m s^{-1}) at ML 19 from the 00UTC run of the 1th of March.

1.4 When did "*start the blowing up*" of the experiment NH _ Low Diff _ PC?

With the analysis of the fields of the pressure departure and the components of the wind (principally with the analysis of the u-component of the wind), it seemed that the "*blowing up*" started at the 2h forecast (Figs 1.33-1.37).

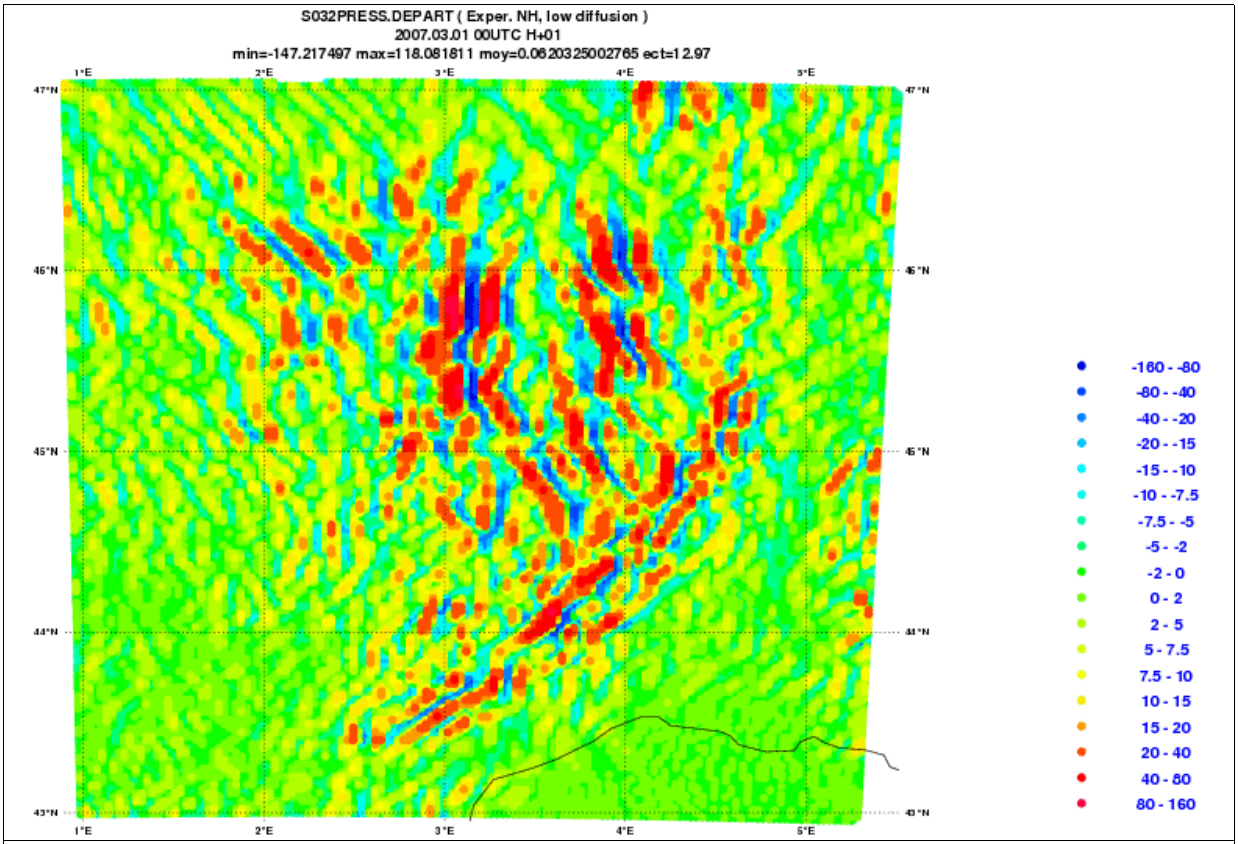

Figure 1.33 ***NH _ Low Diff _ PC*****: forecast H+01 of the pressure departure (Pa) at ML 32 from the 00UTC run of the 1th of March (zoom at the** ***Massif Central*** **zone).**

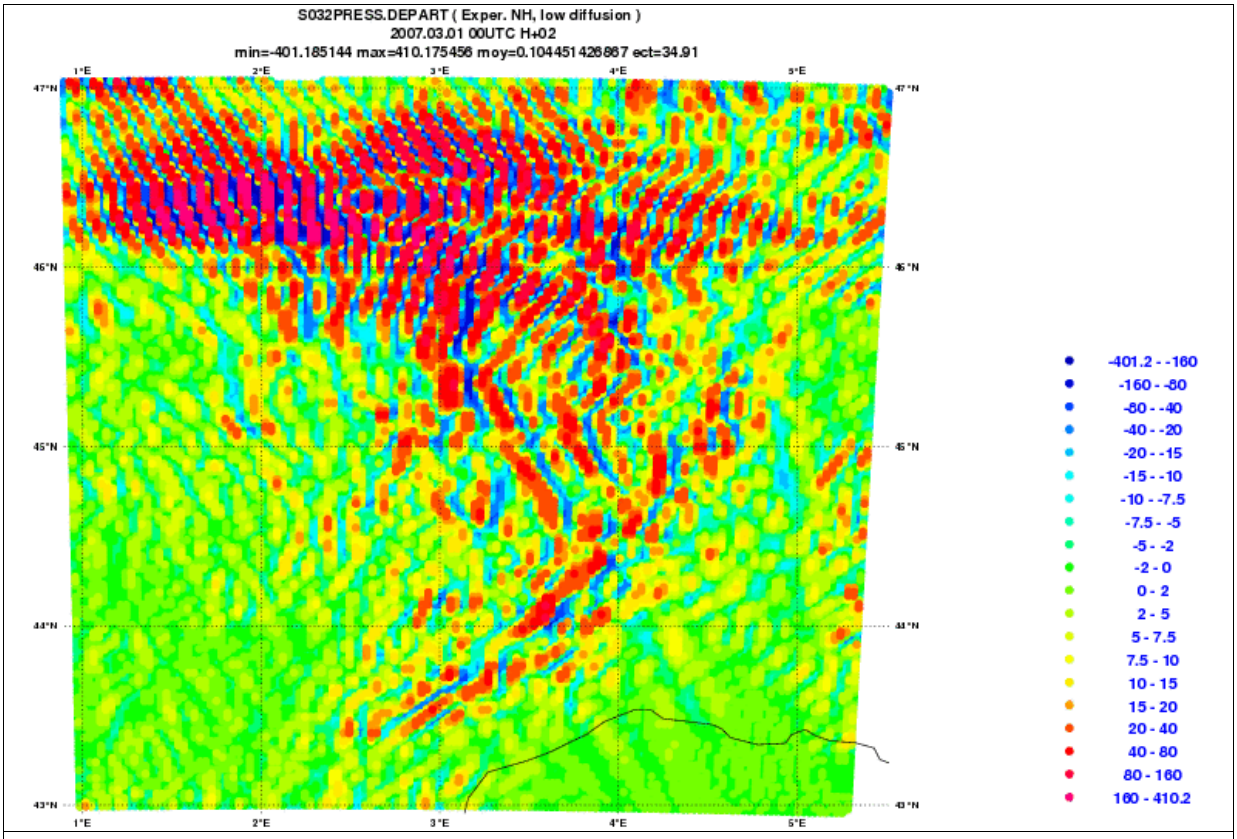

Figure 1.34 *NH _ Low Diff _ PC*: forecast H+02 of the pressure departure (Pa) at ML 32 from the 00UTC run of the 1th of March (zoom at the *Massif Central* zone)..

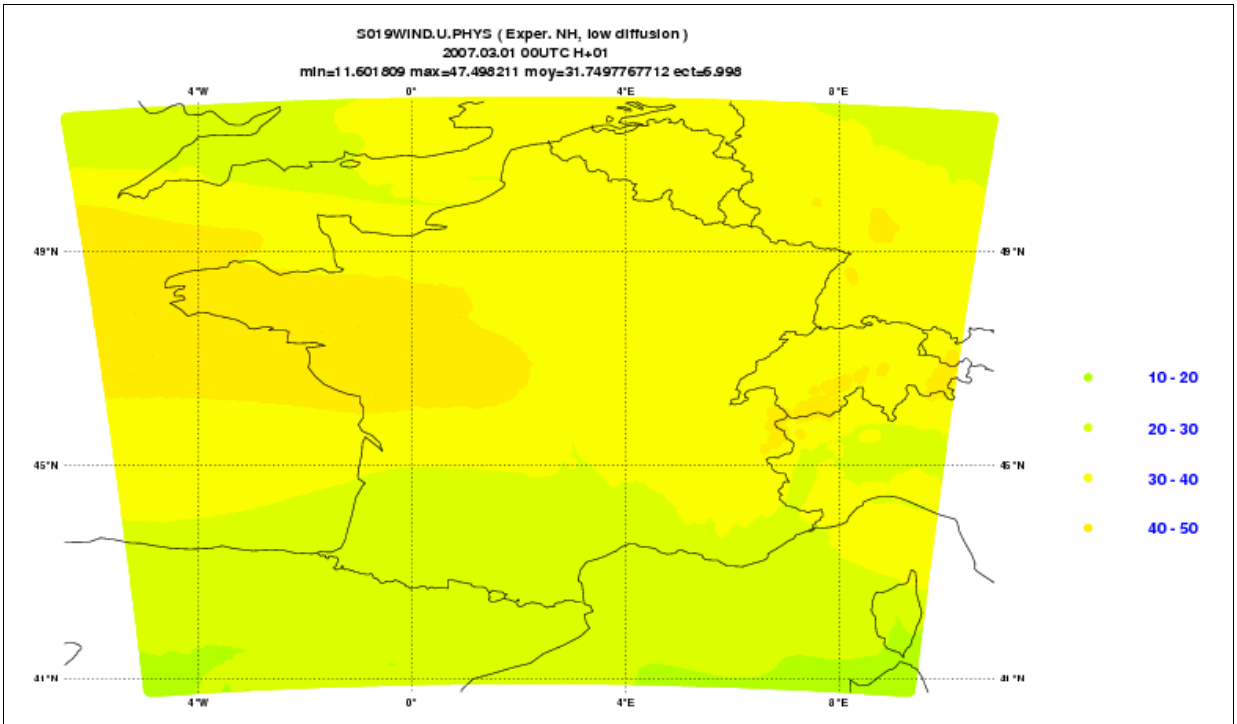

Figure 1.35 *NH _ Low Diff _ PC*: forecast H+01 of the u-component of the wind (m s^{-1}) at ML 19 from the 00UTC run of the 1th of March.

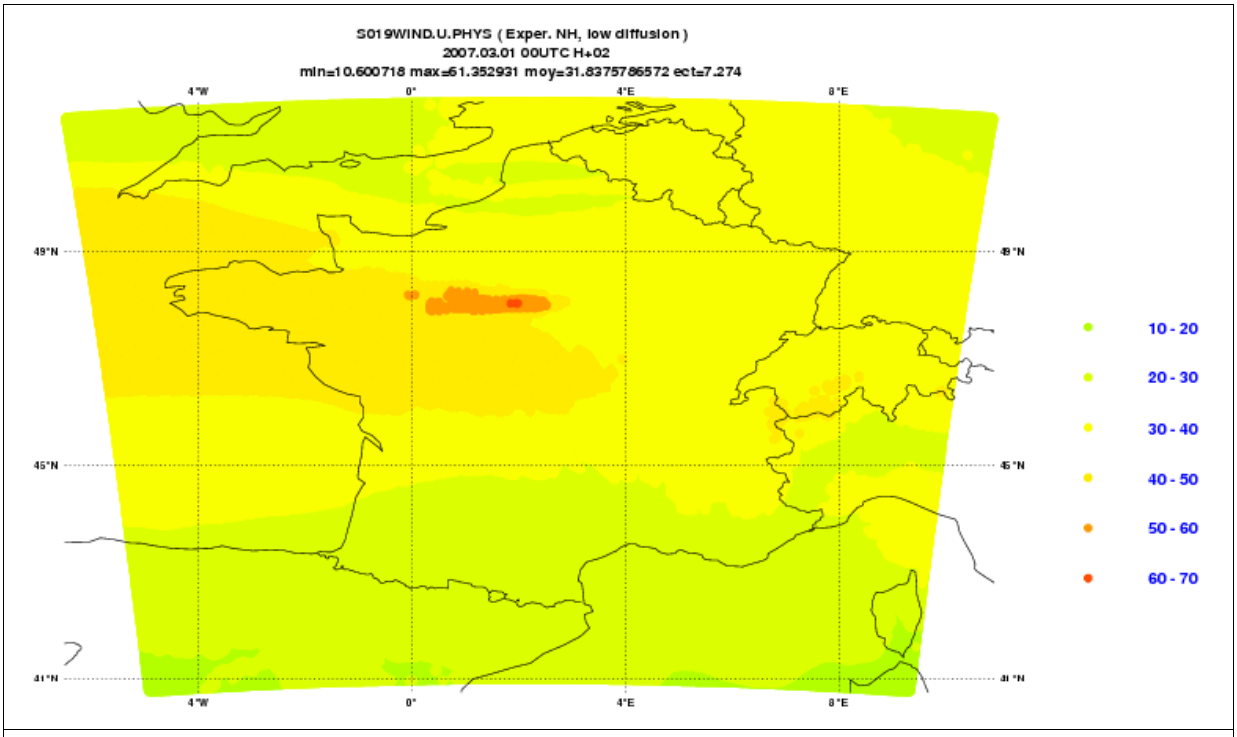

Figure 1.36 *NH _ Low Diff _ PC*: forecast H+02 of the u-component of the wind (m s^{-1}) at ML 19 from the 00UTC run of the 1th of March.

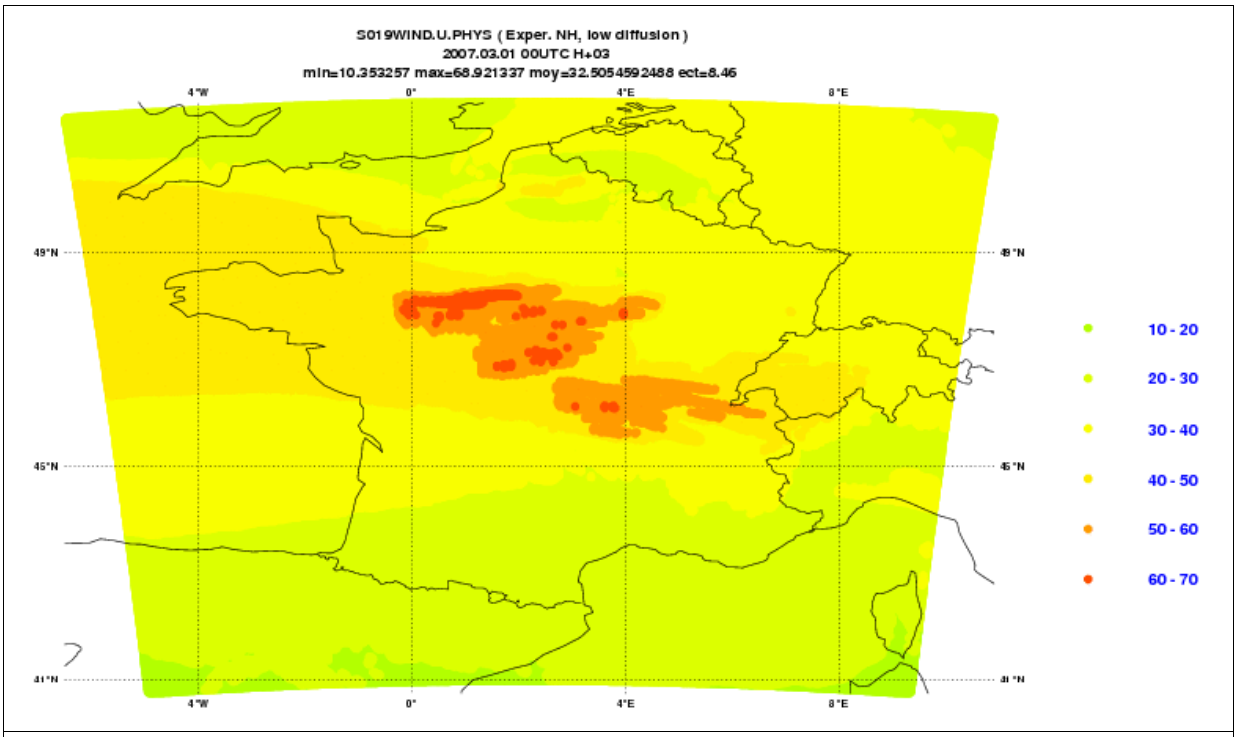

Figure 1.37 *NH _ Low Diff _ PC*: forecast H+03 of the u-component of the wind field (m s^{-1}) at ML 19 from the 00UTC run of the 1th of March.

Some considerations for the case study of the 1th of March 2007:

- Contrarily to the experiment *NH_ Low Diff _ PC*, the new experiment *NH _ Low Diff _ No PC* ran all the forecast part well, which means that maybe there exists a problem with the *PC* used on this case.

- The orographical waves were identified not only on the fields derived from the *NH* experiments but also on the fields derived from the *H* experiments.

- As would be expected, the magnitude of vertical velocity derived from the *NH* experiments is higher than the magnitude of vertical velocity produced by the *H* experiments.

- By contrast, the u and v-components of the wind (ML19) produced by the *H* experiments are similar to the same components forecasted by the *NH* experiments (*Std Diff_PC* and *Low Diff _ No PC*).

- On this case, the forecasted fields derived from the experiments *Low Diff* (not taking account the experiment *NH_ Low Diff _ PC* that blows up) were in general similar to the forecasted fields derived from the experiments *Std Diff* for each dynamical mode.

- The strange behaviour on the forecasts derived from experiment *Low Diff _ PC* was more evident on pressure departure (ML32), on the wind (in particular, on the u-component of the wind) and on the temperature (vertical-cross section).

- At 13h forecast the components of the wind at ML 19 derived from the experiment *NH _ Low Diff _ PC* show a non-physical behaviour (more clear on the u-component) that can be probably related with strong and oscillating winds at the origin of the model explosion. Furthermore, it seems that the instability of the PC already started at 2h forecast.

2. – AROME experiments for the 06th of September 2005

In this situation characterized by a low on the Mediterranean Sea the convection was very strong along the Southern Coast of France and also in some zones inland like the Southern Part of the *Massif Central* and the SW Part of the Alps.

The experiments made with AROME model are identical to the ones made for the first case study.

Also in this case, the area used is FRAN004 but sometimes with a zoom over the region with very heavy precipitation defined by the SW point 42°N 3°E and the NE point 45°N 7°E.

2.1 Forecasts from the *NH* experiments

(A) Accumulated precipitation in 24h

With the analysis of the forecasted accumulated precipitation in 24h and their differences, it can be verified that:

- The patterns of the fields are similar presenting the same main features (figures 2.1-2.3).

- The fields forecasted by the experiments *Low Diff* show more fragmented structures than the field forecasted by the experiment *Std Diff _ PC* (or REF experiment).

- All the forecasts alert to the possibility of very heavy precipitation in the same regions. However, in the zones of the maximums values the differences of accumulated precipitation between the experiments *Low Diff* and the REF experiment can be very significant (figures 2.4 and 2.5).

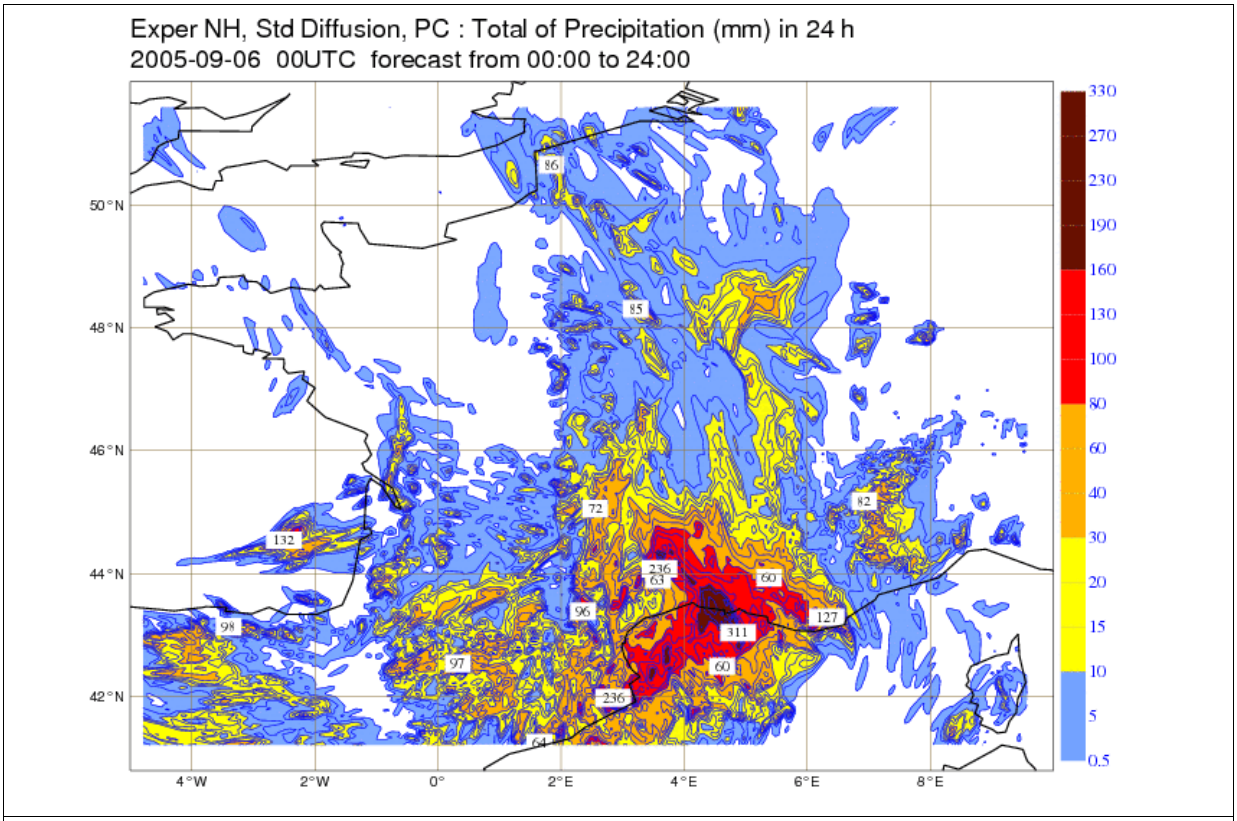

Figure 2.1 *NH _ Std Diff _ PC*: forecast of the accumulated precipitation (mm) from 00UTC to 24UTC of the 6th of September (cylindrical projection).

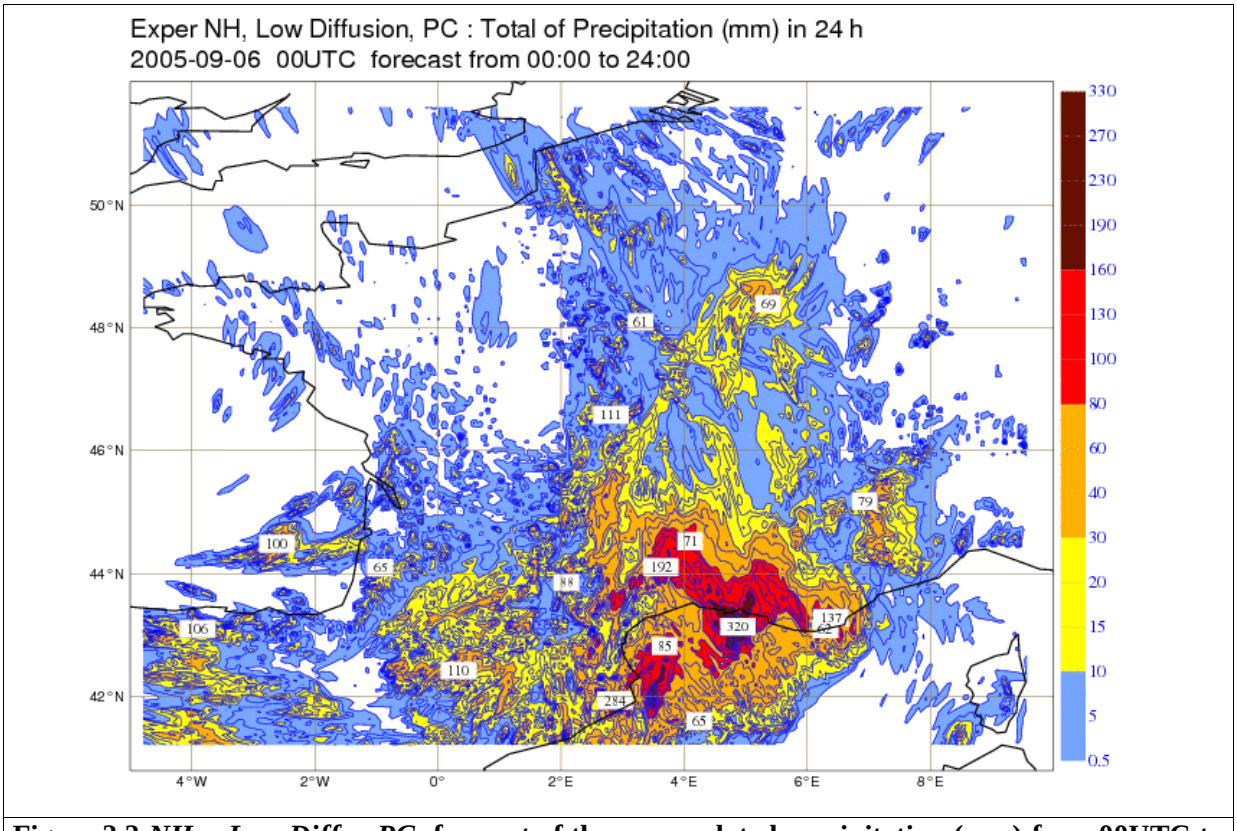

Figure 2.2 *NH _ Low Diff _ PC*: forecast of the accumulated precipitation (mm) from 00UTC to 24UTC of the 6th of September (cylindrical projection).

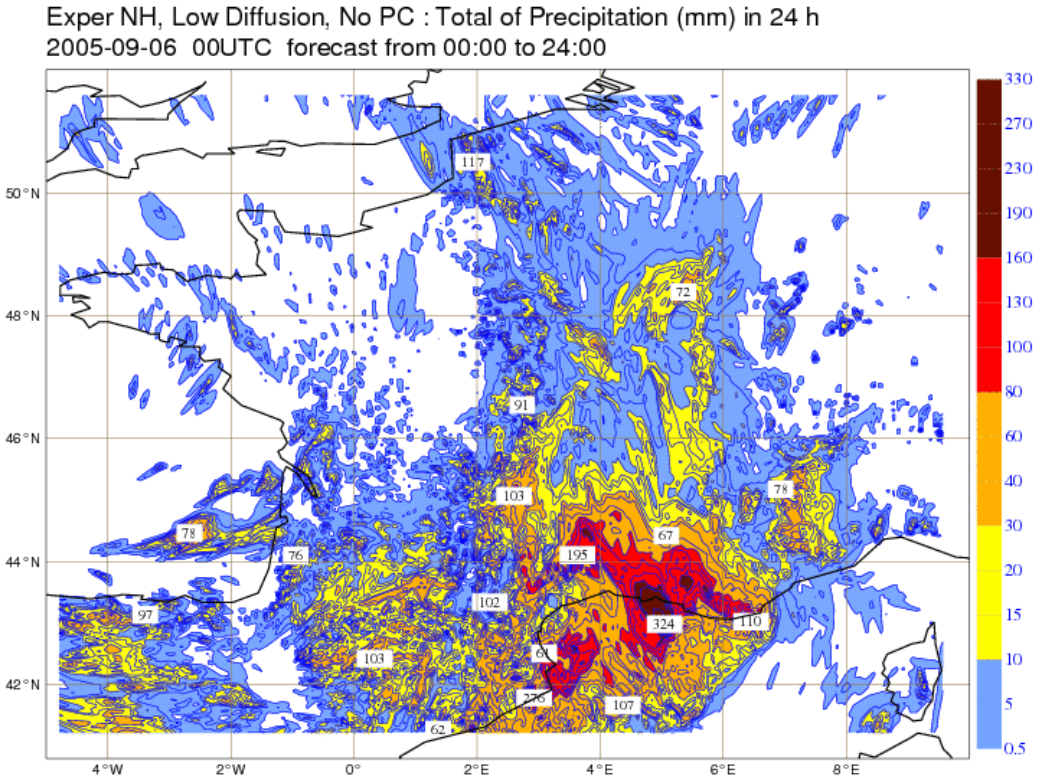

Figure 2.3 *NH _ Low Diff _ No PC*: forecast of the accumulated precipitation (mm) from 00UTC to 24UTC of the 6th of September (cylindrical projection).

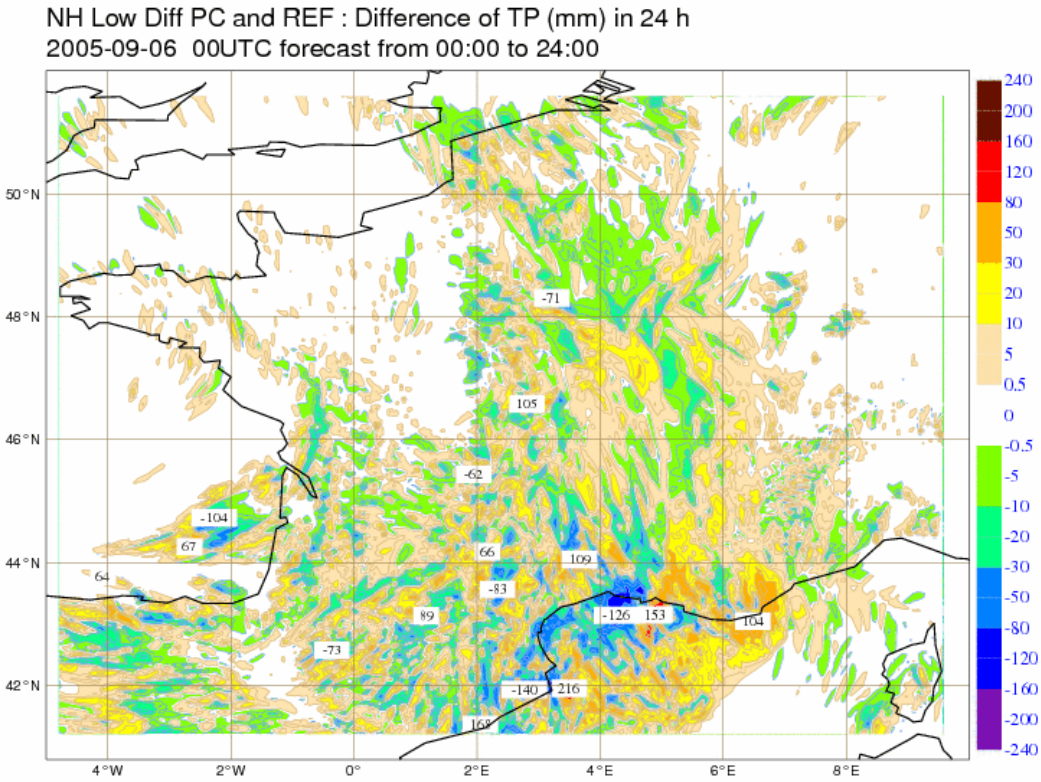

Figure 2.4 Difference between accumulated precipitations (mm) [(*NH _ Low Diff _ PC*) – (*NH _ Std Diff _ PC*)] from 00UTC to 24UTC of the 6th of September (cylindrical projection).

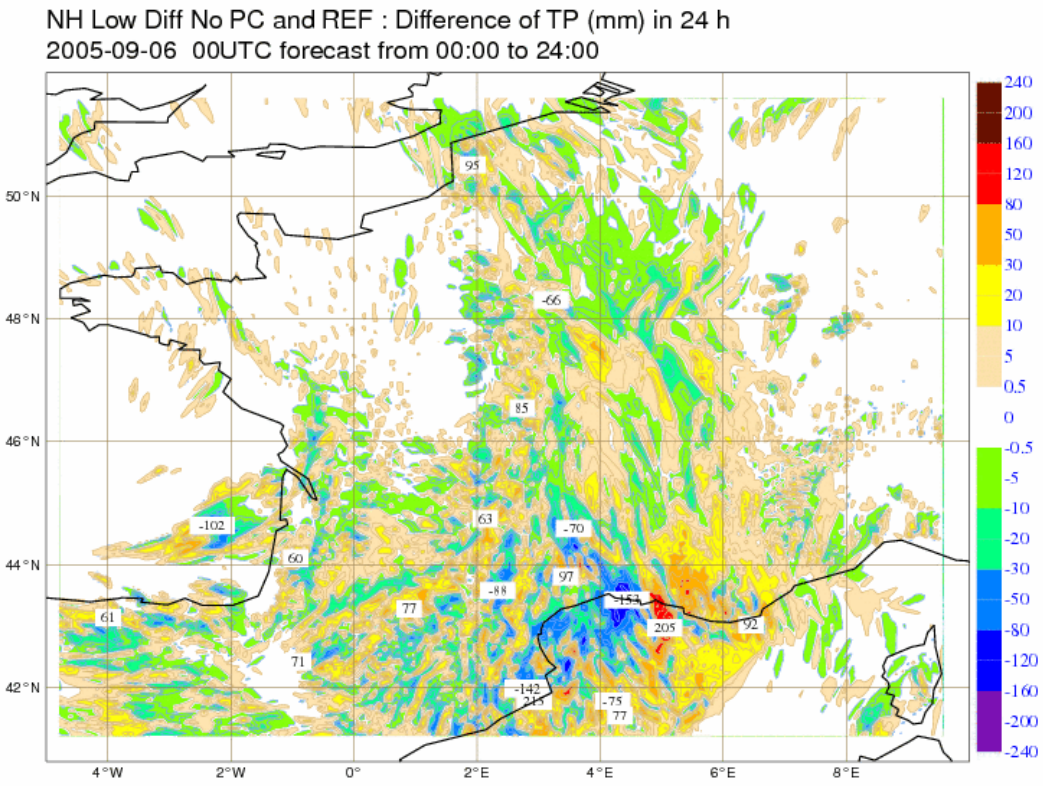

Figure 2.5 Difference between accumulated precipitations (mm) [*(NH _ Low Diff _ No PC) – (NH _ Std Diff _ PC)*] from 00UTC to 24UTC of the 6th of September (cylindrical projection).

(B) Accumulated precipitation from 21UTC to 24UTC

For the period between 21UTC and 24UTC the forecasts of the three NH experiments show a big area with very high values of accumulated precipitation (figures 2.6-2.8). A large precipitation system extends from the Mediterranean (region of *Côte d'Azur*) to the *Massif Central.*

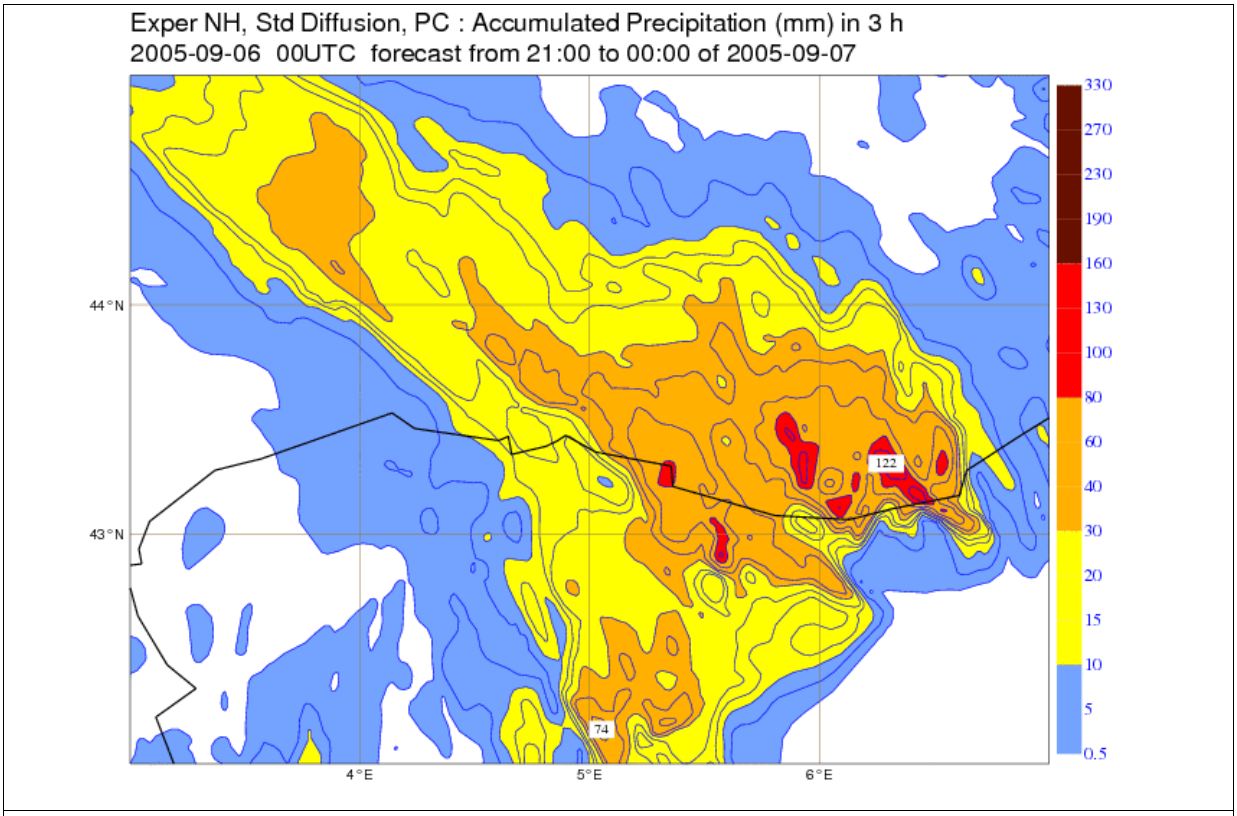

Figure 2.6 *NH _ Std Diff _ PC*: forecast of the accumulated precipitation (mm) from 21UTC to 24UTC of the 6th of September (zoom on the zone with heavy precipitation; cylindrical projection).

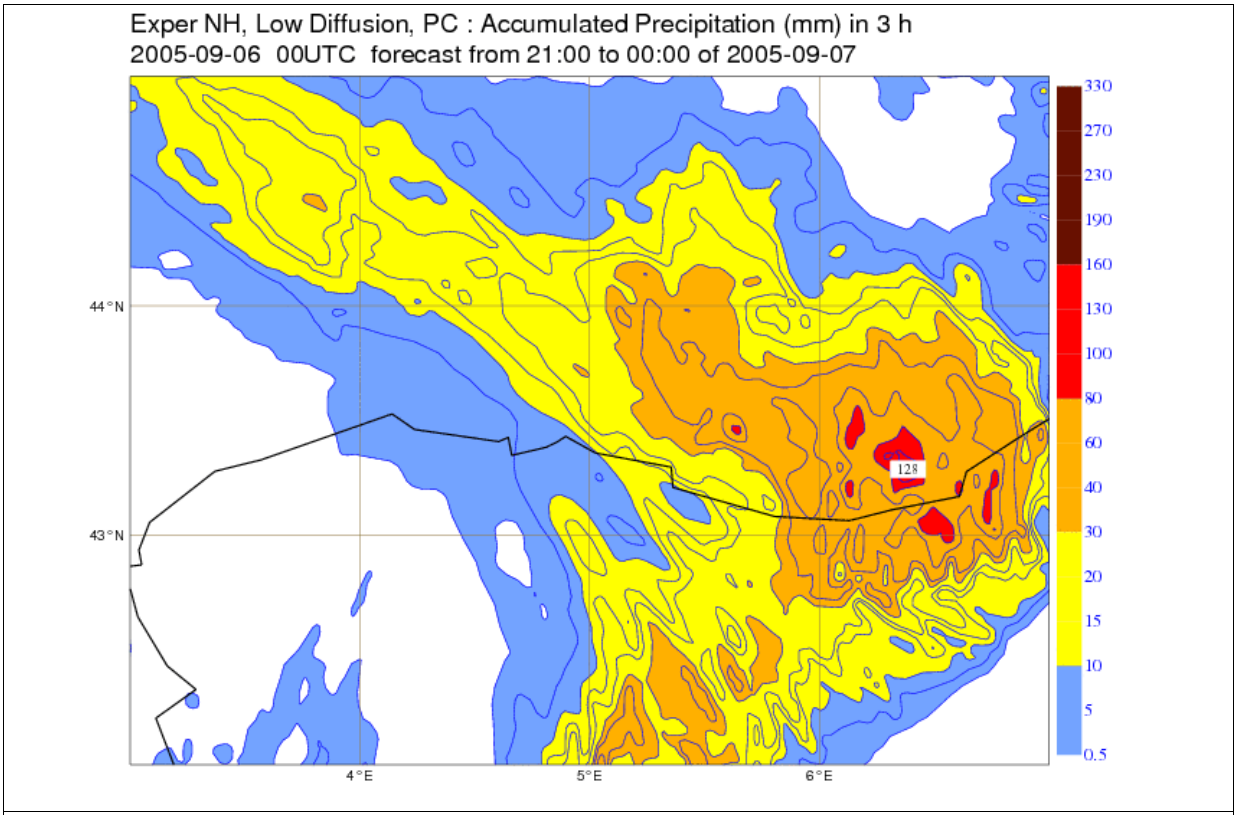

Figure 2.7 *NH _ Low Diff _ PC*: forecast of the accumulated precipitation (mm) from 21UTC to 24UTC of the 6th of September (zoom on the zone with heavy precipitation; cylindrical projection).

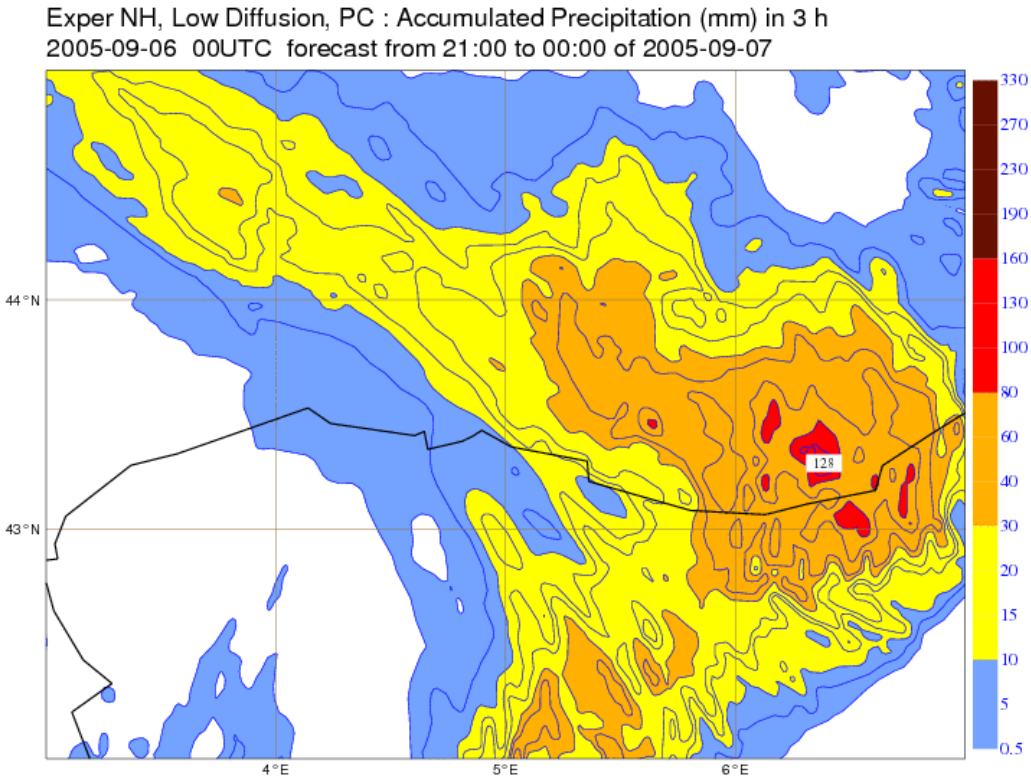

Figure 2.8 ***NH _ Low Diff _ No PC*****: forecast of the accumulated precipitation (mm) from 21UTC to 24UTC of the 6th of September (zoom on the zone with heavy precipitation; cylindrical projection).**

(C) Forecast of Pressure Departure (P_{NH} - P_H) for 21h

By the comparison of the accumulated precipitation (figures 2.6-2.8) with the pressure departure (2.9-2.13), it can be verified that:

- The magnitude of pressure departure is stronger on the zones with higher amounts of precipitation and on their surroundings.

- The pressure departure field derived from the experiment *Std Diff _ PC* is smoother than the pressure departure fields derived from the experiments *Low Diff* (*_PC* and *_No PC*).

- On this situation, the pressure departure field derived from the experiment *Low Diff _ No PC* presents an non-physical behaviour west of the meridian 6°E, approximately, where it shows an numerical anomaly with very strong magnitudes. In particular, the maximum intensity of pressure departure produced by *Low Diff _ No PC* (13 hPa) is four times bigger than the maximum intensity of the field produced from *Low Diff _ PC* and six times bigger than the maximum intensity of the *Std Diff _ PC*.

- Also the pressure departure forecasted by the experiment *Low Diff _ No PC* for the surface (figure 2.12) and for the tropopause levels (figure 2.13) present numerical anomalies.

- Consequently, it seems that on this situation it is important to have the *PC*.

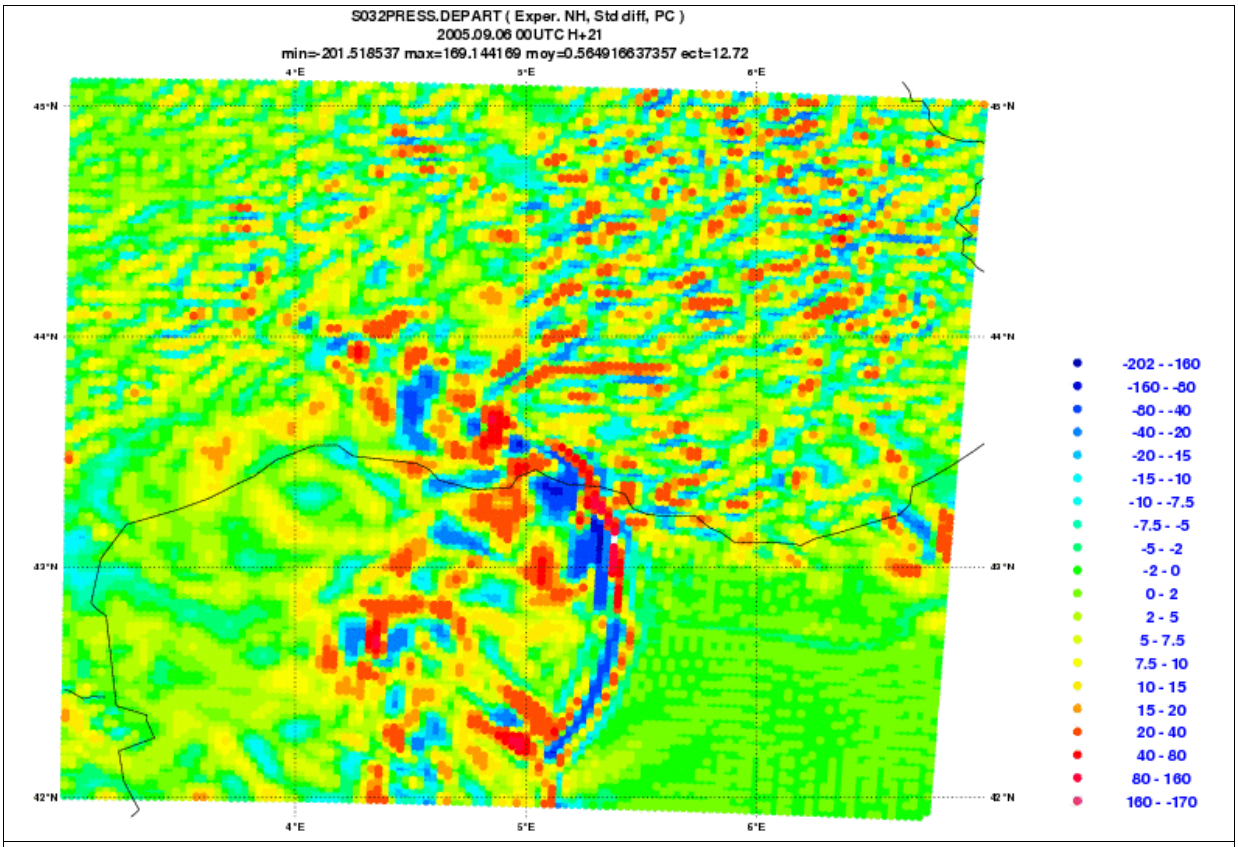

Figure 2.9 *NH _ Std Diff _ PC*: forecast H+21 of Pressure Departure (Pa) at ML 32 from the 00UTC run of the 6th of September (zoom on the zone with heavy precipitation).

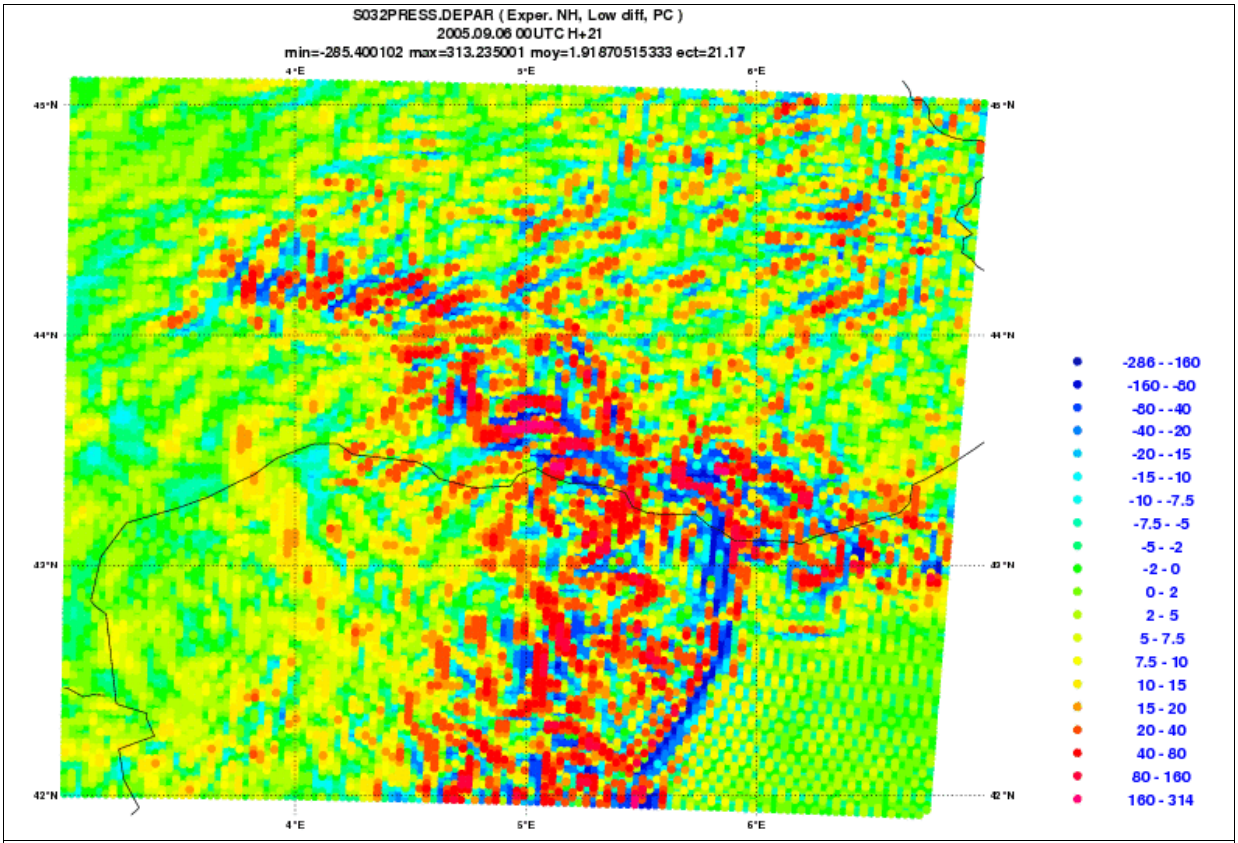

Figure 2.10 *NH _ Low Diff _ PC*: forecast H+21 of Pressure Departure (Pa) at ML 32 from the 00UTC run of the 6th of September (zoom on the zone with heavy precipitation).

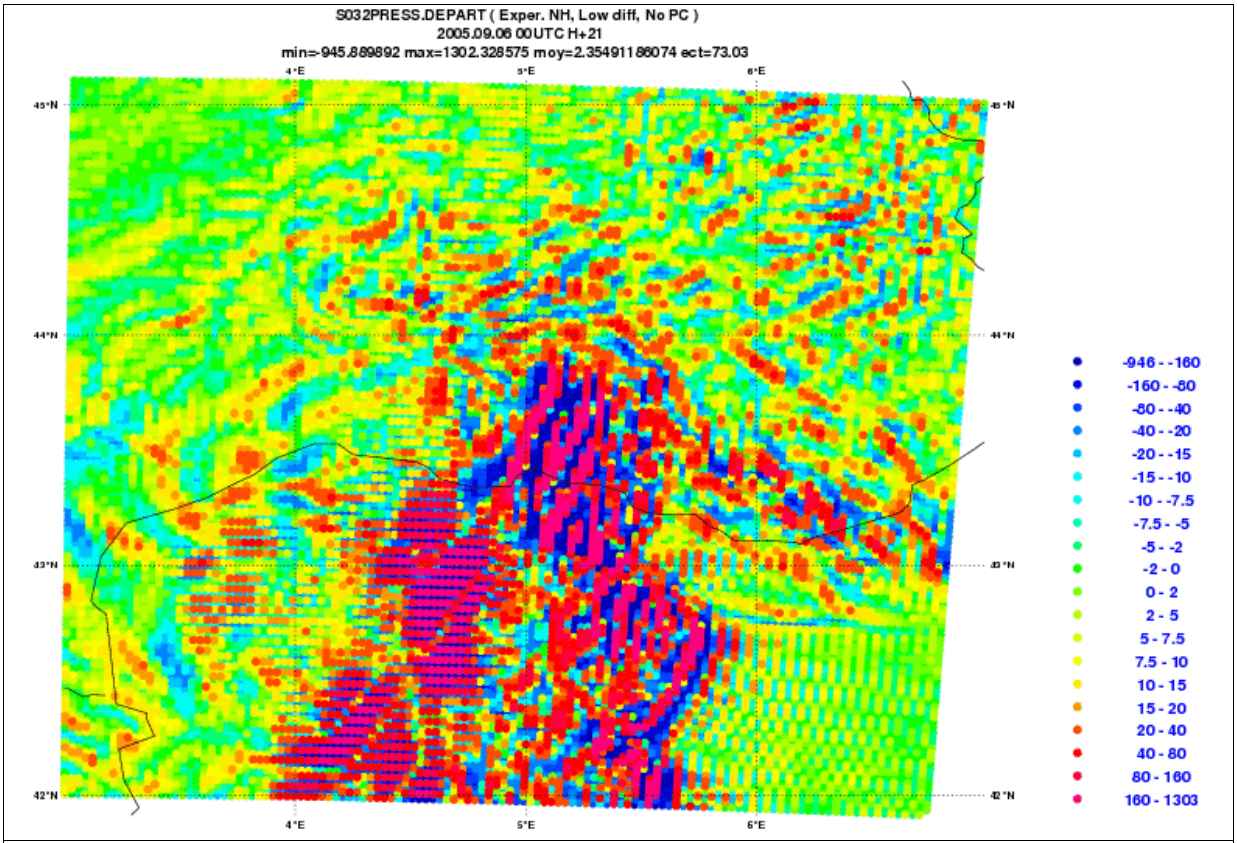

Figure 2.11 *NH _ Low Diff _ No PC*: forecast H+21 of Pressure Departure (Pa) at ML 32 from 00UTC run of the 6th of September (zoom on the zone with heavy precipitation).

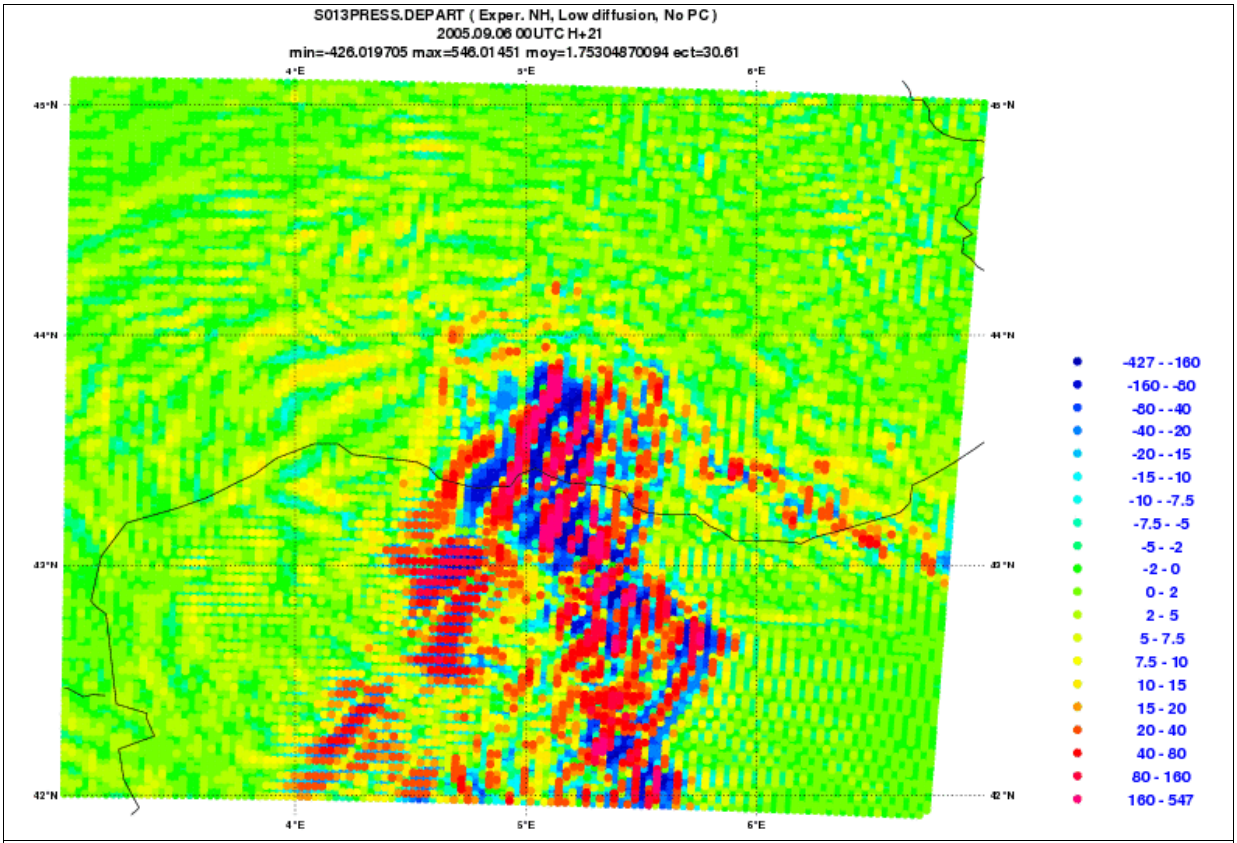

Figure 2.12 *NH _ Low Diff _ No PC*: forecast H+21 of Pressure Departure (Pa) at ML 13 from 00UTC run of the 6th of September (zoom on the zone with heavy precipitation).

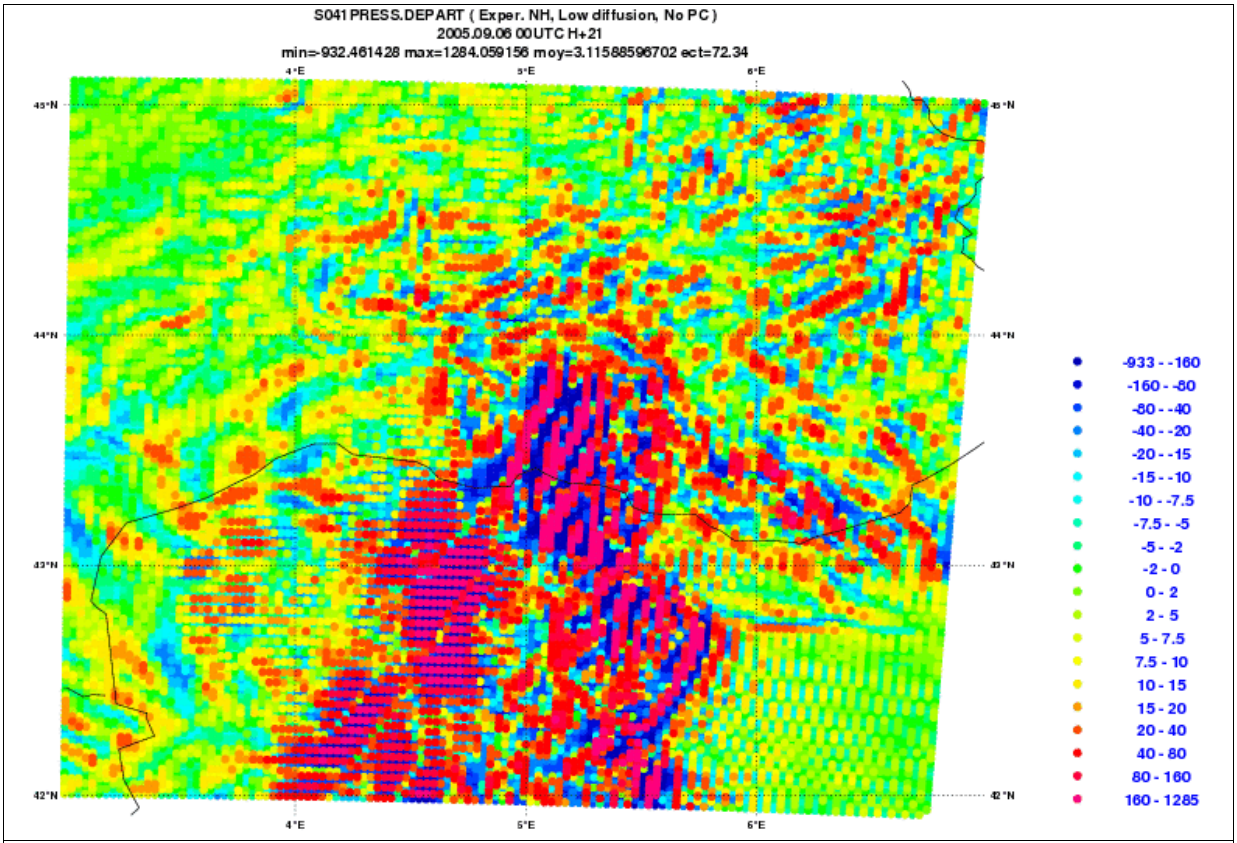

Figure 2.13 *NH _ Low Diff _ No PC*: forecast H+21 of Pressure Departure (Pa) at ML 41 from 00UTC run of the 6th of September (zoom on the zone with heavy precipitation).

2.2 Forecasts for 21h from the *NH* and the *H* experiments

(A) Relative Humidity and Vertical Velocity at 850hPa

By the comparison of the forecasted precipitation for the period 21-24UTC (figures 2.6-2.8) with the forecasts of the relative humidity (RH) and the vertical velocity (ω) at 850hPa for 21h (figures 2.14 – 2.23), it can be concluded that:

- In general the forecasts of humidity produced by the *NH* experiments indicate the existence of high levels of humidity on the areas with heavy precipitation.

- The forecasts of ω derived from the *NH* experiments indicate mostly upward motion on the area of the precipitation system and also a very strong upward forcing inside this area.

- The coexistence at 850hPa of high humidity and upward motion is favourable to deep convection and to the occurrence of heavy precipitation.

- The forecasts of humidity and ω derived from the *H* experiments present only small differences to the corresponding forecasts derived from the *NH.*

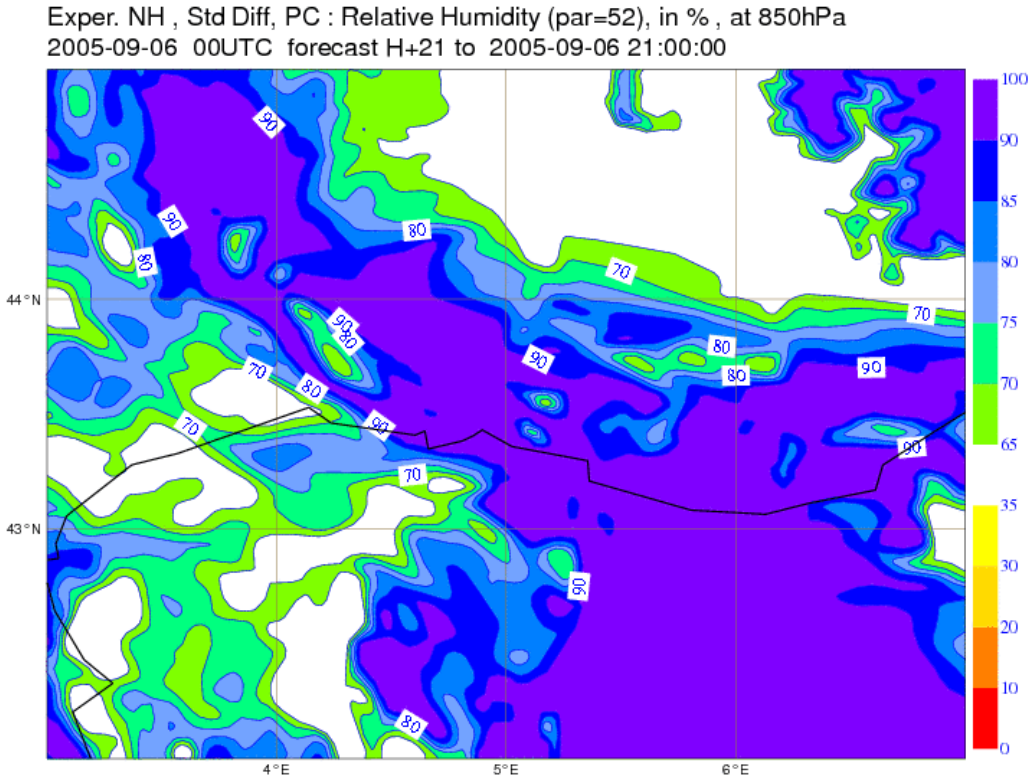

Figure 2.14 *NH _ Std Diff _ PC*: forecast H+21 of RH (%) at 850hPa from 00UTC run of the 6th of September (zoom on the zone with heavy precipitation; cylindrical projection).

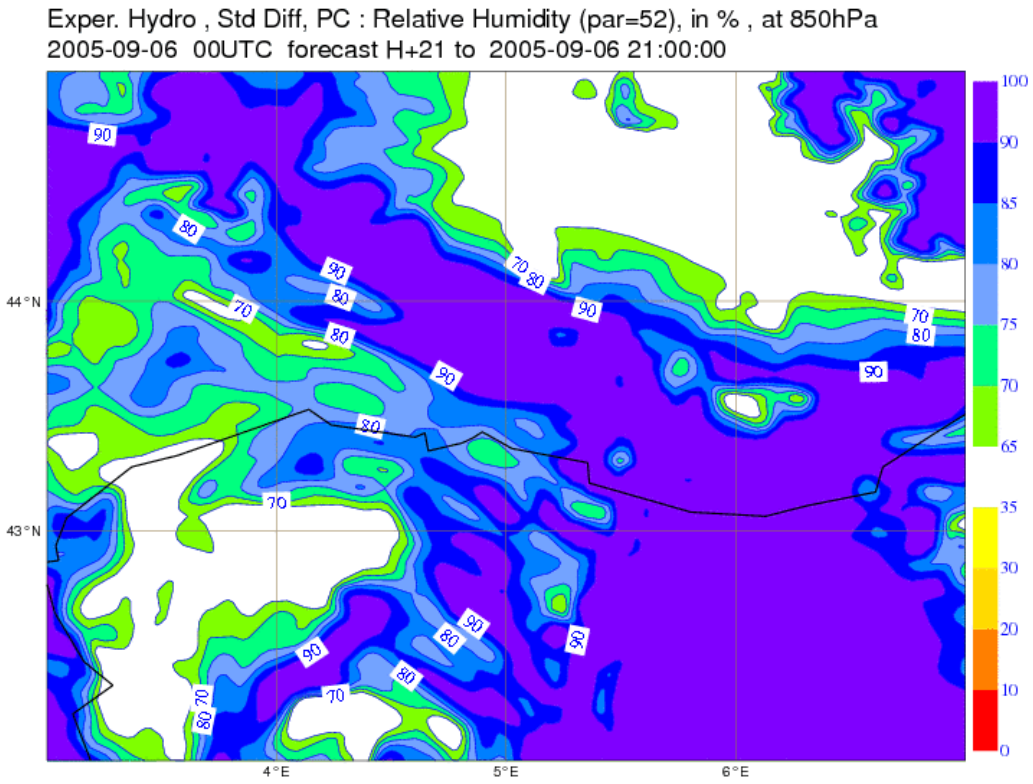

Figure 2.15 *H _ Std Diff _ PC*: forecast H+21 of RH (%) at 850hPa from 00UTC run of the 6th of September (zoom on the zone with heavy precipitation; cylindrical projection).

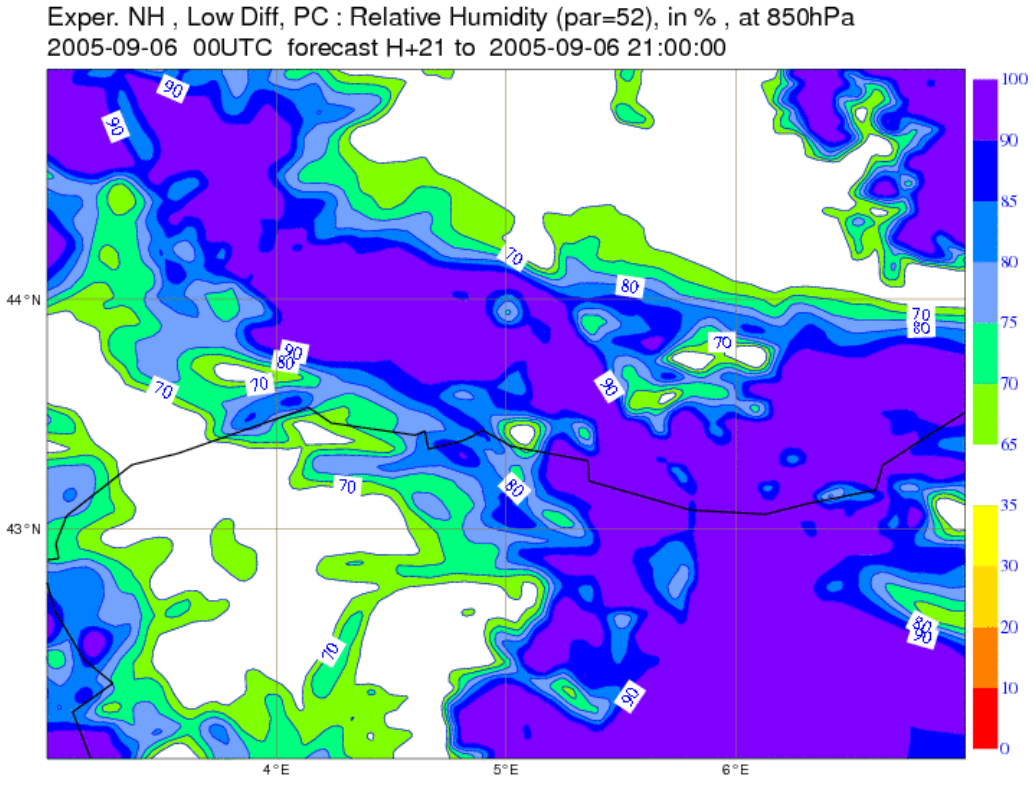

Figure 2.16 *NH _ Low Diff _ PC*: forecast H+21 of RH (%) at 850hPa from 00UTC run of the 6th of September (zoom on the zone with heavy precipitation; cylindrical projection).

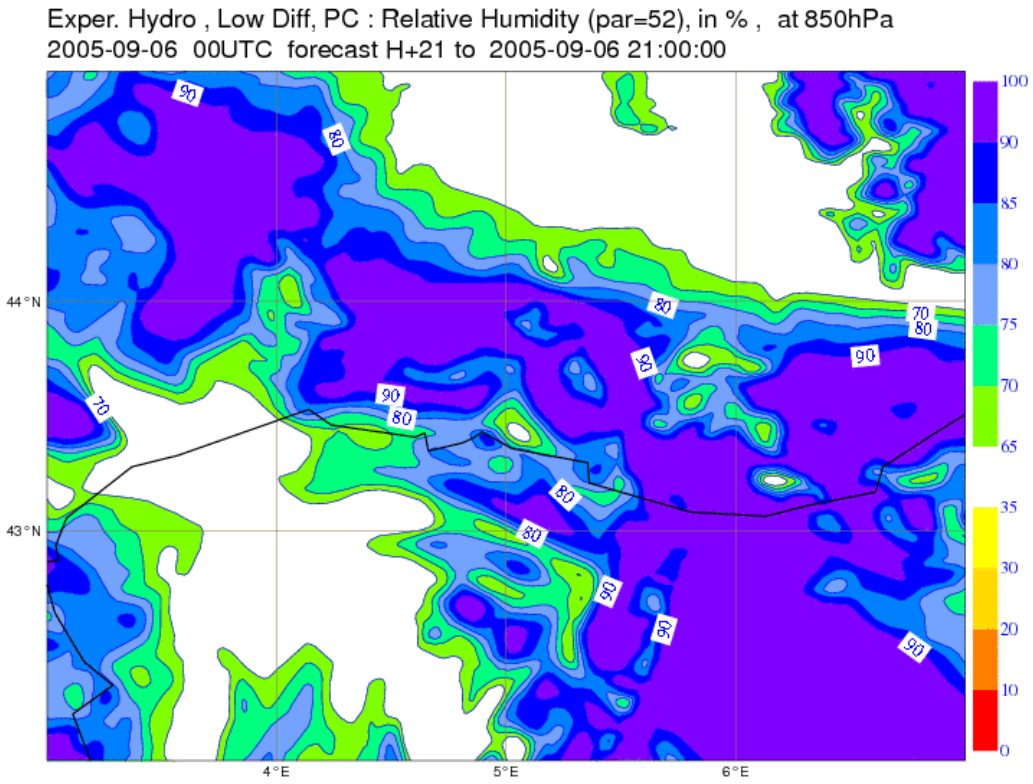

Figure 2.17 *H _ Low Diff _ PC*: forecast H+21 of RH (%) at 850hPa from 00UTC run of the 6th of September (zoom on the zone with heavy precipitation; cylindrical projection).

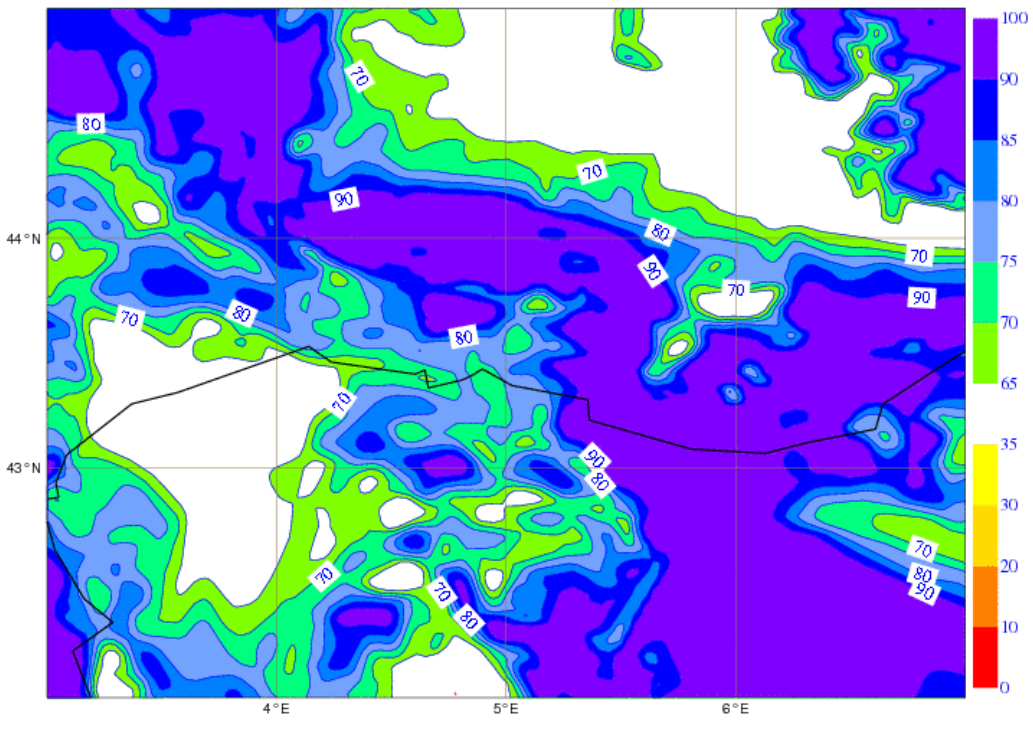

Figure 2.18 *NH _ Low Diff _ No PC*: forecast H+21 of RH (%) at 850hPa from 00UTC run of the 6th of September (zoom on the zone with heavy precipitation; cylindrical projection).

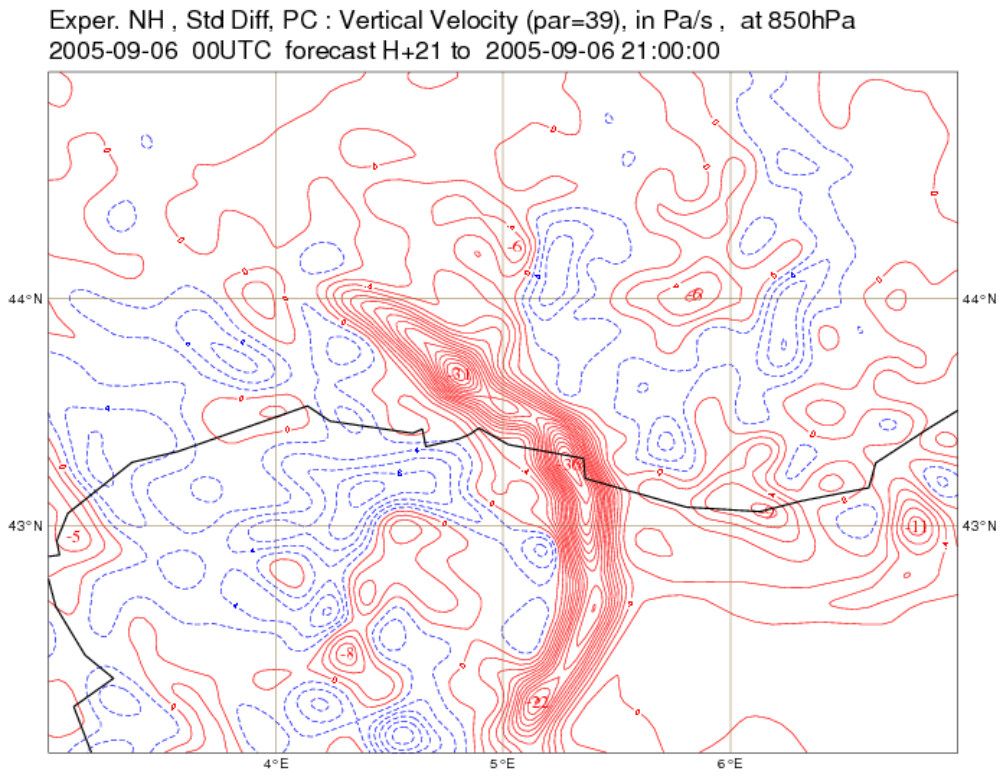

Figure 2.19 *NH _ Std Diff _ PC*: forecast H+21 of ω (Pa s^{-1}) at 850hPa from 00UTC run of the 6th of September (zoom on the zone with heavy precipitation; cylindrical projection).

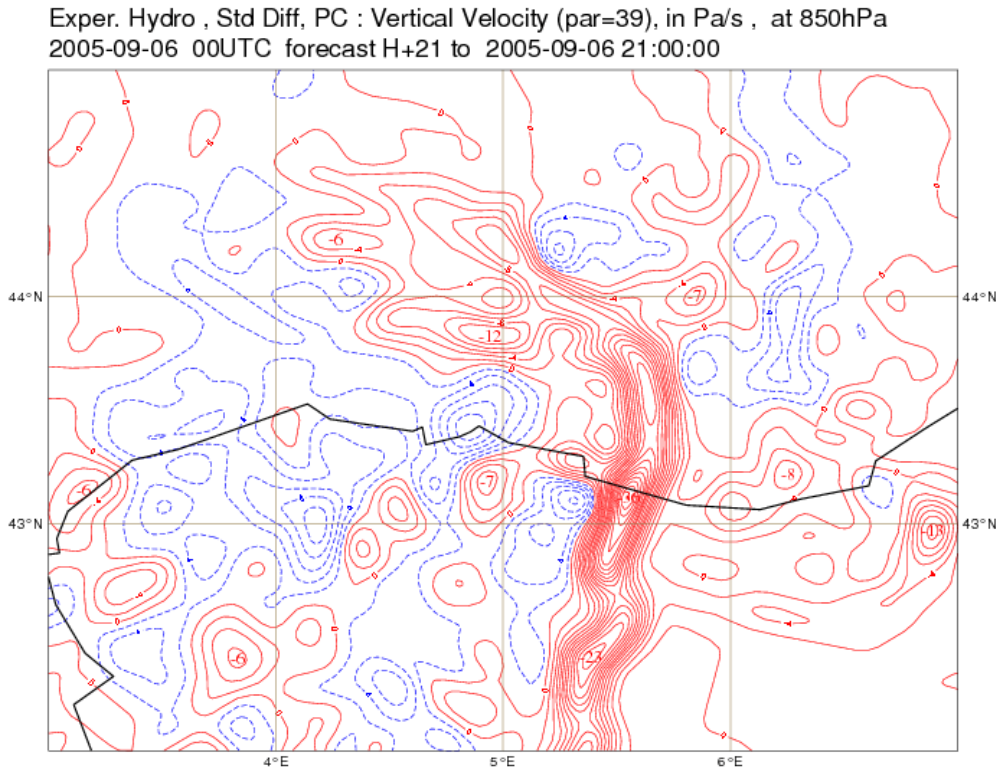

Figure 2.20 *H _ Std Diff _ PC*: forecast H+21 of ω at 850hPa from 00UTC run of the 6th of September (zoom on the zone with heavy precipitation; cylindrical projection).

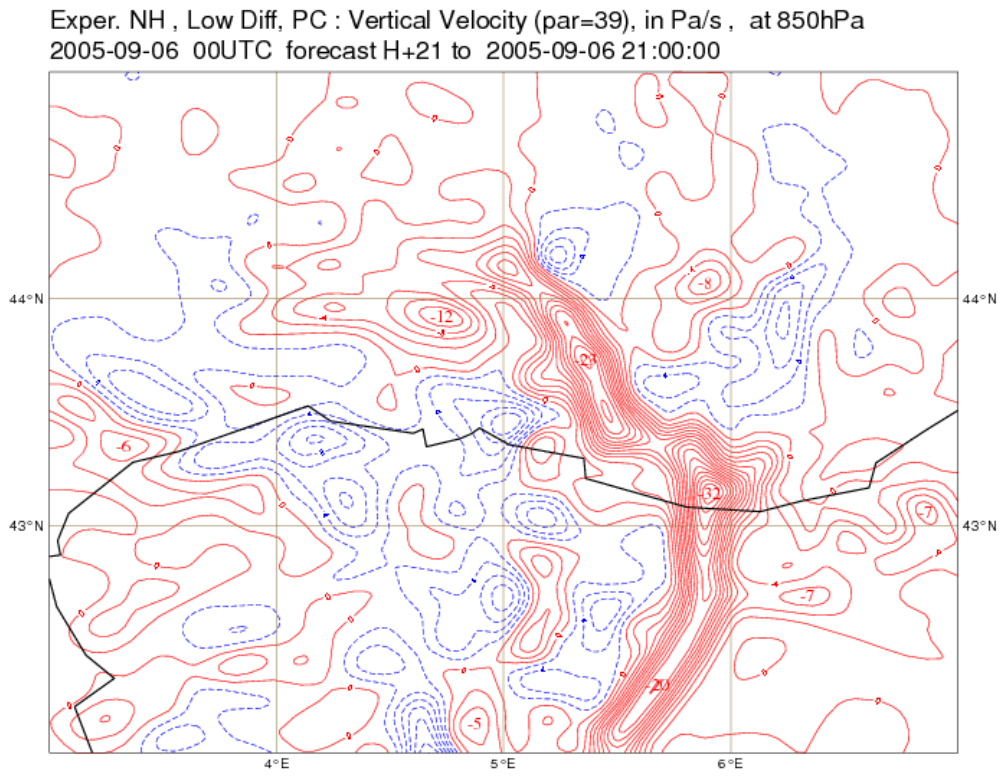

Figure 2.21 *NH _ Low Diff _ PC*: forecast H+21 of ω at 850hPa from 00UTC run of the 6th of September (zoom on the zone with heavy precipitation; cylindrical projection).

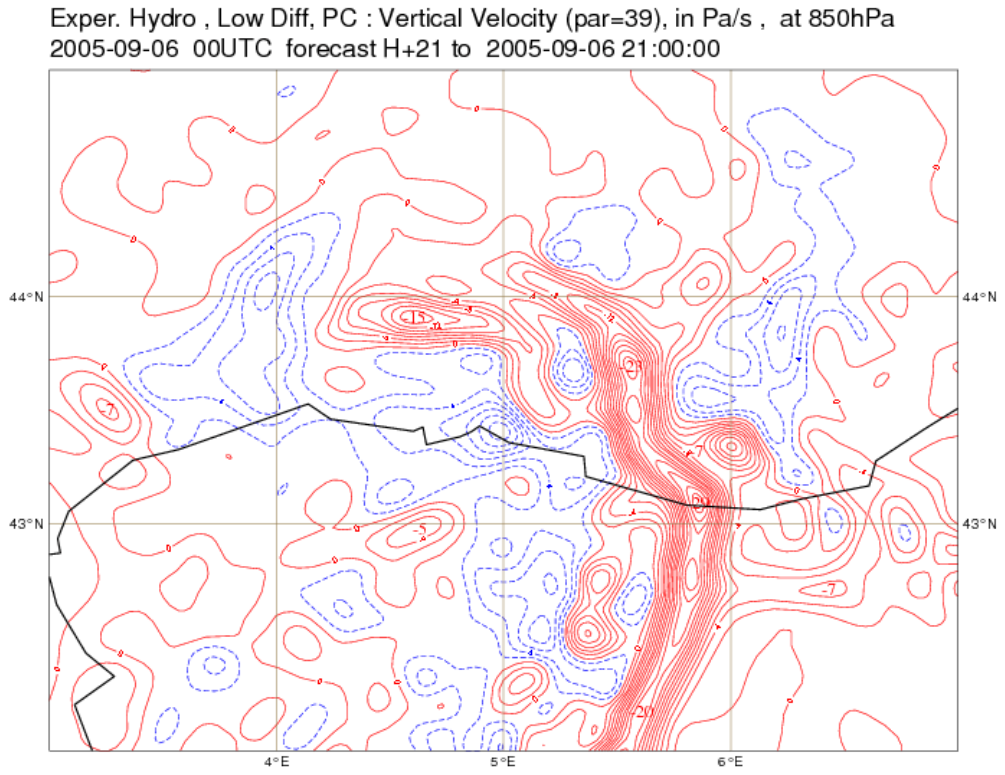

Figure 2.22 *H _ Low Diff _ PC*: forecast H+21 of ω at 850hPa from 00UTC run of the 6th of September (zoom on the zone with heavy precipitation; cylindrical projection).

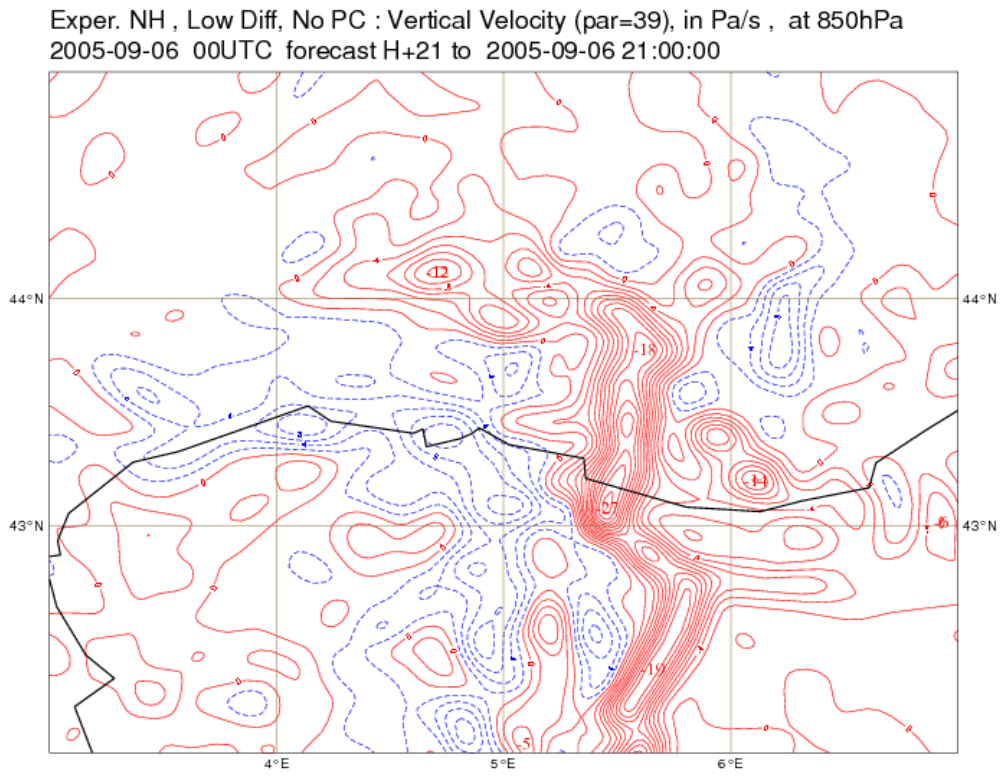

Figure 2.23 *NH _ Low Diff _ No PC*: forecast H+21 of ω at 850hPa from 00UTC run of the 6th of September (zoom on the zone with heavy precipitation; cylindrical projection).

(B) Vertical cross-sections of Temperature (T), Ice Crystal (IC) and Vertical Velocity (ω)

Vertical cross-sections of the forecasts H+21 of T, IC and ω were made between the points 43.5°N 3.5°E and 43.5°N 7°E located in the zone of forecasted heavy precipitation.

(B.1) Temperature

The forecasts of T produced by the experiments *Std Diff* show less perturbation principally on the medium and higher levels than the ones produced by the experiments *Low Diff* (figures 2.24 – 2.28).

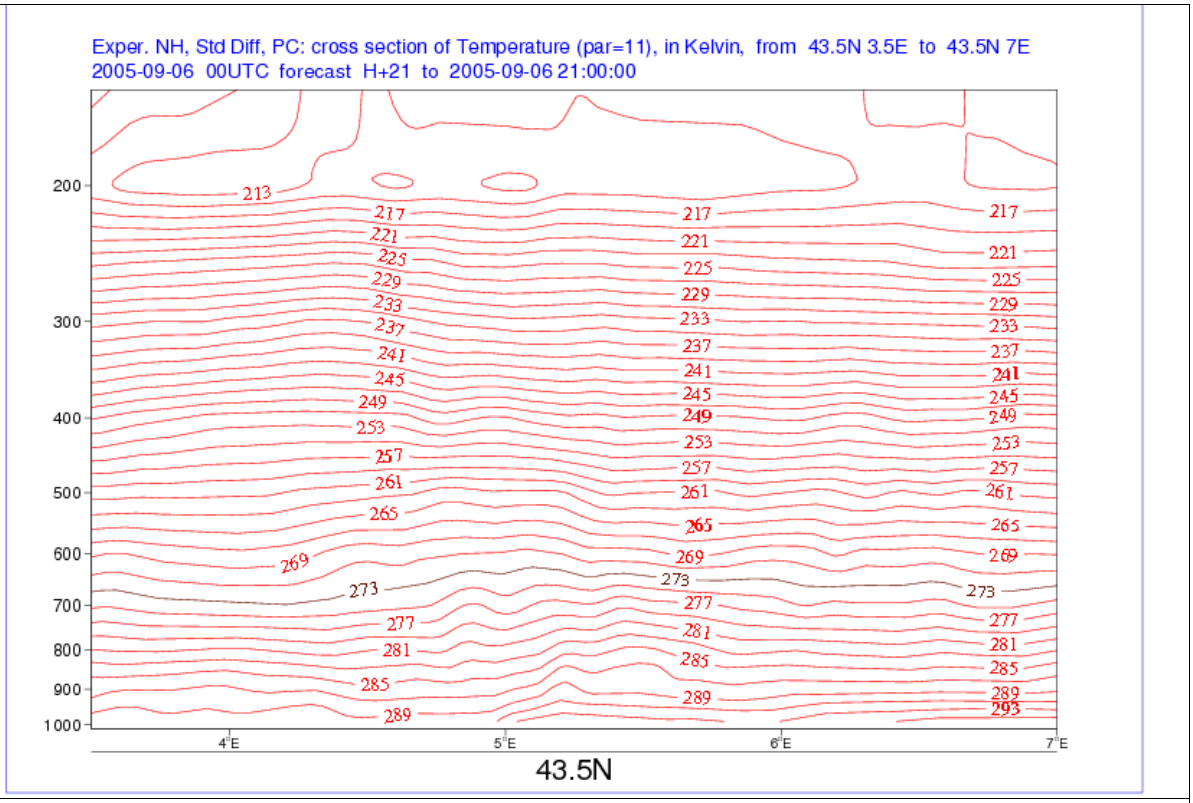

Figure 2.24 *NH _ Std Diff _ PC*: forecast H+21 of Temperature (K) from 00UTC run of the 6th of September.

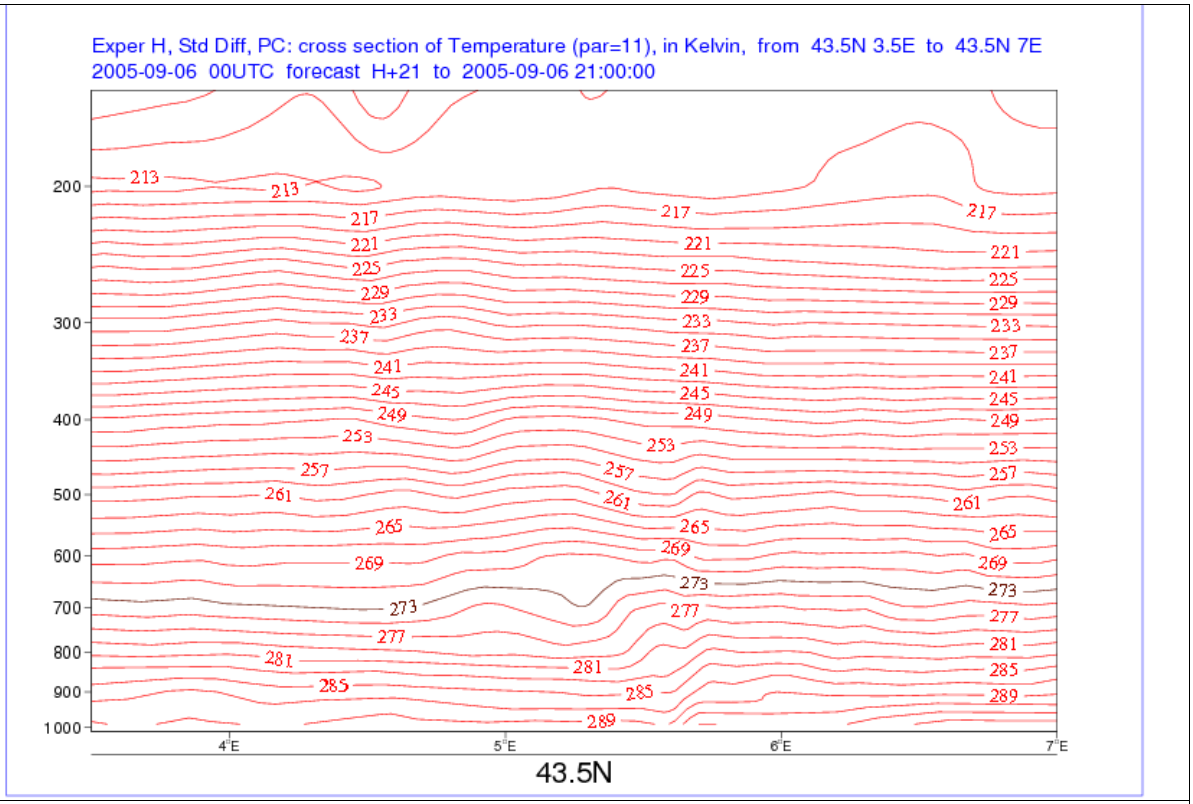

Figure 2.25 *H _ Std Diff _ PC*: forecast H+21 of Temperature (K) from 00UTC run of the 6th of September.

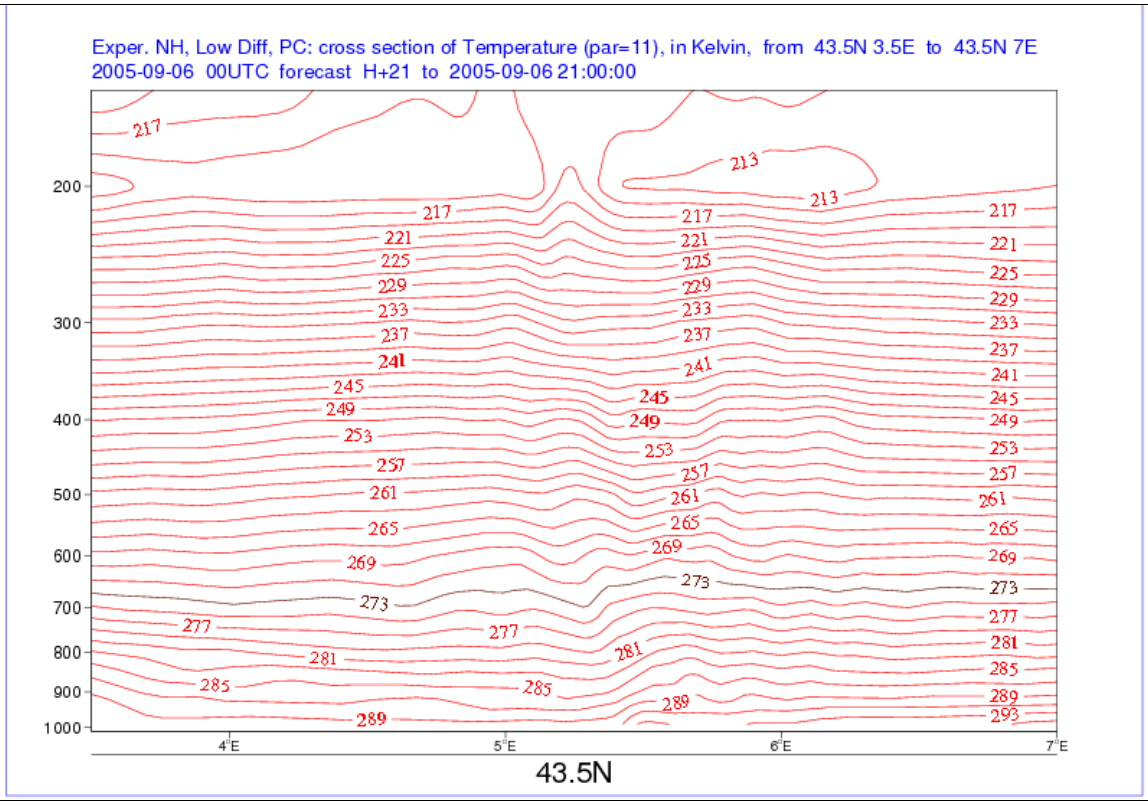

Figure 2.26 *NH _ Low Diff _PC*: forecast H+21 of the Temperature (K) from 00UTC run of the 6th of September.

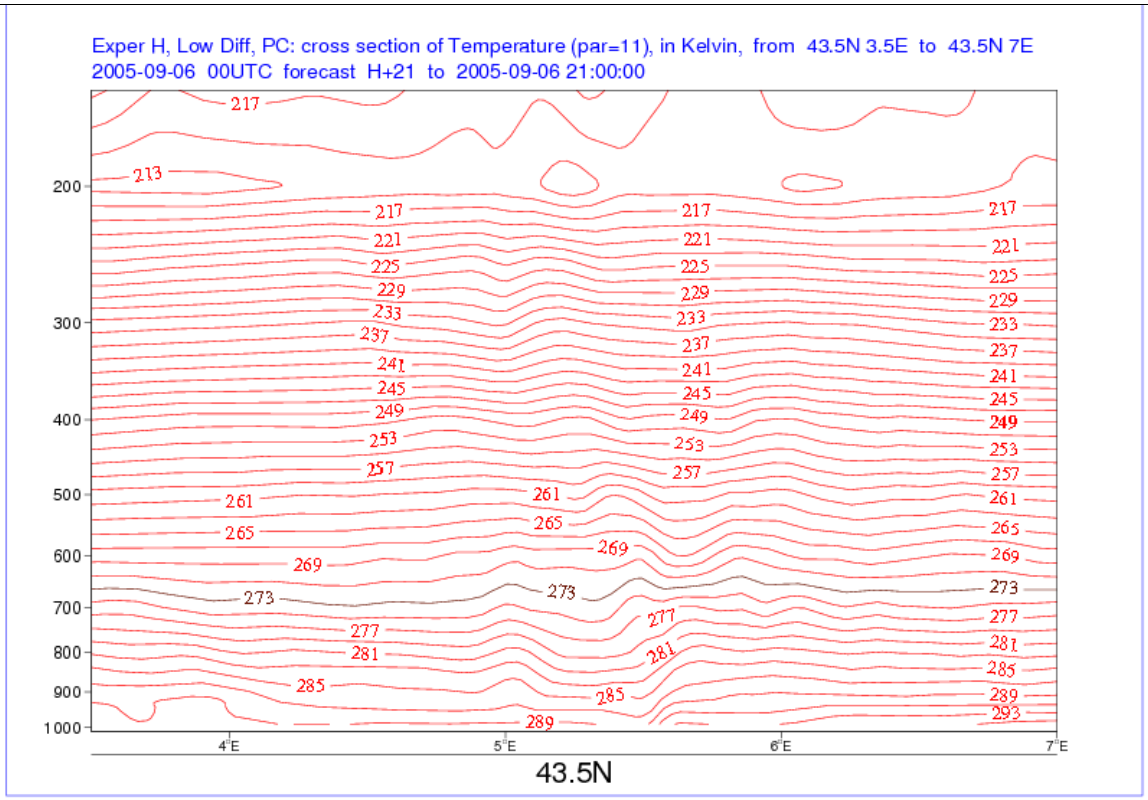

Figure 2.27 *H _ Low Diff _PC*: forecast H+21 of the Temperature (K) from 00UTC run of the 6th of September.

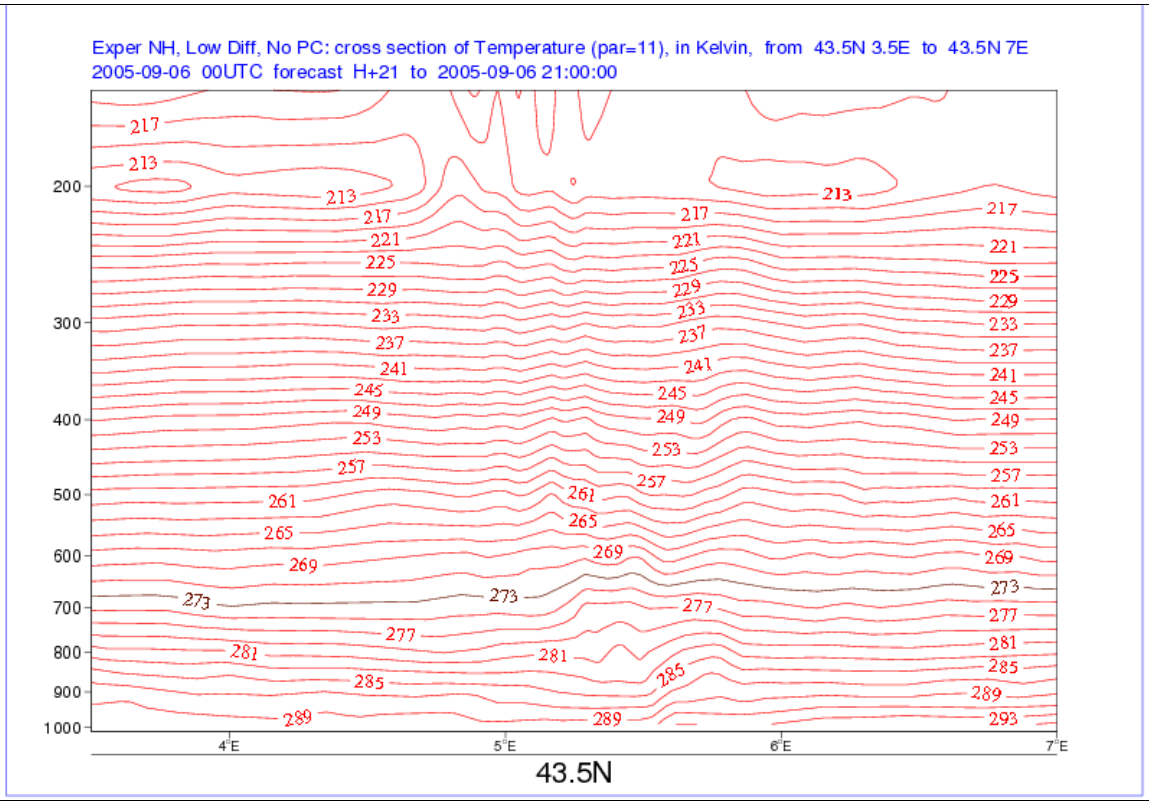

Figure 2.28 *NH _ Low diff _ No PC*: forecast H+21 of the Temperature (K) from 00UTC run of the 6th of September.

(B.2) Ice Crystal

By the analysis of the cross-sections of IC (figures 2.29-2.33), it can be verified that the forecasted fields derived from the experiments with the same intensity of diffusion (e.g., *Std Diff* or *Low Diff*) are much similar then the forecasts derived from the experiments with the same dynamical mode (e.g., *NH* or *H*). Consequently, the intensity of diffusion is more important than the dynamical mode on this case.

The forecasts of IC indicate high quantities of water in a very deep layer of the troposphere, between 550/450hPa and 200/150hPa approximately. This is in agreement with the existence of very thick convective clouds (*cumulonimbus*) in this region that most probably reached the tropopause.

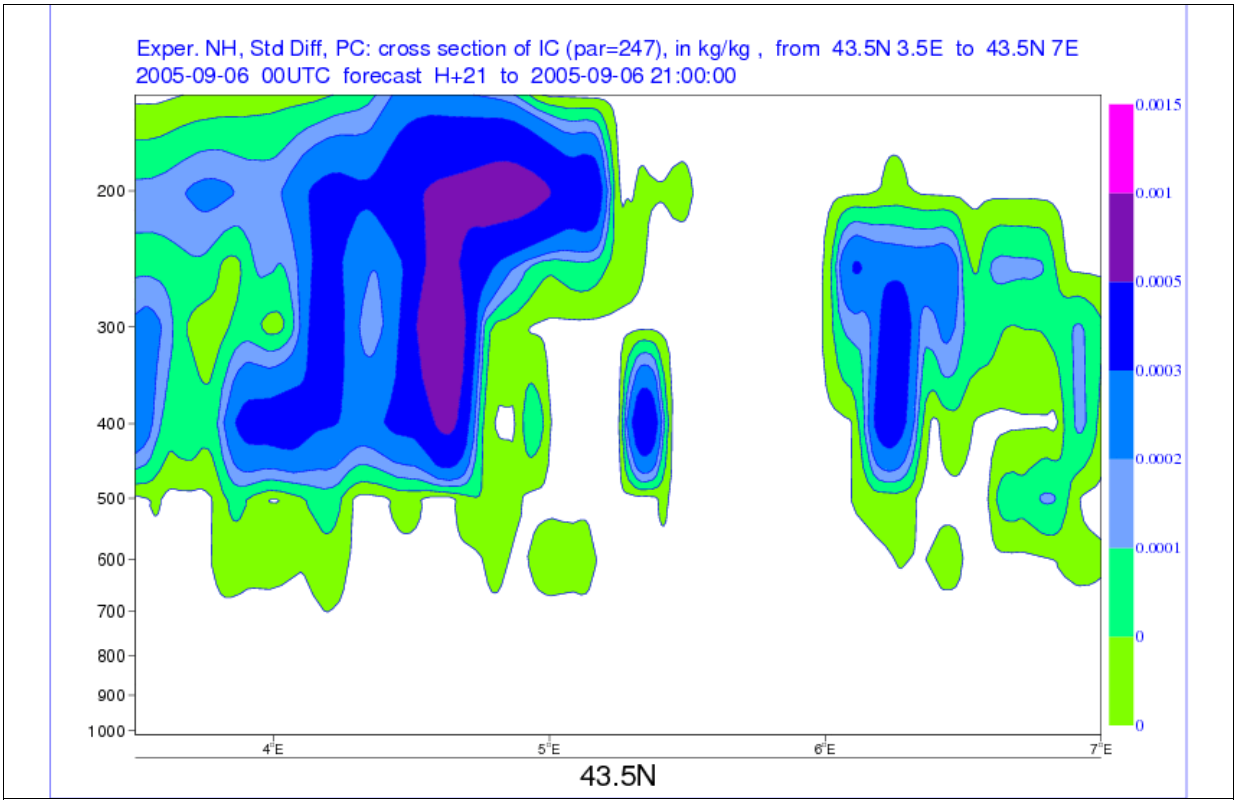

Figure 2.29 *NH _ Std Diff _PC*: forecast H+21 of the Ice Crystal (Kg Kg^{-1}) from 00UTC run of the 6th of September.

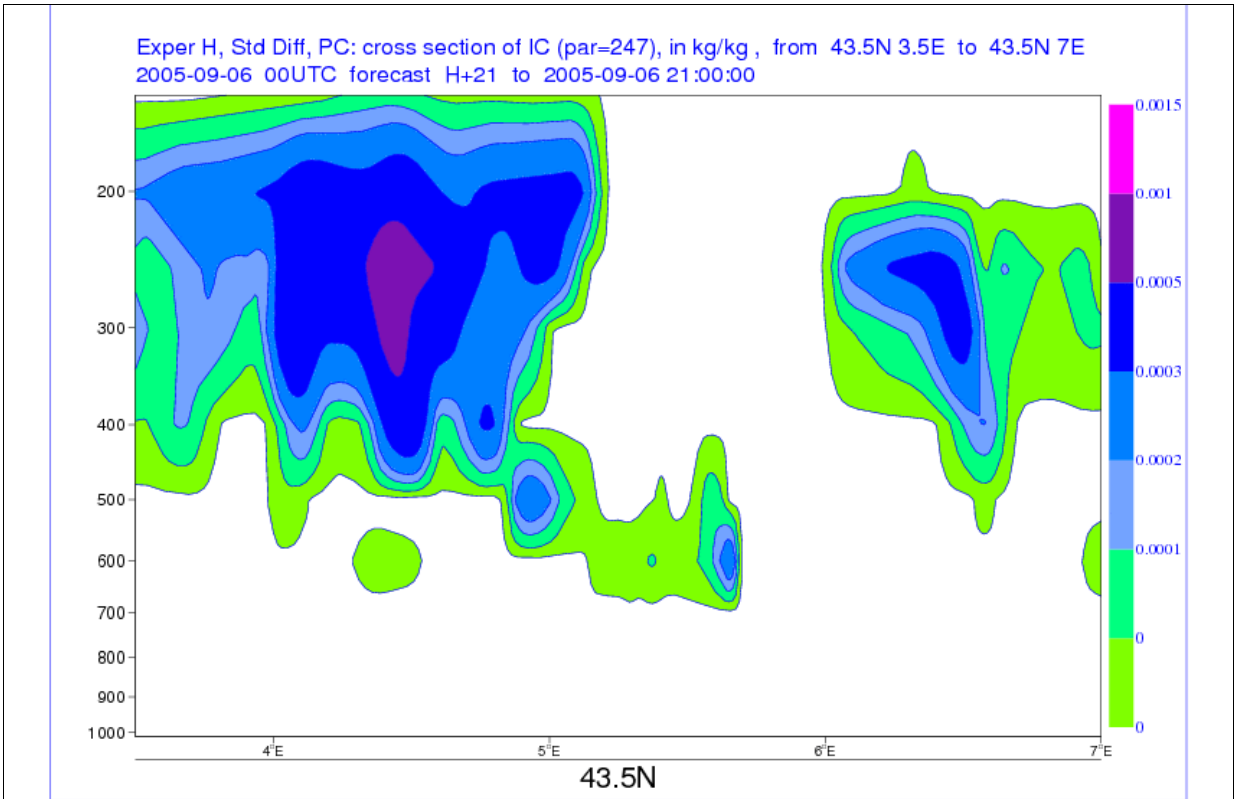

Figure 2.30 *H _ Std Diff _PC*: forecast H+21 of the Ice Crystal (Kg Kg^{-1}) from 00UTC run of the 6th of September.

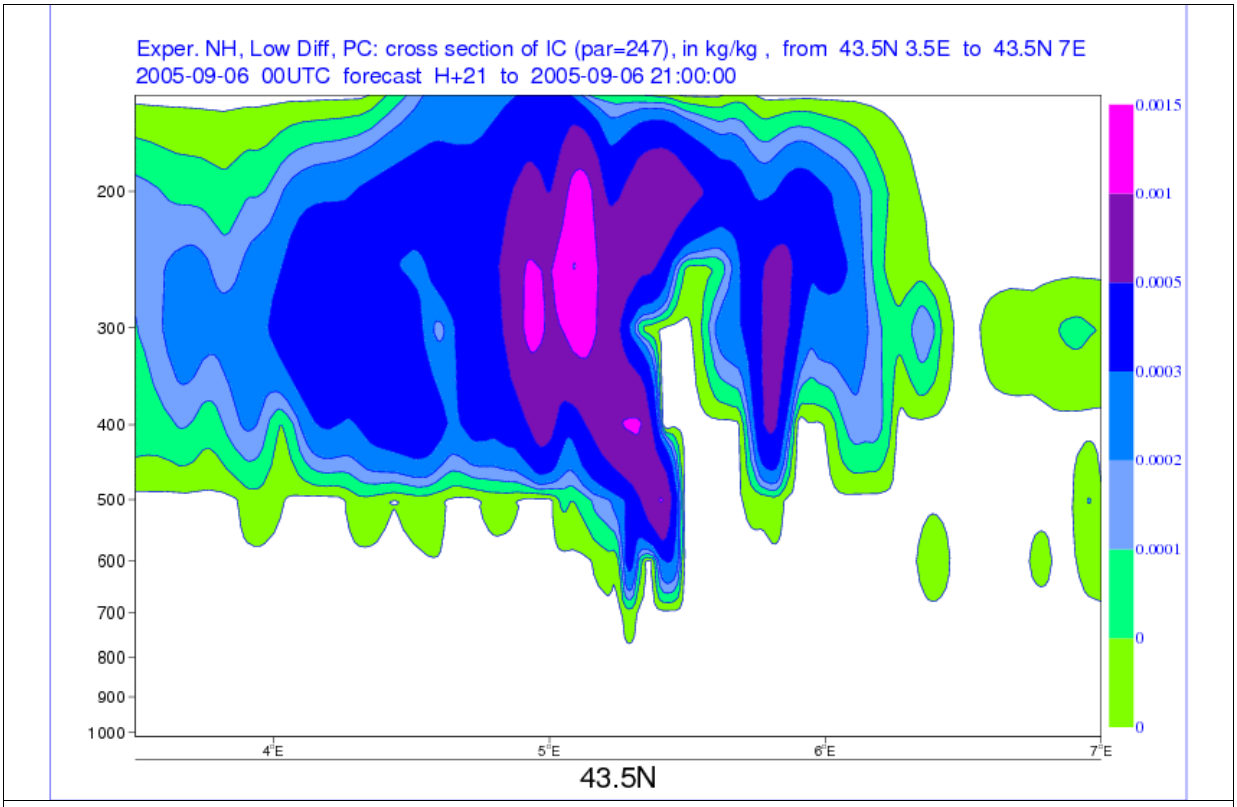

Figure 2.31 *NH _ Low Diff _ PC*: forecast H+21 of the Ice Crystal (Kg Kg^{-1}) from 00UTC run of the 6th of September.

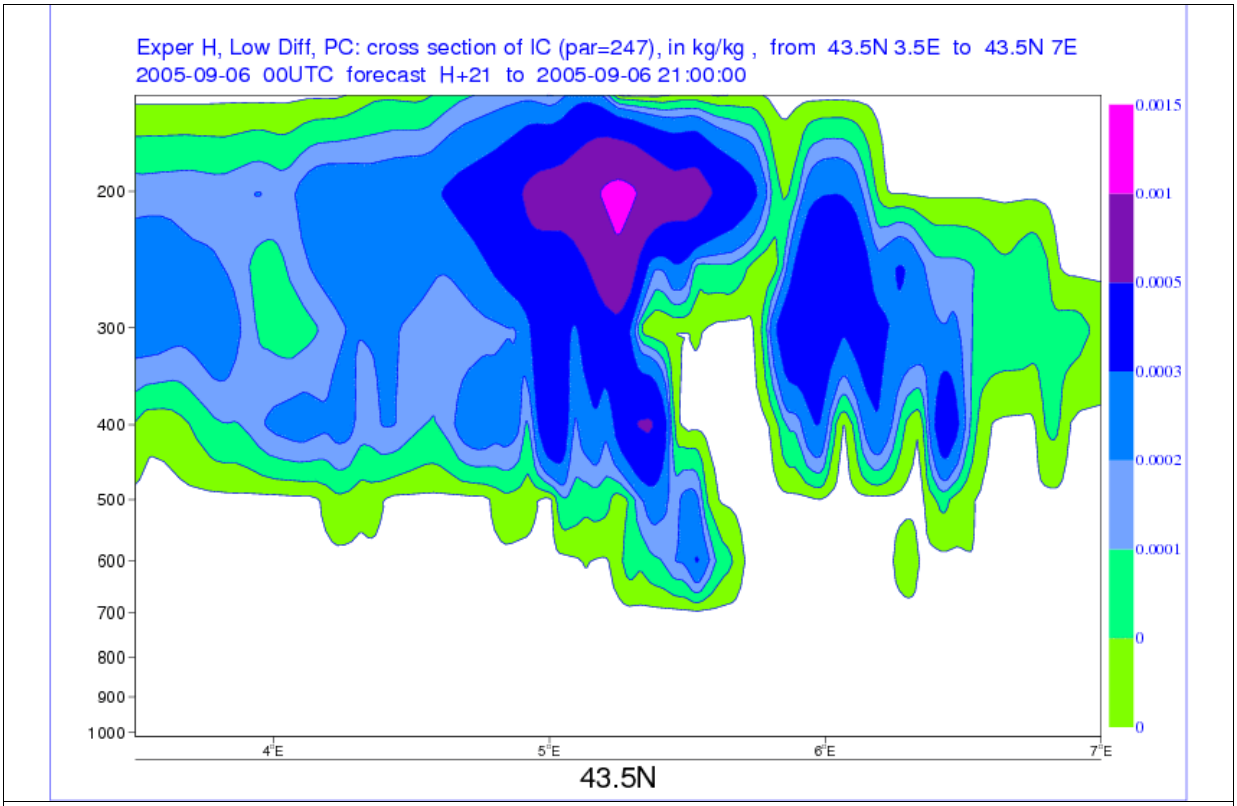

Figure 2.32 *H _ Low Diff _ PC*: forecast H+21 of the Ice Crystal (Kg Kg^{-1}) from 00UTC run of the 6th of September.

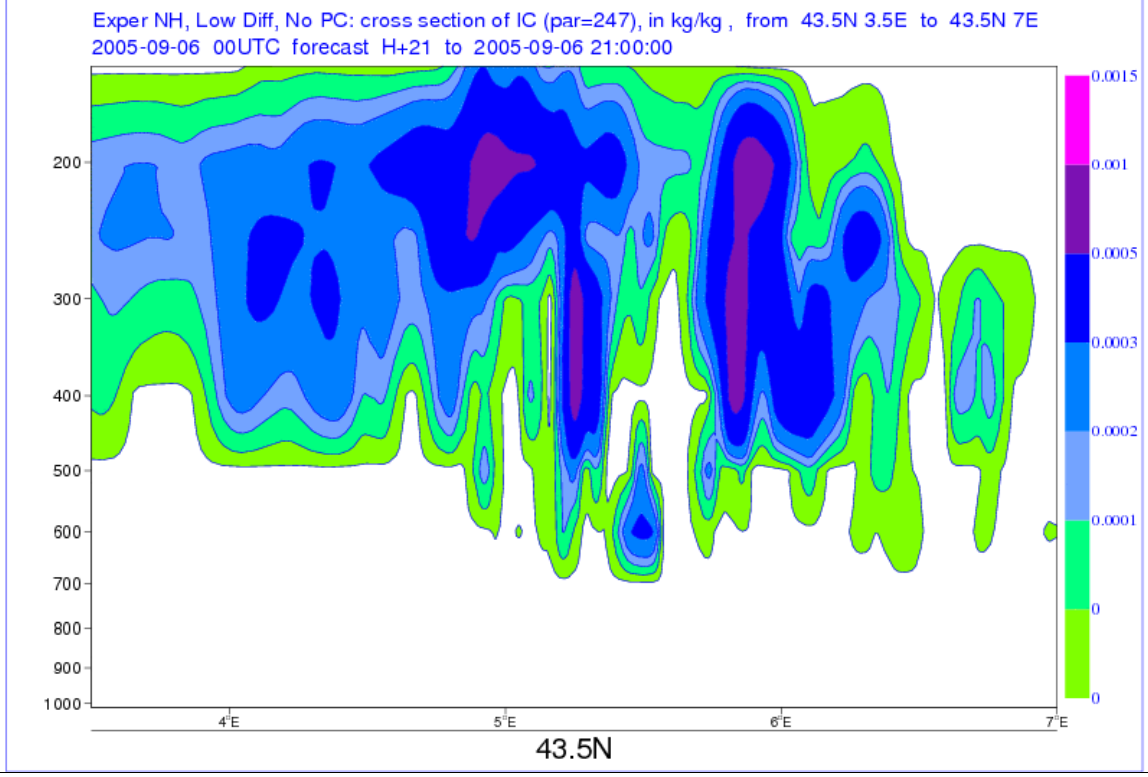

Figure 2.33 *NH _ Low Diff _ No PC*: forecast H+21 of the Ice Crystal (Kg Kg^{-1}) from 00UTC run of the 6th of September.

(B.3) Vertical velocity

With the comparison of the cross-sections of IC and the cross-sections of ω, it can be concluded that on the zones of high values of IC there are mostly upward motion that contributes to deep convection.

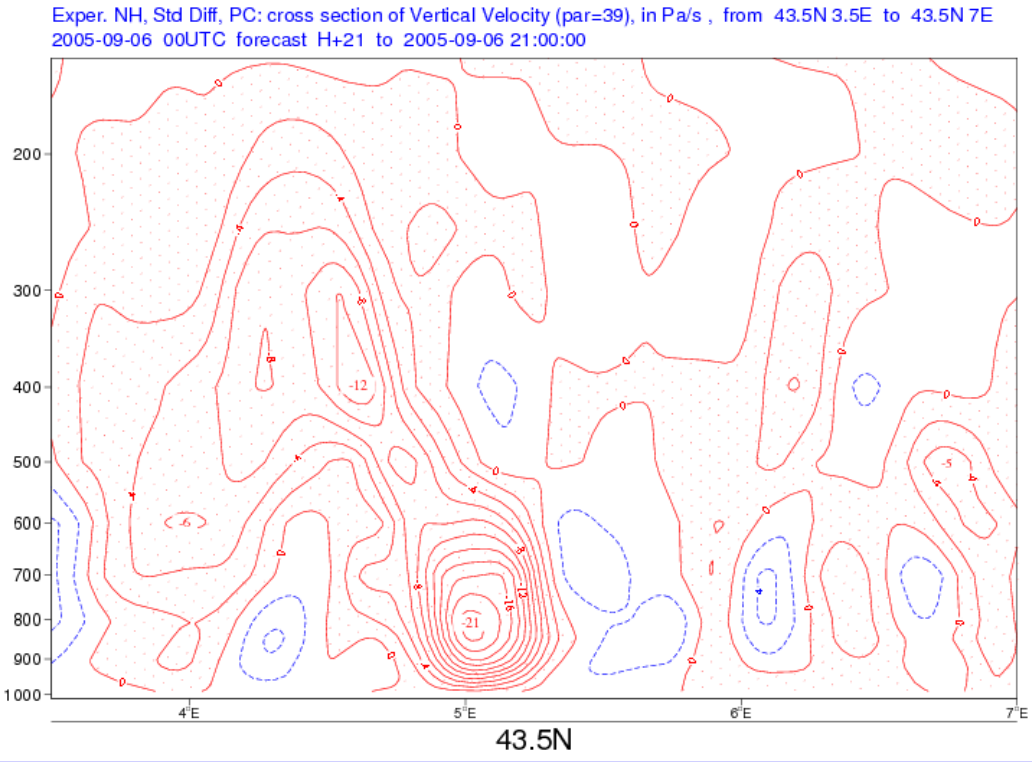

Figure 2.34 *NH _ Std Diff _ PC*: forecast H+21 of the Vertical Velocity (Pa s^{-1}) from 00UTC run of the 6th of September.

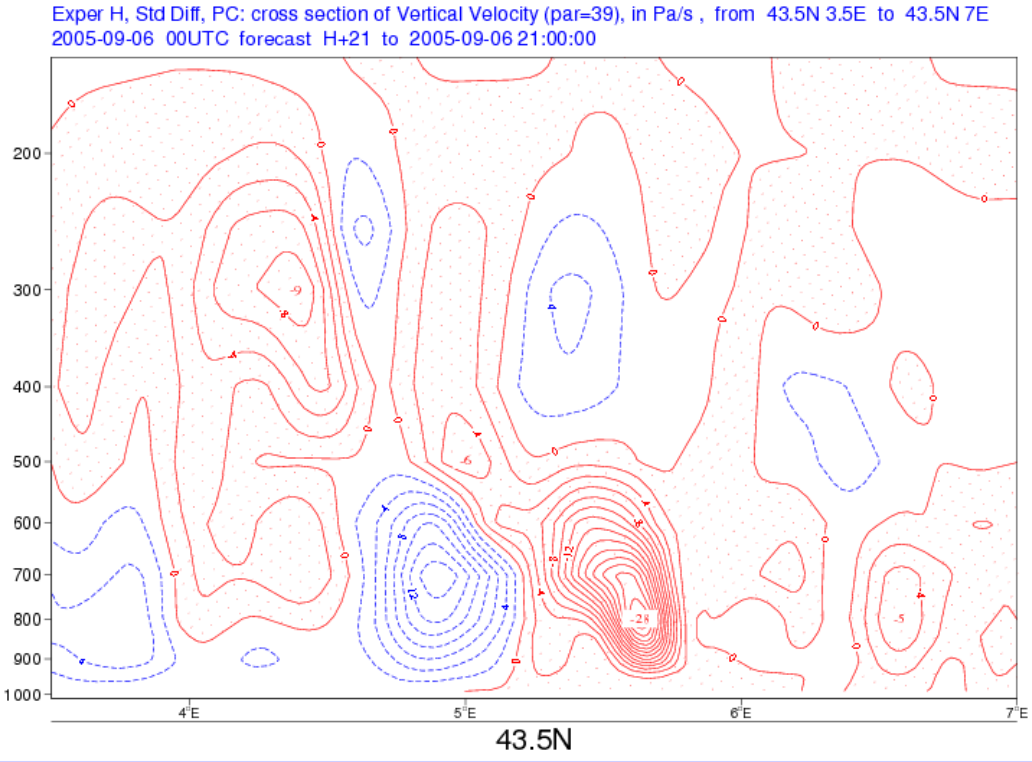

Figure 2.35 *H _ Std Diff _ PC*: forecast H+21 of the Vertical Velocity (Pa s^{-1}) from 00UTC run of the 6th of September.

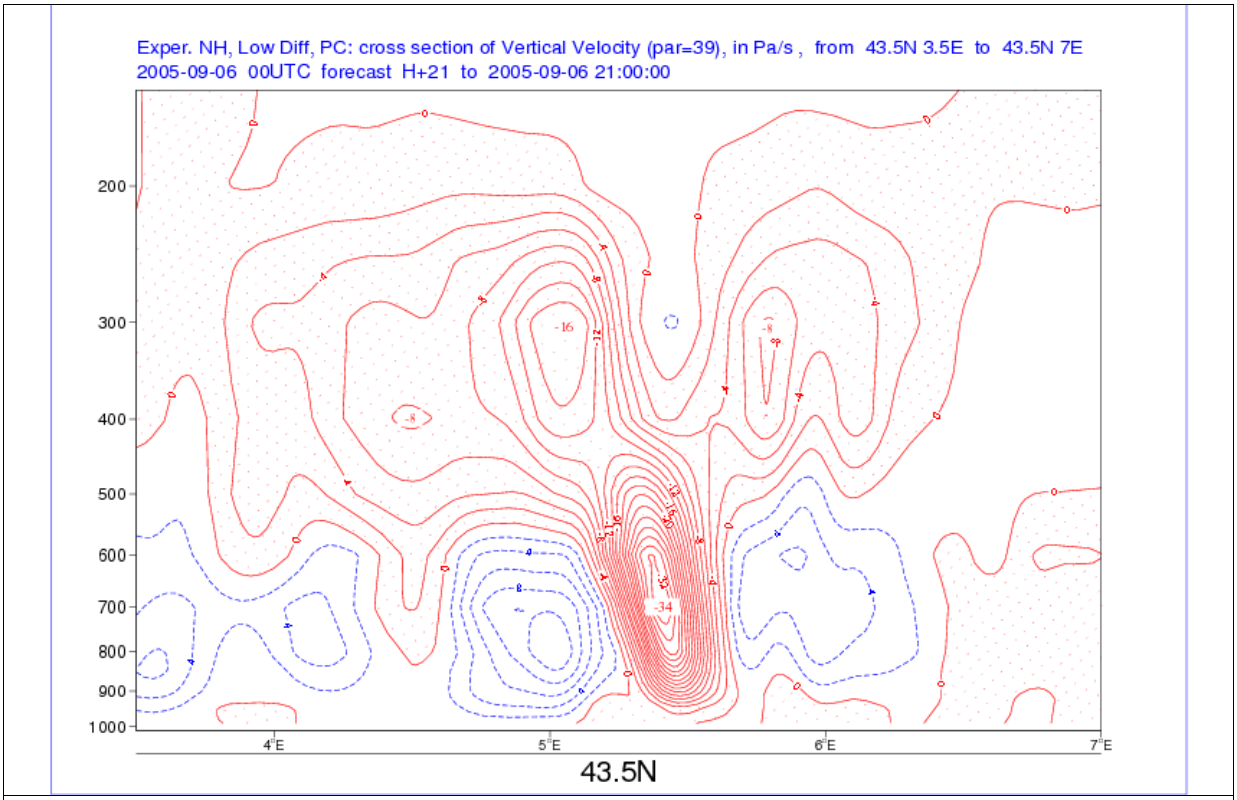

Figure 2.36 *NH _ Low Diff _ PC*: forecast H+21 of the Vertical Velocity (Pa s^{-1}) from 00UTC run of the 6th of September.

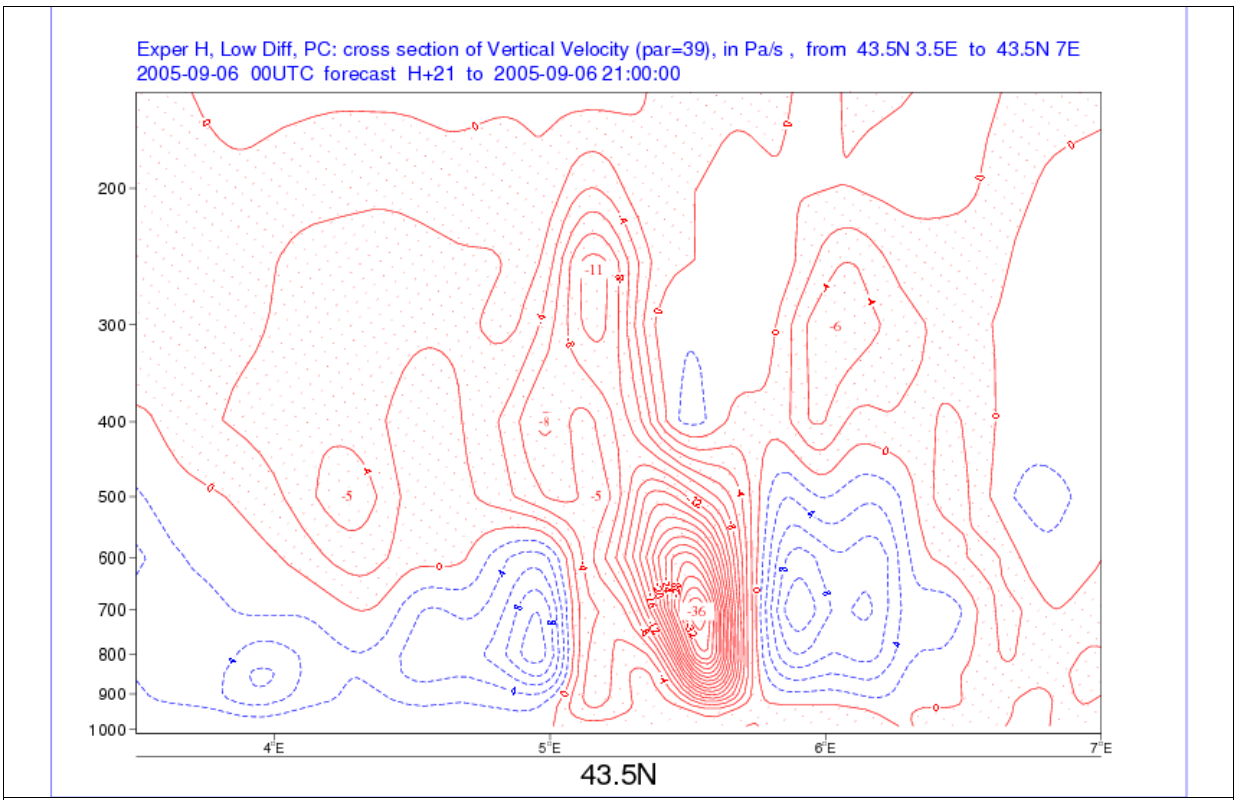

Figure 2.37 *H _ Low Diff _ PC*: forecast H+21 of the Vertical Velocity (Pa s^{-1}) from 00UTC run of the 6th of September.

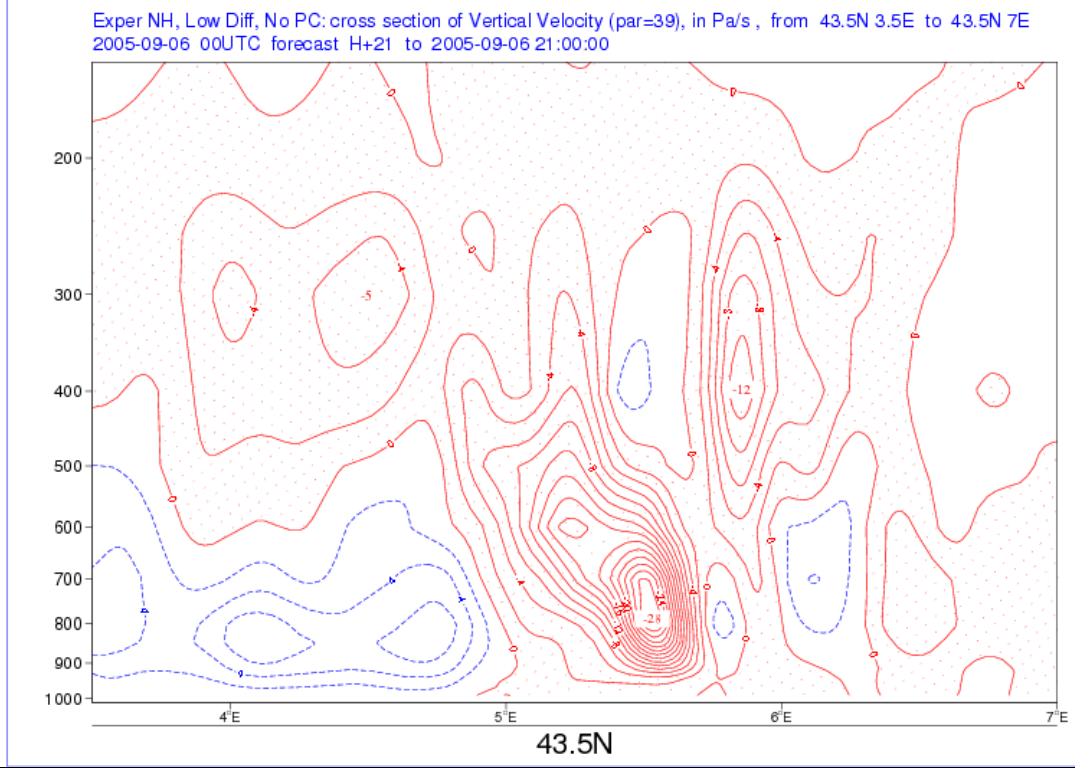

Figure 2.38 ***NH _ Low Diff _ No PC*****: forecast H+21 of the Vertical Velocity (Pa s^{-1}) from 00UTC run of the 6th of September.**

Some considerations for the case study of the 6th of September 2005:

♦ Forecasts of accumulated precipitation for the period 00-24h

- In general, the patterns of the accumulated precipitation produced by the experiments *NH _ Low Diff* are similar to the pattern of the same field derived from the experiment *NH _ Std Diff*.

- As would be expected, the precipitation field derived from the experiments *NH _ Low Diff* seems to be less smooth than the precipitation field produced by the *NH _ Std Diff* , showing the first fields more fragmented structures than the last one.

- All the forecasts derived from the *NH* experiments alert to the possibility of very heavy precipitation on the same regions.

- However, in the zones of deep convection where the amounts of precipitation are very high the differences between the experiments *Low diff* and the experiment *Std Diff* can be very significant.

♦ Forecasted fields for 21h

- As would be expected, the magnitude of pressure departure is stronger on the zones with deep convection.

- The pressure departure derived from the experiment *Low diff _ No PC* presents a non-physical behaviour which means that the Predictor/Corrector can be important on this case.

- The maximum magnitude of pressure departure derived from the *Low Diff _ PC* is around 2 times bigger than the one derived from the *Std Diff._ PC.*

- The forecasts of ω and RH produced by the *NH* experiments present only small differences to the same forecasts produced by the *H* experiments.

- On the forecasts of IC, the intensity of diffusion seems to be more important than the dynamical mode: the forecasts derived from the experiments with the same intensity of diffusion are much similar than the ones derived from the experiments with identical dynamical mode.

3. – AROME experiments for the 21th of November 2007

On this frontal situation two *NH* experiments with Low Diffusion and No Predictor/Corrector were made: one with the AROME shallow cumulus convection scheme from the cycle al32t3_arome-main.01 (REF version); the other one with a new shallow cumulus convection scheme from a tested version (Malardel, 2007).

The area used on this case is FRAN004.

3.1 Forecasts of the low cloud cover (LCC) for 09UTC and 12UTC

Looking at the image of the visible channel for 09UTC (figure 3.1), is possible to identify some bands of low clouds (with light grey tonality) on the South of England and on the Western Part of France, following the extensive band of thick cloudiness (white and bright) associated to a cold front (source: *Images Satellite des 20 derniers jours 1536*1536 fixes* http://www.meteo.fr/test/meteotel/pics/MSGJJHH_new.htm).

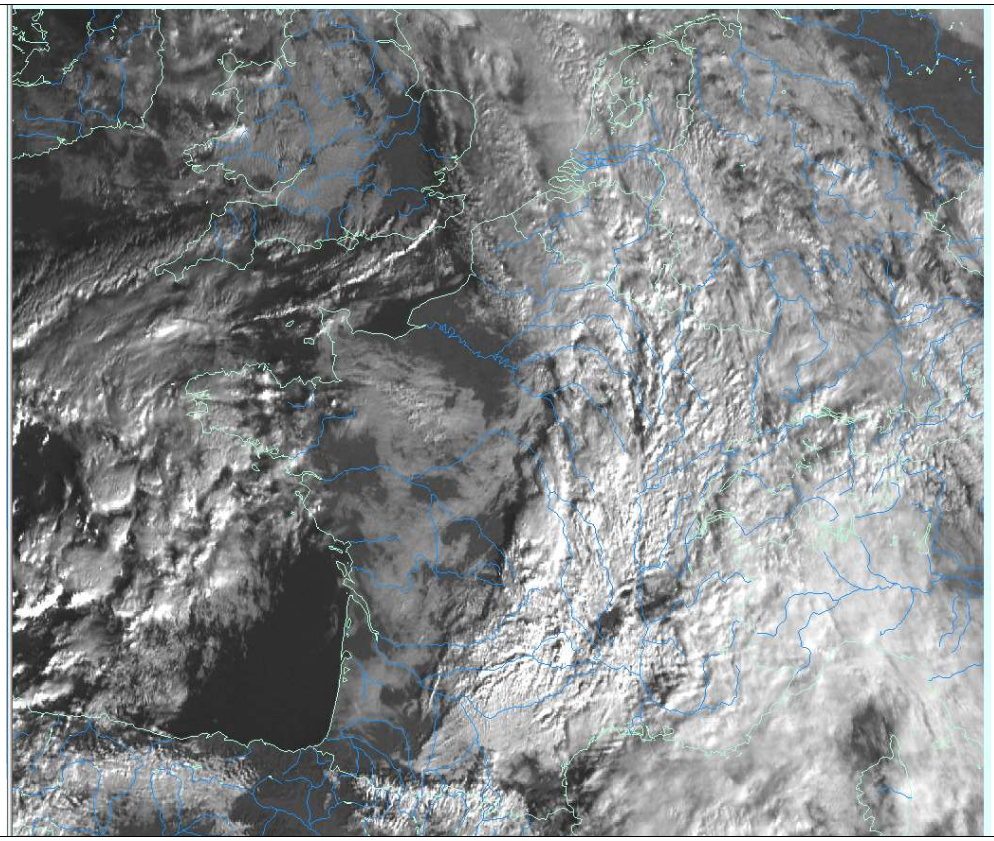

Figure 3.1 MGS: image from the visible channel for 09UTC of the 21th of November.

By the comparison of the forecasts (figures 3.2 and 3.3) with the satellite image, it can be verified that the forecasts are similar and give a general idea of the zones with low clouds. However, the forecasts overestimate these clouds a little on the Western Part of France and over sea, close to the parallel 45° and between France and England.

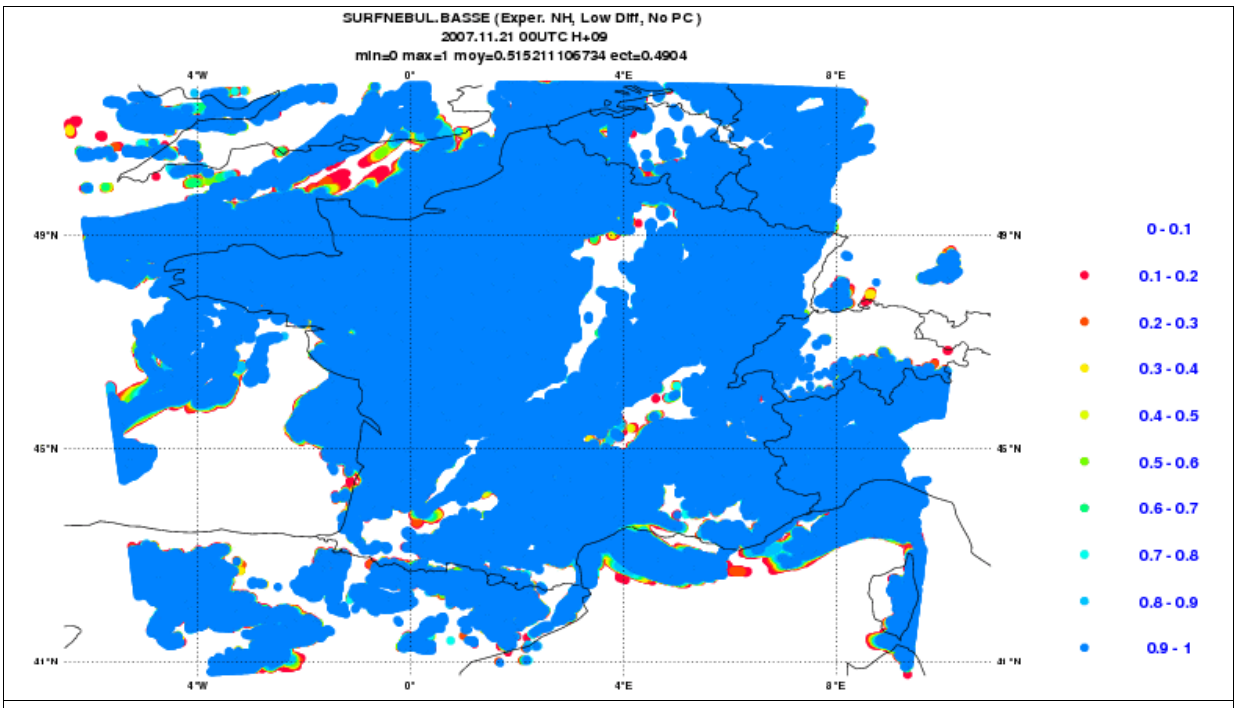

Figure 3.2 *NH _ Low Diff _ No PC* (REF version): forecast H+09 of LCC from the 00UTC run of the 21th of November.

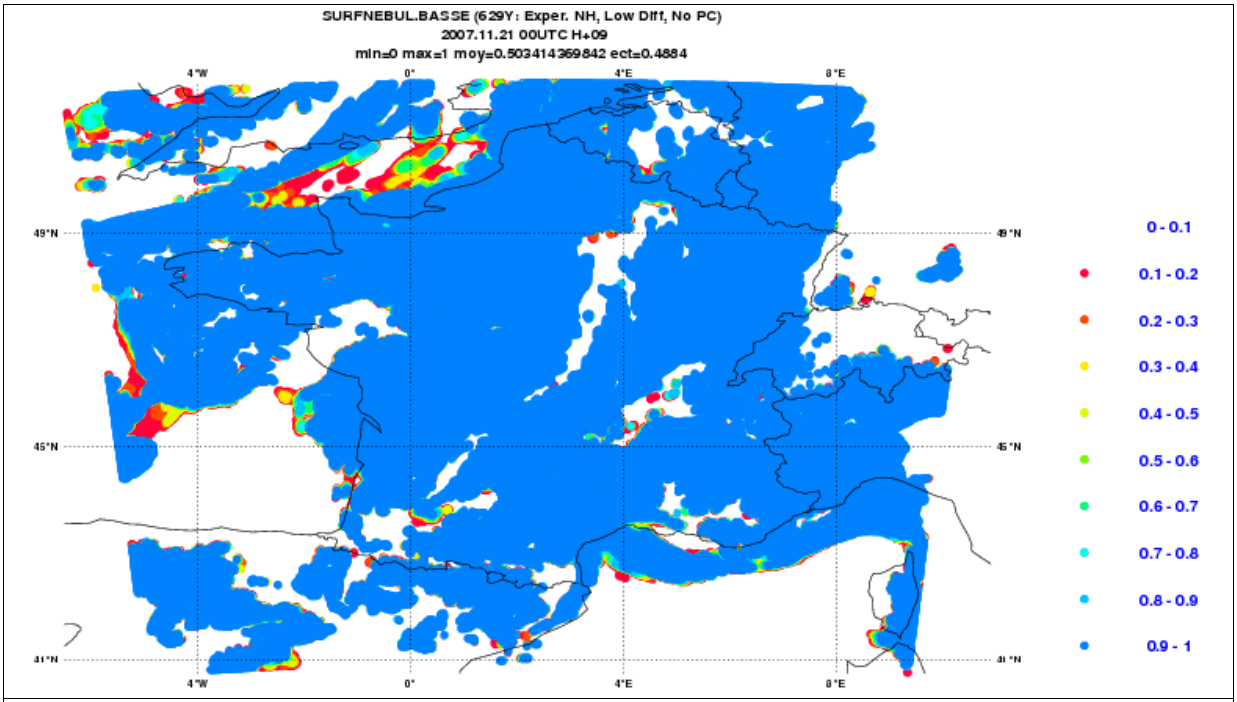

Figure 3.3 *NH _ Low Diff _ No PC* (tested version): forecast H+09 of LCC from the 00UTC run of the 21th of November.

At 12UTC most part of the low clouds are already dissipating over land (figure 3.4) due to the surface warming. The comparison of this image with the forecasts for the same hour (figures 3.5 and 3.6) leads to identical conclusions to those made for the 09h forecasts.

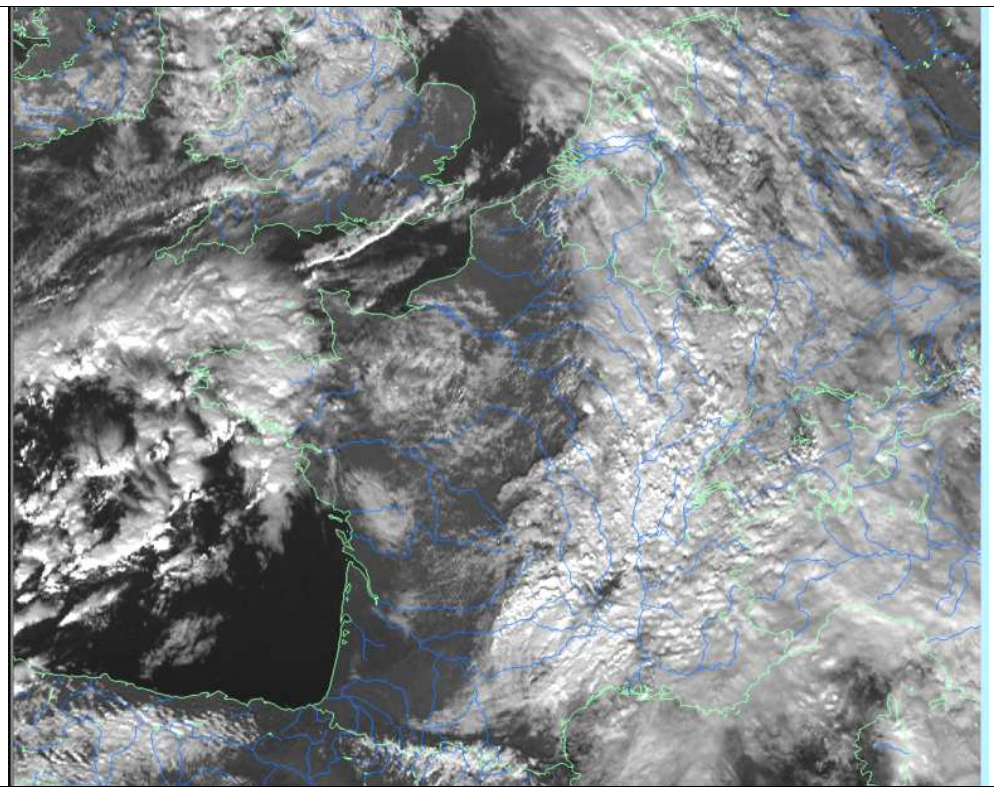

Figure 3.4 MGS: image from the visible channel for 12UTC of the 21th of November.

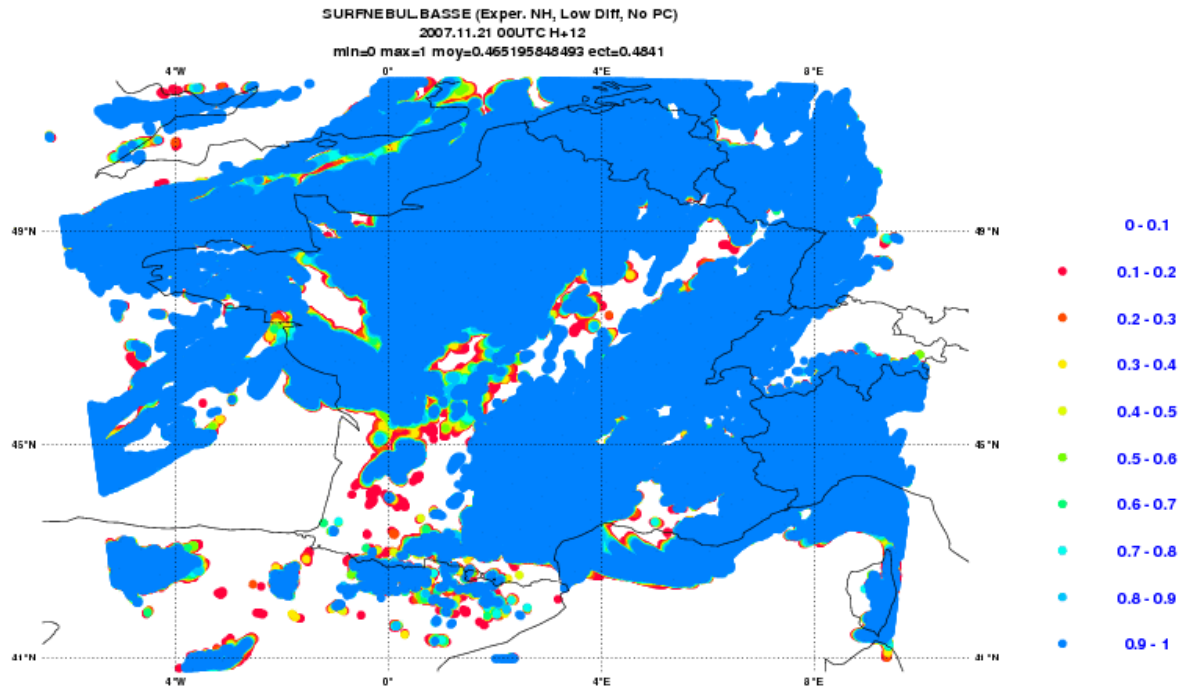

Figure 3.5 *NH _ Low Diff _ No PC* (REF version): forecast H+12 of LCC from the 00UTC run of the 21th of November.

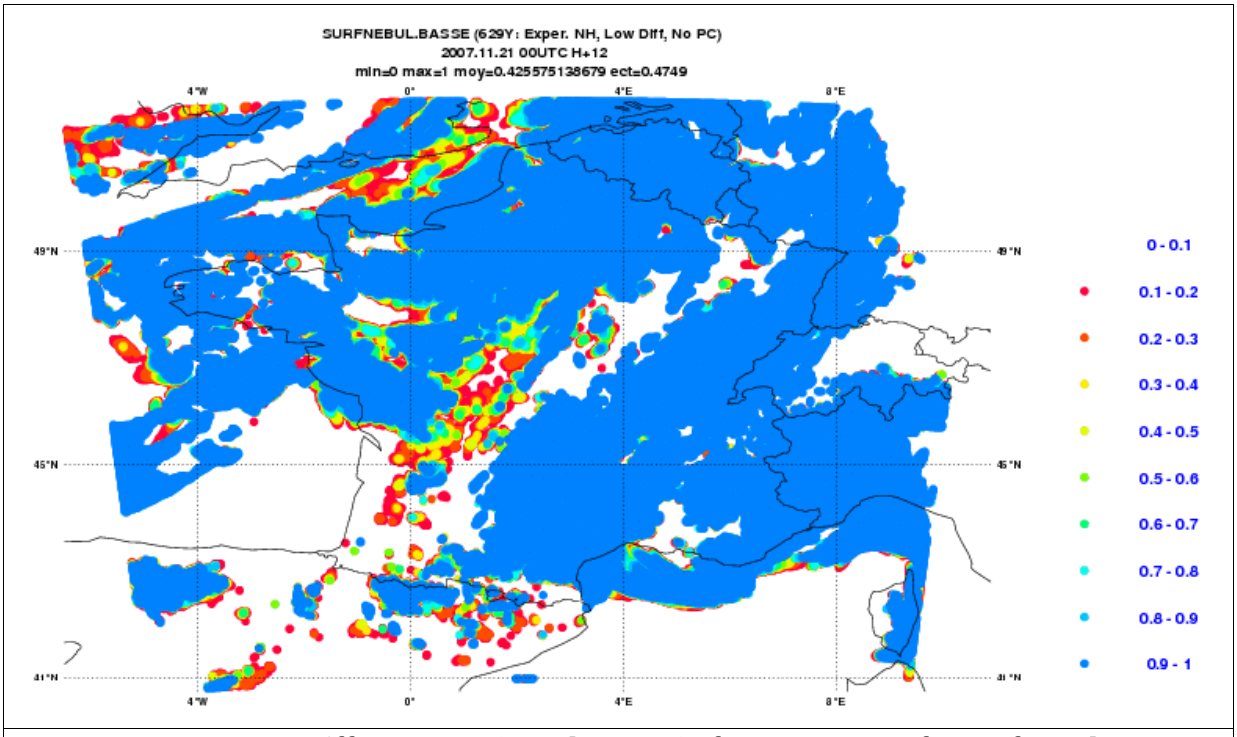

Figure 3.6 *NH _ Low Diff _ No PC* (tested version): forecast H+12 of LCC from the 00UTC run of the 21th of November.

3.2 Forecasts of precipitation

(A) Accumulated from 9 to 12UTC and from 12 to 15UTC

The sequence of the composites of the RADAR image – intensity of precipitation – with the lightening strikes information (figures 3.7-3.9) gives an approximated idea of the activity and the evolution of the frontal system on the period 09-15UTC (*source: http://www.meteo.fr/test/meteotel/pics/DEP/FOUDREMMJJHH.HTM*).

By the comparison of the forecasts of the accumulated precipitation for the period from 9 to 12UTC (figures 3.10-3.12) and for the period from 12 to 15UTC (figures 3.13-3.15), it can be concluded that:

- For each period, the forecast derived from the REF version is similar to the forecast derived from the tested version.

- Furthermore, the regions with forecasted heavy precipitation are the same.

- The differences of the accumulated precipitation are small on the frontal zone and only locally significant on the post-frontal zone, where the convective activity was more intensive (as shown by the lightening strikes information).

- The location of the forecasted precipitation bands is consistent with the information provided by the composites. Furthermore, the most active zones (e.g.,

with lightening strikes and higher intensities of precipitation) show a good superimposition with the areas of high amounts of forecasted precipitation.

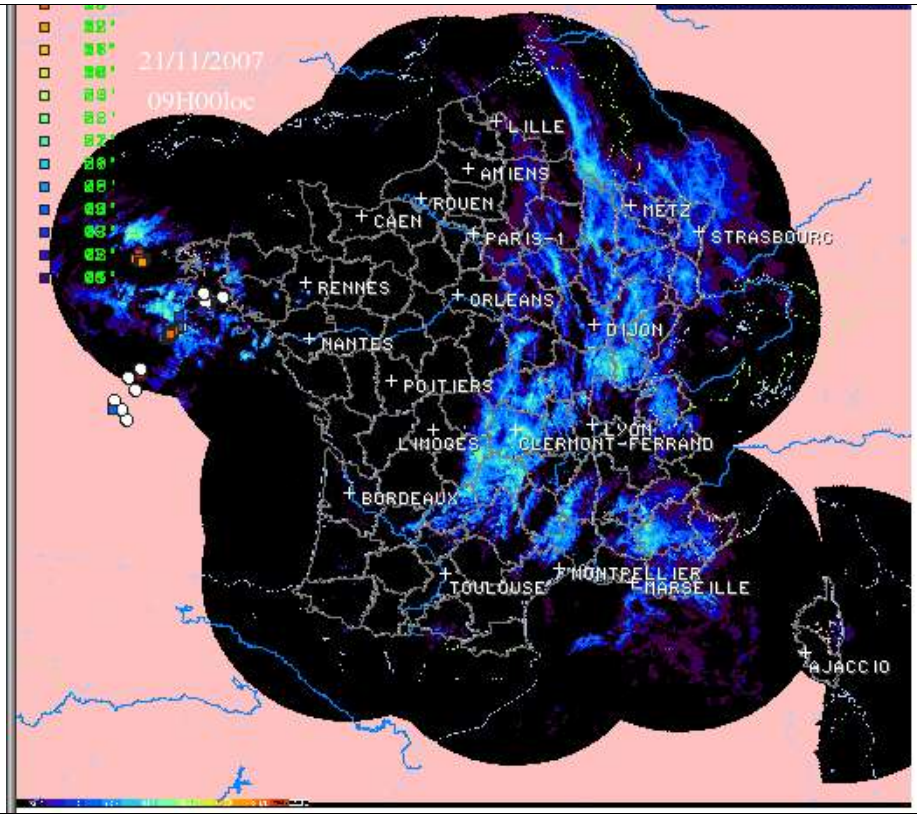

Figure 3.7 Composite of the RADAR image – precipitation intensity (mm/h) - for 09UTC with the lightening strikes occurred on the last 3h.

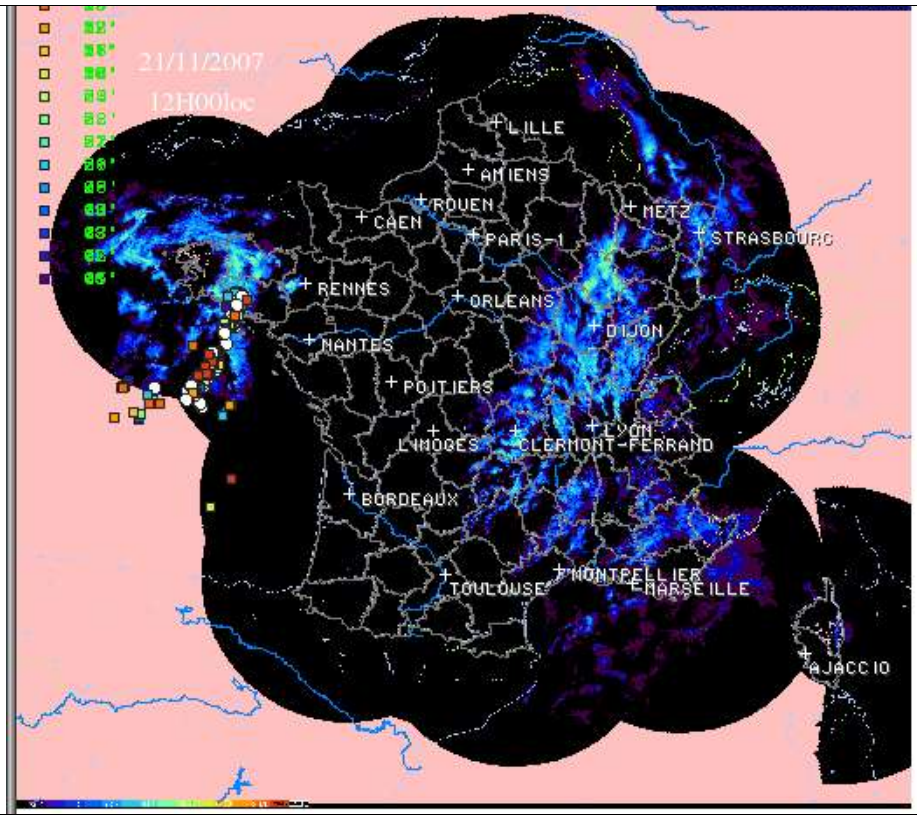

Figure 3.8 Composite of the RADAR image – precipitation intensity (mm/h) - for 12UTC with the lightening strikes occurred on the last 3h.

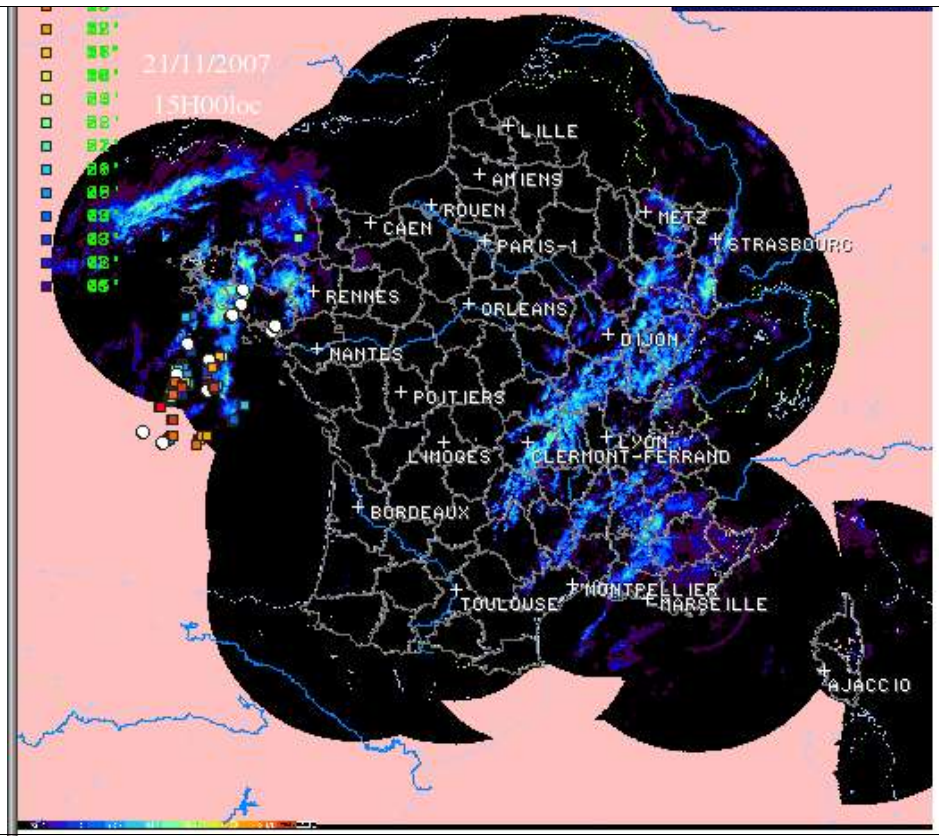

Figure 3.9 Composite of the RADAR image – precipitation intensity (mm/h) - for 15UTC with the lightening strikes occurred on the last 3h.

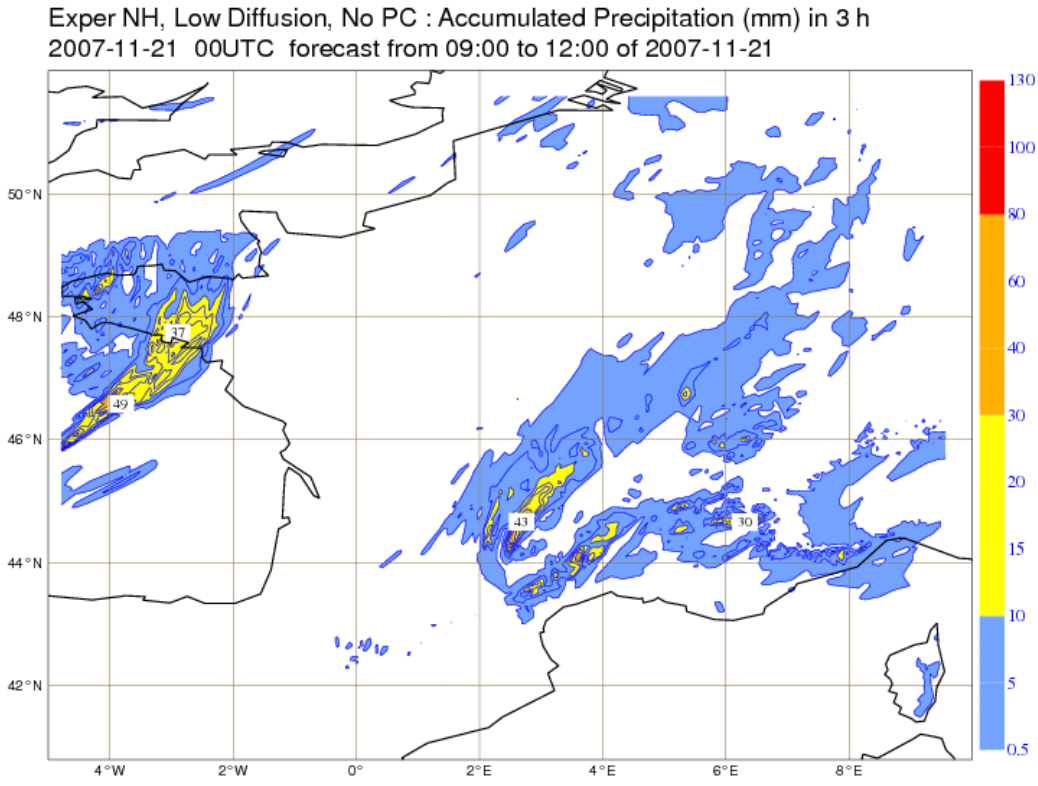

Figure 3.10 *NH _ Low Diff _ No PC* (REF version), run 00UTC: forecast of the accumulated precipitation (mm) for the period 09-12UTC of the 21th of November (cylindrical projection).

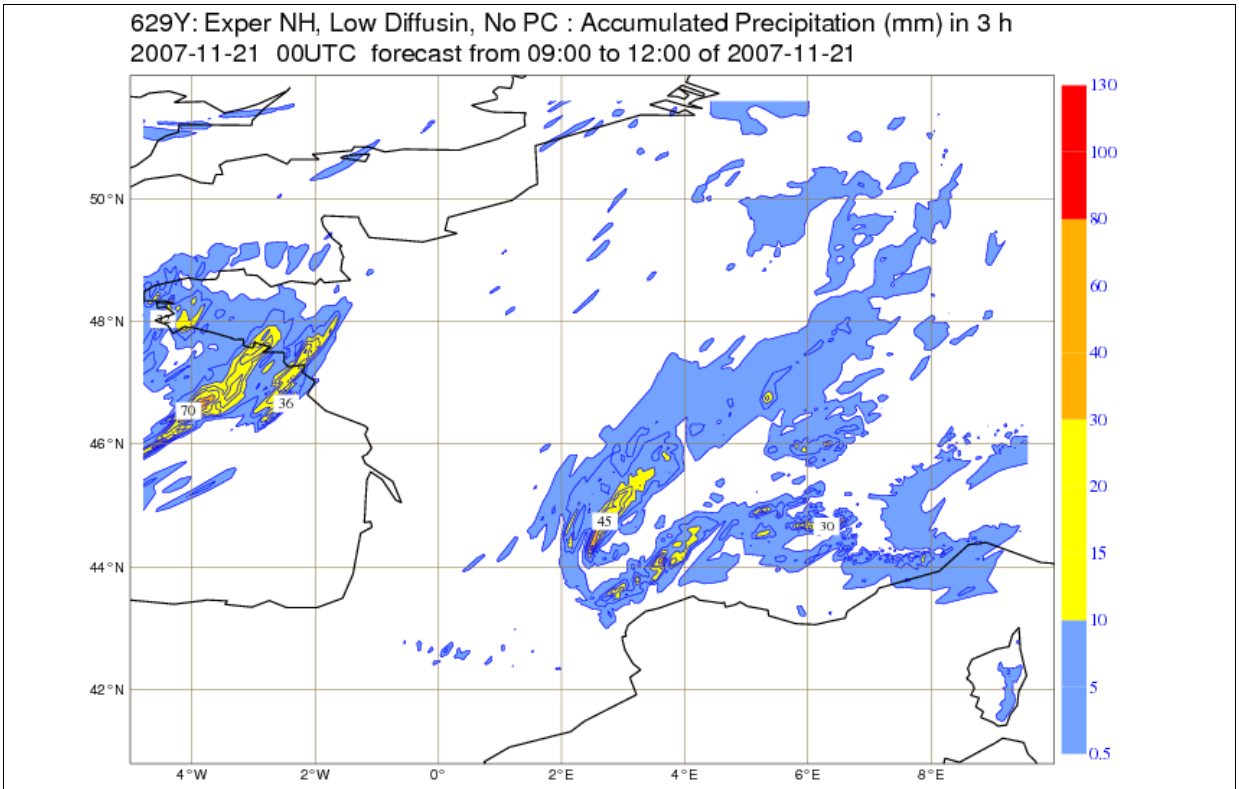

Figure 3.11 *NH _ Low Diff _ No PC* (tested version), run 00UTC: forecast of the accumulated precipitation (mm) for in the period 09-12UTC of the 21th of November (cylindrical projection).

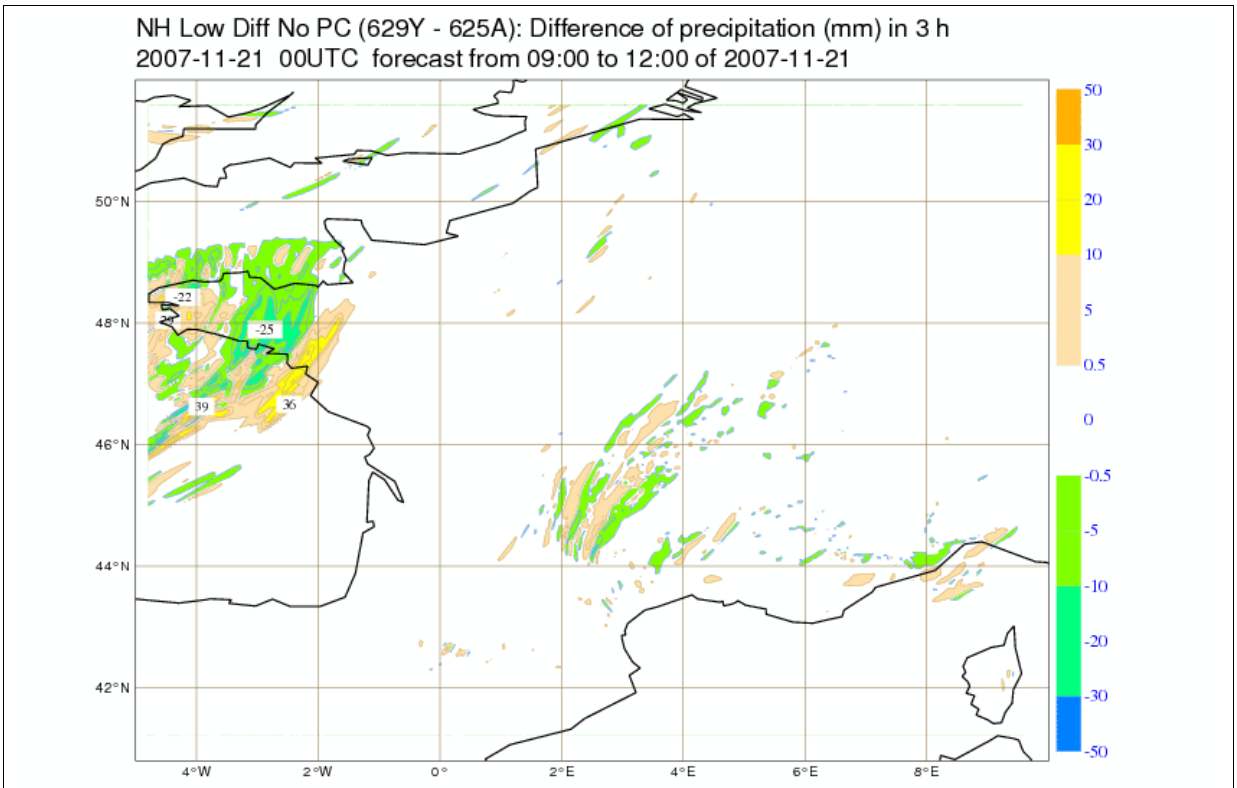

Figure 3.12 Difference between the forecasts of the accumulated precipitation (mm) [tested version – REF version] in the period 09-12UTC of the 21th of November (cylindrical projection).

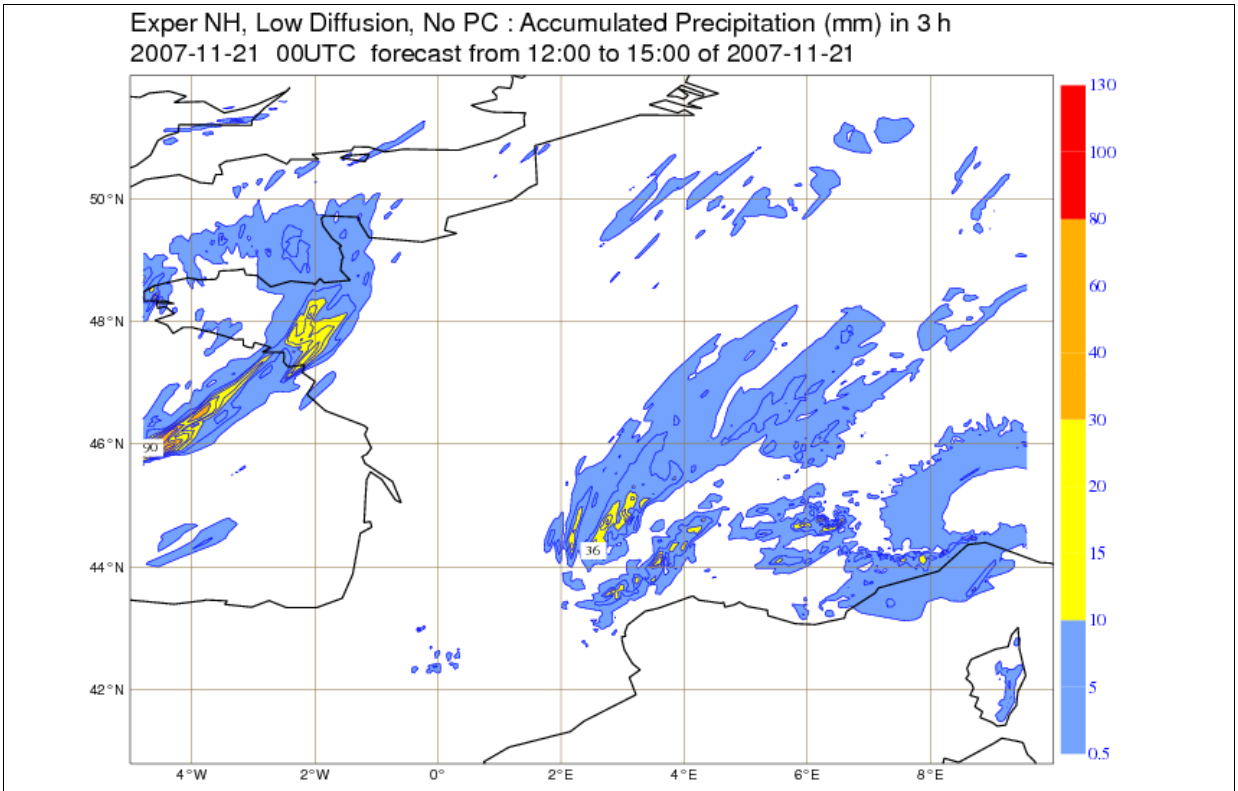

Figure 3.13 *NH _ Low Diff _ No PC* (REF version), run 00UTC: forecast of the accumulated precipitation (mm) in the period 12-15UTC of the 21th of November (cylindrical projection).

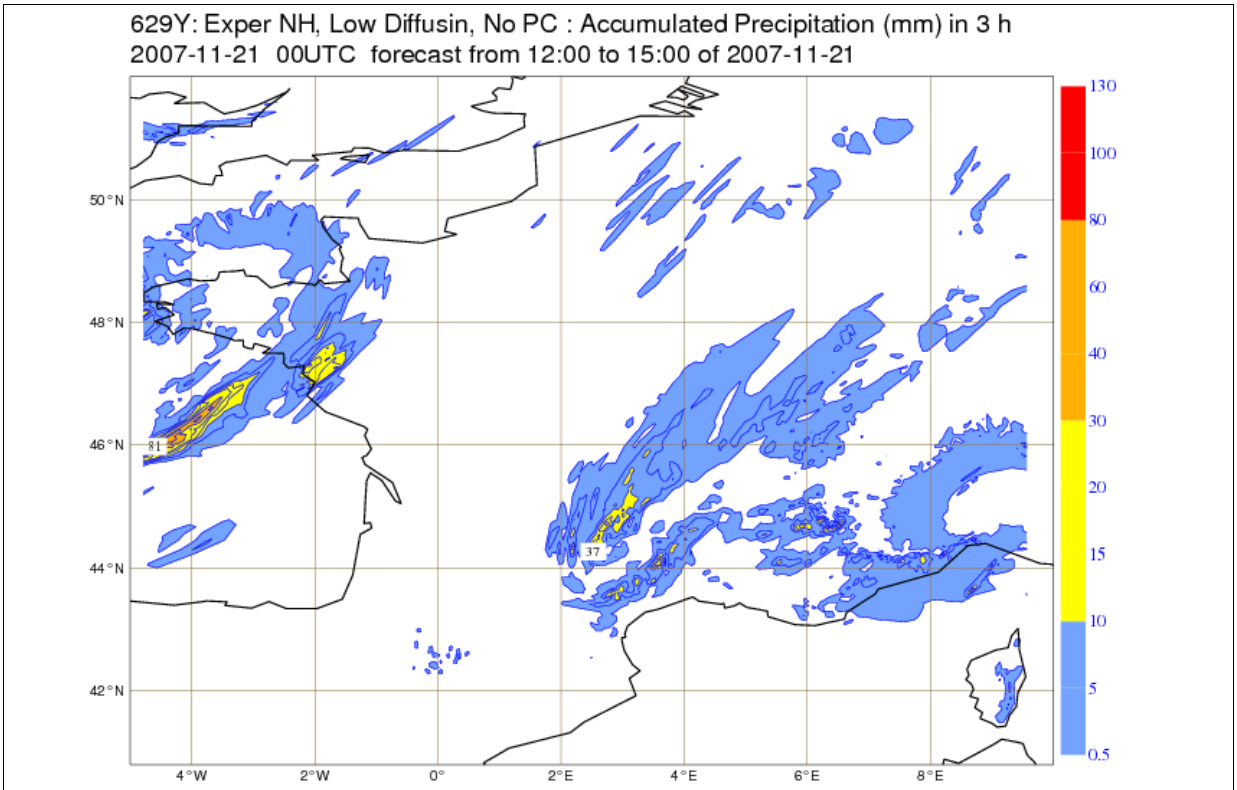

Figure 3.14 *NH _ Low Diff _ No PC* (tested version), run 00UTC: forecast of the accumulated precipitation (mm) in the period 12-15UTC of the 21th of November (cylindrical projection).

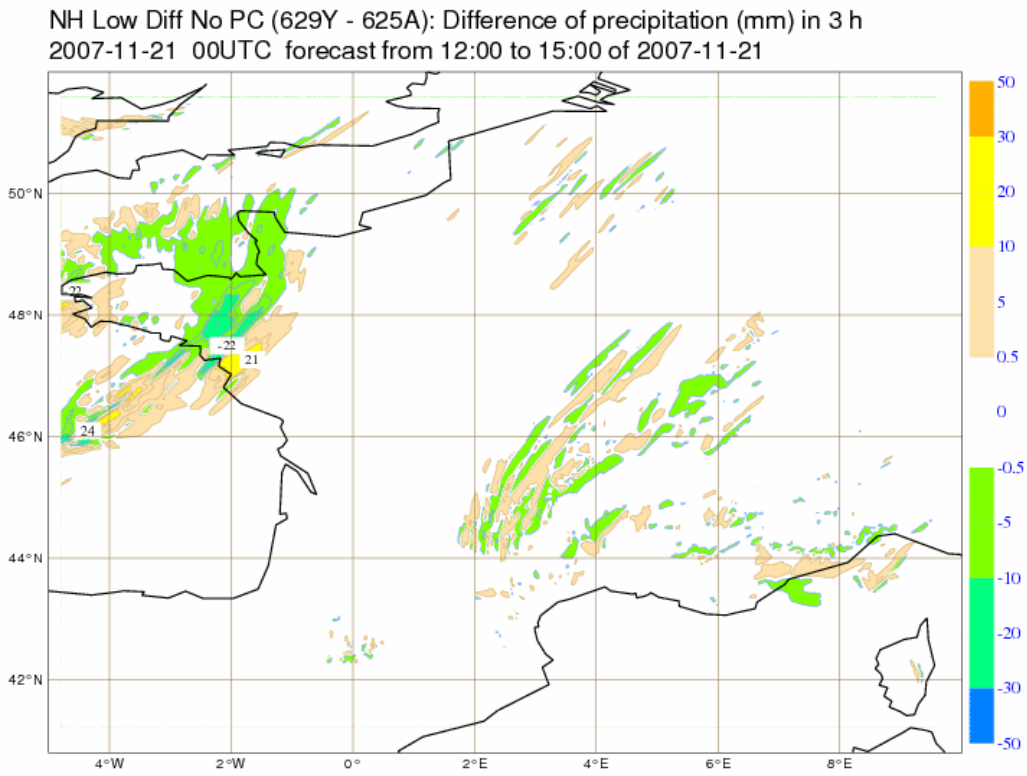

Figure 3.15 Difference between the forecasts of the accumulated precipitation (mm) [tested version – REF version] in the period 12-15UTC of the 21th of November (cylindrical projection).

(B) Accumulated from 00UTC to 24UTC

With the analysis of the forecasted accumulated precipitation in 24h, it is verified that:

- The patterns of the precipitation fields are very similar (figures 3.16 and 3.17).

- On the frontal zone the differences of accumulated precipitation (figure 3.18) are in general small while on the regions of the post-frontal zone where the convective activity was strong the differences are locally very significant.

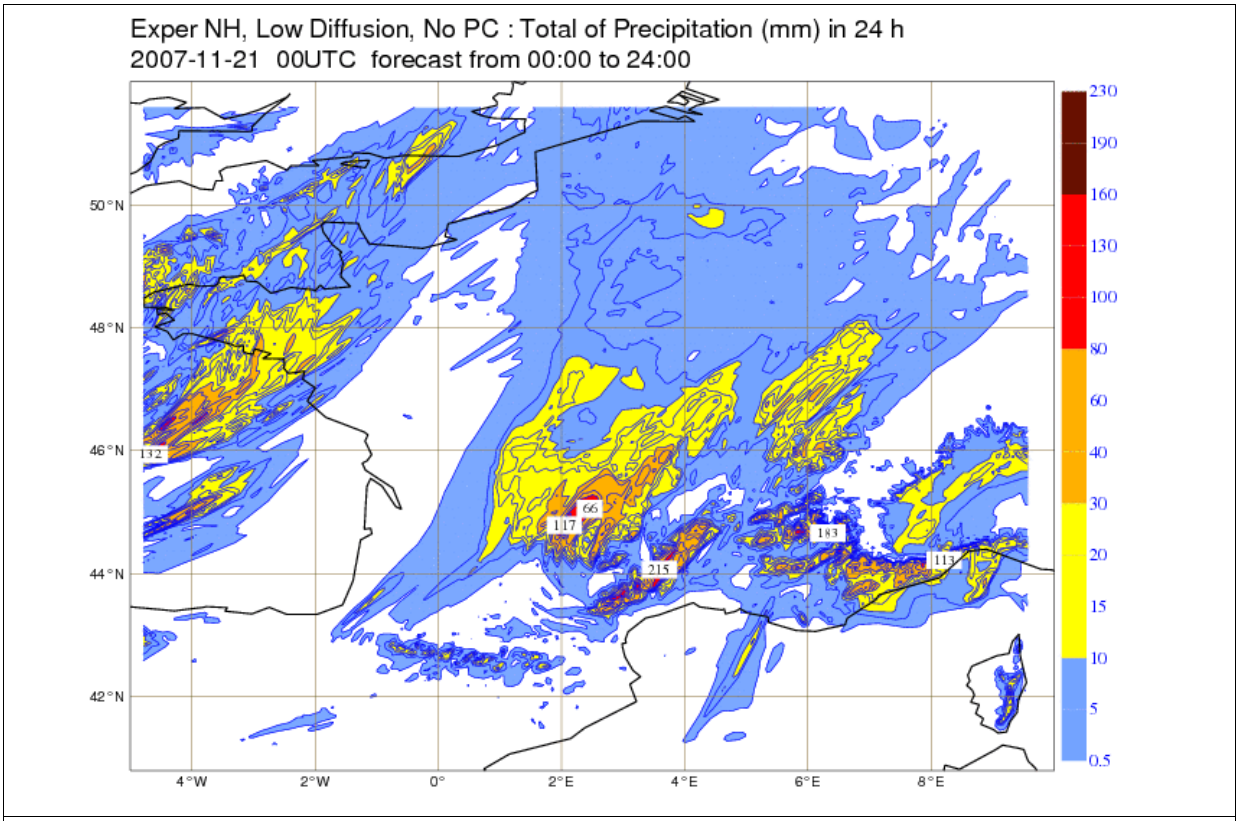

Figure 3.16 *NH _ Low Diff _ No PC* (REF version), run 00UTC: forecast of the accumulated precipitation (mm) in the period 00-24UTC of the 21th of November (cylindrical projection).

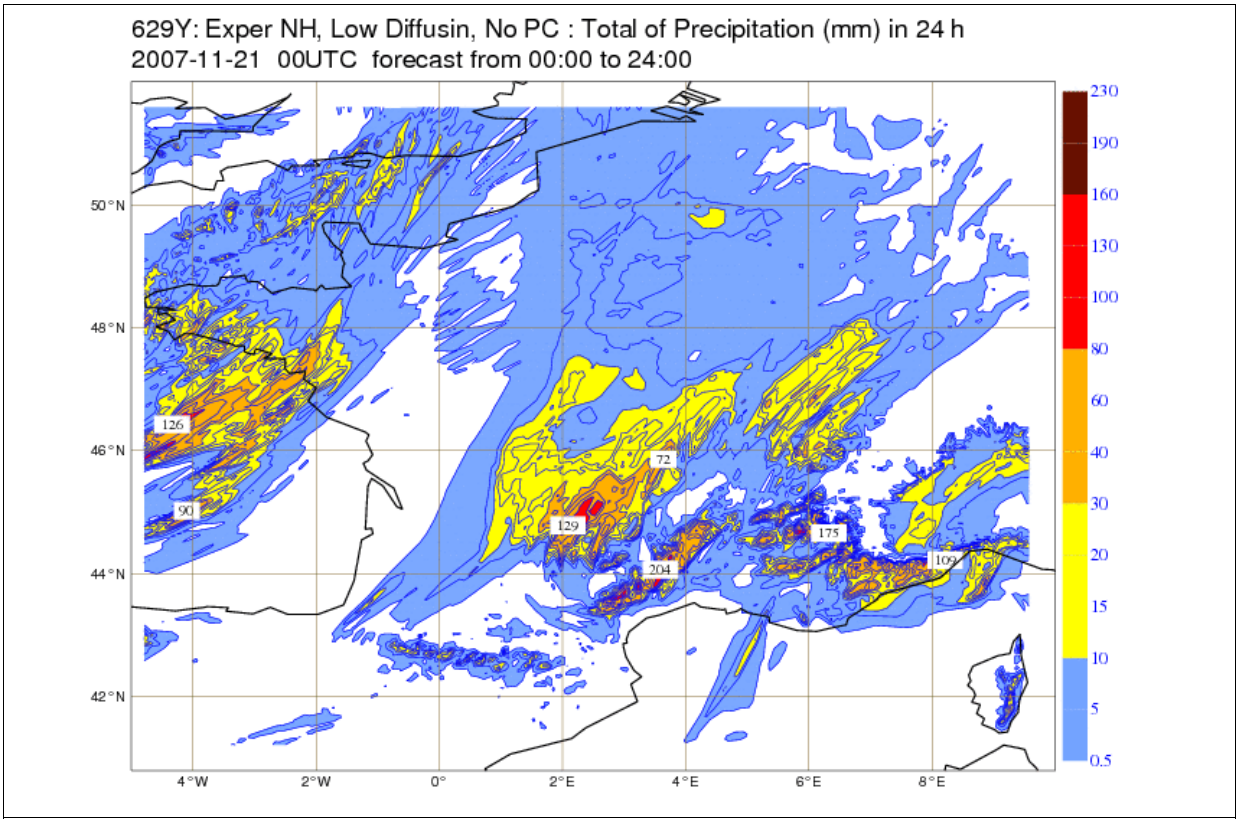

Figure 3.17 *NH _ Low Diff _ No PC* (tested version), run 00UTC: forecast of the accumulated precipitation (mm) in the period 00-24UTC of the 21th of November (cylindrical projection).

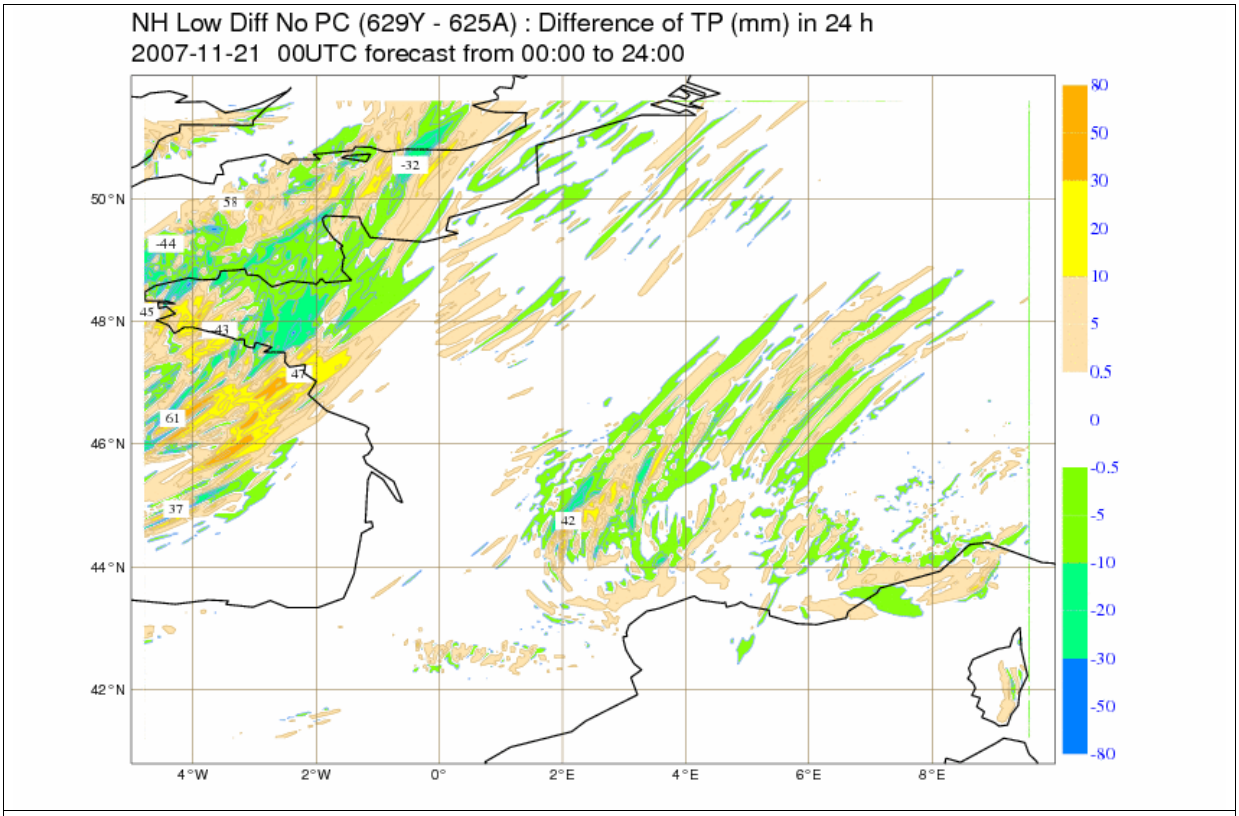

Figure 3.18 Difference between the forecasts of the accumulated precipitation (mm) [tested version – REF version] in the period 00-24UTC of the 21th of November (cylindrical projection).

Some considerations for the case study of the 21th of November 2007:

♦ Forecasts of LCC for 09 and 12h

- The LCC field produced by the experiment with the shallow cumulus convection scheme from the cycle al32t3_arome-main.01 (REF version) is similar to the one produced by the experiment with the new shallow cumulus convection scheme (tested version).

- Both forecasts of LCC give a general idea of the zones with low clouds but overestimate these clouds a little in some areas over land and over sea.

♦ Forecasts of accumulated precipitation

- The accumulated precipitation fields derived from the REF version for the periods 9-12h and 12-15h are similar to the correspondent fields derived from the tested version.

- For each one of these periods, the regions of forecasted heavy precipitation derived from each version are the same. Furthermore, those regions show a good superimposition with the most active zones detected on the observations (images of RADAR + lightening strikes).

- The differences of accumulated precipitation are small on the frontal zone and locally significant on the post-frontal regions where the convective activity was more intensive.

- The forecasts of accumulated precipitation for the period 00-24h derived from each version show very similar patterns.

- These forecasts for the period 00-24h show some consistence with the forecasts for the 3h periods by presenting in general small differences on the frontal zone and differences locally very significant on the more active post-frontal regions.